THESIS

THICKNESS EFFECTS IN THE FREE VIBRATION OF LAMINATED MAGNETO-ELECTRO-ELASTIC BEAMS AND PLATES

Submitted by

Chao Jiang

Department of Civil and Environmental Engineering

In partial fulfillment of the requirements

For the Degree of Master of Science

Colorado State University

Fort Collins, Colorado

Fall 2016

Master's Committee:

Advisor: Paul R. Heyliger

Bruce R. Ellingwood
Troy B. Holland

ABSTRACT

THICKNESS EFFECTS IN THE FREE VIBRATION OF LAMINATED MAGNETO-ELECTRO-ELASTIC BEAMS AND PLATES

A semi-analytical discrete-layer approach is used to evaluate thickness effects in the free vibration of laminated magneto-electro-elastic beams and plates under various lateral boundary conditions. To match the primary physical phenomenon and simplify the study, piecewise continuous approximations are used through the thickness direction and either continuous global polynomial or trigonometric functions are used to simulate the deflection in axial or planar displacement fields. Thin plate models can be recovered to predict frequency estimation for various boundary conditions and compared with continuum-based theories using more complex approximations. Based on symmetry the natural vibratory modes can be grouped to optimize computation. Numerical examples are used to show the thickness effects, with non-dimensional frequencies computed to multiple plates under six lateral boundary conditions: simply supported, clamped, and four different combinations of free and clamped/simply-supported edges. As the out-of-plate dimension becomes small and two opposite sides are free, this methodology can also be applied to beams under simply-supported, fixed-fixed and cantilever support conditions. Along with the influence of electro-elatstic and magneto-elastic coupling, the results of these analyses clearly illustrate the thickness effects within laminated plates by showing how the results vary with length/thickness ratio. Finding the accurate ratio varied with thickness is expected to provide useful specifications for the further study and design of multilayered magneto-electro-elastic beams and plates.

TABLE OF CONTENTS

ABSTRACT ii

CHAPTER 1 INTRODUCTION 1

CHAPTER 2 THEORY 5

2.1 Governing Equations 5

2.2 Ritz Approximations 10

2.3 Boundary Conditions 12

2.4 General Group Theories 15

CHAPTER 3 ISOTROPIC BEAMS 18

3.1 Free Vibrations of Simply Supported Isotropic Beams 19

3.1.1 *Frequency Comparison with EB/ Axial/ Torsion Theory* 19

3.1.2 *Comparison with Other Theories* 21

3.1.3 *Influence of a/h* 22

3.1.4 *Mode Shapes* 25

3.1.5 *Slenderness* 26

3.2 Free Vibrations of Fixed-fixed Isotropic Beams 28

3.2.1 *Frequency Comparison with EB/ Axial/ Torsion Theory* 28

3.2.2 *Influence of a/h* 30

3.2.3 *Mode Shapes* 30

3.2.4 *Slenderness* 32

3.3 Free Vibrations of Cantilever Beams 33

3.3.1 *Frequency Comparison with EB/ Axial/ Torsion Theory* 33

3.3.2 *Influence of a/h*....34

3.3.3 *Mode Shapes*....35

3.3.4 *Slenderness*....35

3.4 Characteristics of Isotropic Beams....39

CHAPTER 4 COMPOSITE MEE BEAMS....41

4.1 Characteristics of Composite MEE Beams....41

4.2 Simply Supported Condition....42

4.3 Fixed-fixed Condtion....48

4.4 Fixed-free Condition....53

CHAPTER 5 ISOTROPIC PLATES....59

5.1 Classical Isotropic Plates' Theories....60

5.2 Simply Supported Condition.... 61

5.3 All-Clamped Condition.... 64

5.4 FCFC Condition....67

5.5 CFFF Condition....70

5.6 CCFF Condition....73

5.7 SFSF Condition....75

CHAPTER 6 COMPSITE MEE PLATES....79

6.1 Comparison with Existing Results....79

6.2 SSSS Condition....80

6.3 CCCC Condition....86

6.4 FCFC Condition....92

6.5 CFFF Condition....99

6.6 CCFF Condition..... 105

6.7 SFSF Condition.....111

CHAPTER 7 CONCLUSION.....117

CHAPTER 8 REFERENCE..... 119

CHAPTER 9 APPENDIX A..... 121

CHAPTER 10 APPENDIX B.....124

CHAPTER 1 INTRODUCTION

The free vibration of solids can be used to evaluate elastic constants, study internal friction, and detect the presence of internal voids or flaws among other behaviors. Although closed-form solutions have been found for the vibration of many plate geometrics in simple cases, a large number of problems have not been solved through this methodology. Once the equations of motion have been derived, it is also common to use approximate methods for plates under various boundary conditions. For simply-supported plates, Kirchhoff's plate theory yields many exact solutions that can predict the behavior of elastic deformations and stresses near or across the interface of material layers under static and dynamic loading, but usually only when the planar dimensions are much larger than the thickness. Those methods can also be used for solving more complicated situations for multilayered composites that are more complex than for homogeneous elastic materials. An example of this is smart materials/ structures where piezoelectric (PE) and piezomagnetic (PM) materials have been involved in engineering fields. Applications range from cell phone to space shuttle technology. As piezoelectric solids link the electric and mechanical behaviors, so do piezomagnetic materials link magnetic and mechanical behaviors. From a combination of different materials, this class of smart structure not only contains the characteristics of elastic or electric/magnetic materials but also the potential to model new phenomenon associated with energy conversion, which means the converting energy could be transform from one form (among magnetic, electric, and mechanical energies) to others in the materials.

The free vibration of plates made of PE and PM materials have been investigated by several researchers. By expending the general boundary conditions in terms of series expansion,

Vel and Batra [1] solved the static deformation of multilayered piezoelectric plates using a three-dimensional solution. The corresponding bending vibration problem has been studied by Vel *et al.* [2]. Moreover, as an advanced application, materials labeled magneto-electro-elastic (MEE) materials have recently appeared. These materials contain both characters of electric and magnetic fields. Applications of these types of materials are seeing broader use and are the focus of the present study.

For a simply-supported multilayered MEE plate, the exact free vibration behavior using the exact closed-form solution in deflection has been derived using the pseudo Stroh formulation by Pan and Heyliger [3]. The state-space formulation is another method to analyze the static and dynamic behaviors of MEE multilayered plates [4][5]. This methodology was used by Chen *et al.* [6] in the study of the free vibration of a non-homogeneous isotropic MEE plate. Kondaiah, Shankar, and Ganesan using finite element method investigated beams made of magneto-electro-thermo-elastic smart composite materials with different volume fractions under uniform temperature rise on clamped-free boundary condition [7]. The discrete-layer (DL) and domain-discretization methods have also been widely used in analysis of anisotropic elastic and MEE plates and shells. The free vibration of an anisotropic and MEE plate was

[1] S.S. Vel, R.C. Batra, Three-dimensional analytical solution for hybrid multilayered piezoelectric plates, *ASME Journal of Applied Mechanics* 67 (2000) 558-567.

[2] S.S. Vel, R.C. Mewer, R.C. Batra, Analytical solution for the cylindrical bending vibration of piezoelectric composite plates, *International Journal of Solids and Stuctures* 41 (2004) 1625-1643.

[3] E. Pan, P.R. Heyliger, Free vibrations of simply supported and multilayered magneto-electro-elastic plates, *Journal of Sound and Vibration* 252 (2002) 429-442.

[4] J.G. Wang, L.F. Chen, S.S. Fang, State vector approach to analysis of multilayered magneto-electro-elastic plates, *International Journal of Solids and Structure* 40 (2003) 1669-1680.

[5] J.Y. Chen, H.L. Chen, E. Pan, P.R. Heyliger, Modal analysis of magneto-electro-elastic plates using the state vector approach, *Journal of Sound and Vibration* 304 (2007) 722-734.

[6] W.Q. Chen, K.Y. Lee, H.J. Ding, On free vibration of non-homogeneous transversely isotropic magneto-electro-elastic plates, *Journal of Sound and Vibration* 279 (2005) 237-251.

[7] P. Kondaiah, k. Shankar, N. Ganesan. Studies on magneto-electro-elastic cantilever beam under thermal environment, *Coupled systems mechanics* (2012) pp.205-217

worked out by Chen, Heyliger and Pan [8] corresponding to different lateral boundary conditions. The studies of many computational schemes for the solution of the equations of motions are based on the early work of Demarest [9] and Eer Nisse [10] through algorithms for elastic and piezoelectric parallelepipeds. However, if there is no existing closed-form solution, by expanding the displacements in terms of reasonable approximations, Hamiltons principle can be used to solve the weak form of the equations of motion. Furthermore, at an interface made of different materials, such as elastic, pezoelectric, and piezomagnetic properties, additional considerations may apply. Between two dissimilar materials, interface conditions include continuous stress, normal electric displacement, and normal magnetic induction. At a region of discontinuous material properties, these cause a discontinuity in the slope of the displacement and potential fields. The use of piecewise linear functions through the thickness with continuous global polynomial or trigonometric functions in the plane parallel to the interface allows a relatively accurate solution to be achieved. Via a semi-analytical discrete-layer model, Heyliger [11] developed the governing equations of layered elastic and piezoelectric parallelepipeds and obtained frequencies for a number of geometries and material combinations using this sort of approach.

When the thickness of the plate, h, is at least 10 times smaller than its lateral dimensions, Kirchhoff's classical theory of thin plates can often give sufficiently accurate results instead

[8] J.Y. Chen, P.R. Heyliger, E. Pan, Free Vibration of Three-dimesional Multilayered Magneto-electro-elastic Plates under combined Clamped/Free Boundary Conditions, *Journal of Sound and Vibration* 333 (2014) 4017-4029.

[9] H.H. Demarest, Jr., Cube Resonance Method to Determine the Elastic Constants of Solids,*J. Acoust. Soc. Am.* 49, (1971) 768-775.

[10] E.P. Eer Nisse, Variational Method for Electroelastic Vibration Analysis, *IEEE Trans. Sonics Ultrason.* SU-14(1976) 153-160.

[11] P.R. Heyliger, Traction-free Vibration of Layered Elastic and Piezoelectric Rectangular Parallelepipeds, *The Journal of the Acoustical Society of America* 107, 1235 (2000).

of carrying out a full three-dimensional stress analysis. But accuracy usually decreases with increasing thickness of the plate. Many authors qualify the value of the thickness relative to the larger plate dimensions as being "small" [12], "much smaller" [13], or "significantly smaller" [14]. Several authors have suggested limits with numbers attached: the thickness is "less than 1/20" [15] the lateral dimensions or that the lateral dimensions are "at least ten times" the thickness [16]. There has always been significant latitude assumed in applying these limits, since they are clearly influenced by plate geometry, the nature of the loading, and the material constitution. Such an inherent limitation of classical plate theory for the moderately thick plates necessitated the development of more refined theories in order to obtain reliable results for the behavior of these new materials. By plotting the frequencies as a function of the length-to-thickness ratio a/h, the present results indicate the level of errors influenced by thickness effects. The errors even within prior recommendations of a/h ratios can be significant.

The objective of this studying is to use Hamilton's principle and appropriate approximations to make the link between the thin plate theory and more accurate continuum models to determine at what a/h ratios thin plate theory may be adequate for beams and plates of laminated MEE material.

[12]Rao, S. S. *Vibration of Continuous Systems*, John Wiley and Sons, Hoboken, NJ (2007). Technomic Publishing Co., Lancaster PA (1987).

[13]Whitney, J. M. *Structural Analysis of Laminated Composite Plates*, Technomic Publishing Co., Lancaster PA (1987).

[14]Hjelmstad, K. D. *Fundamentals of Structural Mechanics*, Prentice Hall, Upper Saddle River, NJ (1997).

[15]Ugural, A. C. and Fenster, S. K. *Advanced Strength and Applied Elasticity*, Third Edition, Prentice Hall, Englewood Cliffs, NJ (1995).

[16]Szilard, R. *Theory and Analysis of Plates* Prentice Hall, Englewood Cliffs, NJ (1974).

CHAPTER 2 THEORY

This section details the generation of the discrete-layer model for MEE plates under six boundary conditions. Applying basic mechanical electric and magnetic relations, the variational form of Hamilton's principle for a MEE medium is presented. The equations resulting from this variational statement are solved by reducing the three-dimensional elasticity theory to a two-dimensional theory due to assuming a piecewise linear relationship through the thickness direction. Therefore, the approximate funcitons of the in-plane field variables can be generated respect to various lateral boundary conditions.

2.1 Governing Equations

A plate is a structural element that is flat and thin. The lateral dimension is relatively larger than the thickness, typically at least 10 times bigger. Normally, a plate is formed by multiple off-axis orthotropic layers and all constitutive relations are linear. Hence, Hooke's law applies for each layer. The interest in this work is the free vibration response of the plate. A rectangular Cartesian coordinate is used to formulate the governing equations with the origin located at one of the four corners on the tops surface, as shown in Figure 1.

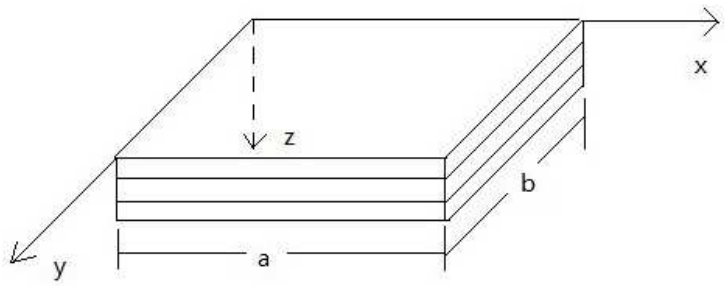

Figure 1: The definition of rectangular Cartesian coordinate

Of primary interest in this work are the thickness effects in laminated plate vibration for plates composed of elastic, electric and magnetic materials. Square laminates with lateral dimensions a=b and a total thickness h are considered in this study. As the plate can be composed of MEE materials, keeping the elastic parameters and changing the electric or magnetic variables and set the appropriate coupling coefficients (either piezomagnetic or piezoelectric constants) to zero can easily carry out the corresponding results for purely PE, PM, or elastic materials. Each layer is homogeneous and each interface is perfectly bonded; therefore, the compatibility of displacements and the potentials are enforced. Even though the elastic displacements, electric and magnetic potentials, elastic traction, and the z-components of the electric displacement and magnetic induction are continuous, there is a discountinuity of the gradient of displacement components, the electrostatic potential and magnetostatic potential at the interface of two layers.

In a linear, isotropic MEE solid, the coupled constitutive law for each lamina can be expressed as:

$$\sigma_{ij} = C_{ijkl}S_{kl} - e_{kij}E_k - q_{kij}H_k, \tag{1}$$

$$D_m = e_{mkl}S_{kl} + \epsilon_{mk}E_k + d_{mk}H_k, \tag{2}$$

$$B_m = q_{mkl}S_{kl} + d_{mk}E_k + \mu_{mk}H_k \tag{3}$$

Here σ_{ij}, D_m and B_m are respectively the components of stress, electric displacement and magnetic induction; S_{kl}, E_k and H_k represent the components of strain, electric field and magnetic field; C_{ijkl}, ϵ_{mk} and μ_{mk} indicate the elastic, dielectric, and magnetic permeability coefficients; and e_{kij}, q_{kij} and d_{mk} are the piezoelectric, piezomagnetic and magnetoelectric coefficients.

In these expressions, the indices, i and j range over the values 1 to 3, which represent the values of the rectangular Cartesian coordinates x, y and z. It is common to use a standard contracted notation that uses a single subscript for the stress components instead of the double subscript notation. The indices can be replaced by 11=1, 22=2, 33=3, 23=4, 13=5 and 12=6, and the matrix form representing the components of the elastic stiffness tensor in Cartesian coordinates can be given by

$$\begin{Bmatrix} \sigma_1 \\ \sigma_2 \\ \sigma_3 \\ \sigma_4 \\ \sigma_5 \\ \sigma_6 \end{Bmatrix} = \begin{bmatrix} C_{11} & C_{12} & C_{13} & 0 & 0 & C_{16} \\ C_{12} & C_{22} & C_{23} & 0 & 0 & C_{26} \\ C_{13} & C_{23} & C_{33} & 0 & 0 & C_{36} \\ 0 & 0 & 0 & C_{44} & C_{45} & 0 \\ 0 & 0 & 0 & C_{45} & C_{55} & 0 \\ C_{16} & C_{26} & C_{36} & 0 & 0 & C_{66} \end{bmatrix} \begin{Bmatrix} \epsilon_1 \\ \epsilon_2 \\ \epsilon_3 \\ \epsilon_4 \\ \epsilon_5 \\ \epsilon_6 \end{Bmatrix} \tag{4}$$

Moreover, by setting the values e_{mkl} or q_{mkl} equal to zero, the results for either purely PE, PM, or elastic material can be achieved.

The relationship between the strain and displacement, electric (magnetic) field and its potential can be written as:

$$S_{ij} = \frac{1}{2}\left(\frac{\partial u_i}{\partial x_j} + \frac{\partial u_j}{\partial x_i}\right), \tag{5}$$

$$E_k = -\frac{\partial \phi}{\partial x_k}, \tag{6}$$

$$H_k = -\frac{\partial \psi}{\partial x_k} \tag{7}$$

Here, u_i are the infinitesimal displacement components and ϕ and ψ are the electric and magnetic potentials, respectively. The components x_k are related to the x, y and z in the rectangular Cartesian coordinates for k=1,2,3.

The weak form of the equations of motion, the charge equation and the electromagnetic equation for a MEE medium within Hamilton's principle can be expressed as [17]:

$$\delta \int_{t_0}^{t} dt \int_V \left[\frac{1}{2}\rho \dot{u}_j \dot{u}_j - H(S_{kl}, E_k, H_k)\right] dV + \int_{t_0}^{t} dt \int_S (T_k \delta u_k - \sigma \delta\phi - I\delta\psi)\, dS = 0 \tag{8}$$

Here, t_0 and t are two specified times, V is the volume of the plate and S is the surface that bounds V. δ is the variational operator. The . superscript represents differentiation with respect to time, and T, σ, and I are surface tractions, surface charge, and surface current. H is the system enthalpy and can be written as

$$H = \frac{1}{2}C_{ijkl}S_{ij}S_{kl} - e_{ijk}E_iS_{jk} - \frac{1}{2}\epsilon_{ij}E_iE_j - q_{ijk}H_iS_{jk} - \frac{1}{2}\mu_{ij}H_iH_j - d_{ik}E_iH_k \tag{9}$$

Based on the specific material properties used in this study, and setting $x_1 = x$, $x_2 = y$, and $x_3 = z$, with the corresponding displacement field as u, v, w, the weak form can be expanded as:

[17] H.F. Tiersten, *Linear Piezoelectric Plate Vibrations*, Plenum, New York (1969).

$$
\begin{aligned}
0 = \int_{t_0}^{t} dt \int_V \Big\{ & \rho\left(\dot{u}\delta\dot{u} + \dot{v}\delta\dot{v} + \dot{w}\delta\dot{w}\right) - \Big[C_{11}\frac{\partial u}{\partial x}\frac{\partial \delta u}{\partial x} + C_{12}\frac{\partial u}{\partial x}\frac{\partial \delta v}{\partial y} + C_{12}\frac{\partial \delta u}{\partial x}\frac{\partial v}{\partial y} \\
& + C_{13}\frac{\partial u}{\partial x}\frac{\partial \delta w}{\partial z} + C_{13}\frac{\partial \delta u}{\partial x}\frac{\partial w}{\partial z} + C_{22}\frac{\partial v}{\partial y}\frac{\partial \delta v}{\partial y} + C_{23}\frac{\partial v}{\partial y}\frac{\partial \delta w}{\partial z} + C_{23}\frac{\partial \delta v}{\partial y}\frac{\partial w}{\partial z} \\
& + C_{33}\frac{\partial w}{\partial z}\frac{\partial \delta w}{\partial z} + C_{16}\frac{\partial u}{\partial x}\left(\frac{\partial \delta u}{\partial y} + \frac{\partial \delta v}{\partial x}\right) + C_{16}\frac{\partial \delta u}{\partial x}\left(\frac{\partial u}{\partial y} + \frac{\partial v}{\partial x}\right) \\
& + C_{26}\frac{\partial v}{\partial y}\left(\frac{\partial \delta u}{\partial y} + \frac{\partial \delta v}{\partial x}\right) + C_{26}\frac{\partial \delta v}{\partial y}\left(\frac{\partial u}{\partial y} + \frac{\partial v}{\partial x}\right) + C_{36}\frac{\partial w}{\partial z}\left(\frac{\partial \delta u}{\partial y} + \frac{\partial \delta v}{\partial x}\right) \\
& + C_{36}\frac{\partial \delta w}{\partial z}\left(\frac{\partial u}{\partial y} + \frac{\partial v}{\partial x}\right) + C_{44}\left(\frac{\partial v}{\partial z} + \frac{\partial w}{\partial x}\right)\left(\frac{\partial \delta v}{\partial z} + \frac{\partial \delta w}{\partial x}\right) \\
& + C_{55}\left(\frac{\partial u}{\partial z} + \frac{\partial w}{\partial y}\right)\left(\frac{\partial \delta u}{\partial z} + \frac{\partial \delta w}{\partial y}\right) + C_{66}\left(\frac{\partial u}{\partial y} + \frac{\partial v}{\partial x}\right)\left(\frac{\partial \delta u}{\partial y} + \frac{\partial \delta v}{\partial x}\right) \\
& + C_{45}\left(\frac{\partial v}{\partial z} + \frac{\partial w}{\partial x}\right)\left(\frac{\partial \delta u}{\partial z} + \frac{\partial \delta w}{\partial y}\right) + C_{45}\left(\frac{\partial \delta v}{\partial z} + \frac{\partial \delta w}{\partial x}\right)\left(\frac{\partial u}{\partial z} + \frac{\partial w}{\partial y}\right) \\
& - e_{15}\delta E_1\left(\frac{\partial u}{\partial z} + \frac{\partial w}{\partial x}\right) - e_{15}E_1\left(\frac{\partial \delta u}{\partial z} + \frac{\partial \delta w}{\partial x}\right) - e_{24}\delta E_2\left(\frac{\partial v}{\partial z} + \frac{\partial w}{\partial y}\right) \\
& - e_{24}E_2\left(\frac{\partial \delta v}{\partial z} + \frac{\partial \delta w}{\partial y}\right) - e_{31}\delta E_3\frac{\partial u}{\partial x} - e_{31}E_3\frac{\partial \delta u}{\partial x} - e_{32}\delta E_3\frac{\partial v}{\partial y} - e_{32}E_3\frac{\partial \delta v}{\partial y} \\
& - e_{33}\delta E_3\frac{\partial w}{\partial z} - e_{33}E_3\frac{\partial \delta w}{\partial z} - q_{15}\delta H_1\left(\frac{\partial u}{\partial z} + \frac{\partial w}{\partial x}\right) - q_{15}H_1\left(\frac{\partial \delta u}{\partial z} + \frac{\partial \delta w}{\partial x}\right) \\
& - q_{24}\delta H_2\left(\frac{\partial v}{\partial z} + \frac{\partial w}{\partial y}\right) - q_{24}H_2\left(\frac{\partial \delta v}{\partial z} + \frac{\partial \delta w}{\partial y}\right) - q_{31}\delta H_3\frac{\partial u}{\partial x} - q_{31}H_3\frac{\partial \delta u}{\partial x} \\
& - q_{32}\delta H_3\frac{\partial v}{\partial y} - q_{32}H_3\frac{\partial \delta v}{\partial y} - q_{33}\delta H_3\frac{\partial w}{\partial z} - q_{33}H_3\frac{\partial \delta w}{\partial z} - \epsilon_{11}E_1\delta E_1 \\
& - \epsilon_{22}E_2\delta E_2 - \epsilon_{33}E_3\delta E_3 - \mu_{11}H_1\delta H_1 - \mu_{22}H_2\delta H_2 - \mu_{33}H_3\delta H_3]\Big\}\, dV \\
& + \int_{t_0}^{t} dt \int_S \left(T_k\delta u_k - \sigma\delta\phi - I\delta\psi\right) dS = 0
\end{aligned}
\tag{10}
$$

It is possible to integrate the weak form by parts and collect the cofficients with respect to δu, δv, δw, $\delta\phi$, and $\delta\psi$. Since we use Ritz method, there is no need for this step. Here the focus is on the quasi-static state which means there is no electric charge or current densities across the surface. Body forces are also assumed to be zero in the results that follow.

2.2 Ritz Approximations

The five primary field variables (u, v, w, ϕ and ψ) can be approximated with x, y, z and t as follows:

$$
\begin{aligned}
u(x,y,z,t) &= \sum_{j=1}^{n} U_j(x,y,t)\,\bar{\Psi}_j^u(z) = \sum_{i=1}^{m}\sum_{j=1}^{n} U_{ji}(t)\,\Psi_i^u(x,y)\,\bar{\Psi}_j^u(z) \\
v(x,y,z,t) &= \sum_{j=1}^{n} V_j(x,y,t)\,\bar{\Psi}_j^v(z) = \sum_{i=1}^{m}\sum_{j=1}^{n} V_{ji}(t)\,\Psi_i^v(x,y)\,\bar{\Psi}_j^v(z) \\
w(x,y,z,t) &= \sum_{j=1}^{n} W_j(x,y,t)\,\bar{\Psi}_j^w(z) = \sum_{i=1}^{m}\sum_{j=1}^{n} W_{ji}(t)\,\Psi_i^w(x,y)\,\bar{\Psi}_j^w(z) \\
\phi(x,y,z,t) &= \sum_{j=1}^{n} \Phi_j(x,y,t)\,\bar{\Psi}_j^v(z) = \sum_{i=1}^{m}\sum_{j=1}^{n} \Phi_{ji}(t)\,\Psi_i^\phi(x,y)\,\bar{\Psi}_j^\phi(z) \\
\psi(x,y,z,t) &= \sum_{j=1}^{n} \Psi_j(x,y,t)\,\bar{\Psi}_j^v(z) = \sum_{i=1}^{m}\sum_{j=1}^{n} \Psi_{ji}(t)\,\Psi_i^\psi(x,y)\,\bar{\Psi}_j^\psi(z)
\end{aligned}
\tag{11}
$$

Here U_{ji}, V_{ji}, W_{ji}, Φ_{ji} and Ψ_{ji} are unknown constants. $\Psi_i(x,y)$ are the in-plane approximation functions, while $\bar{\Psi}_j$ are the one-dimensional Lagrangian interpolation polynomials in the thickness direction respect to each variable.

The corresponding virtual fields can be expressed as:

$$
\begin{aligned}
\delta u = \Psi_i^u(x,y)\,\bar{\Psi}_j^u(z), \quad \delta v = \Psi_i^v(x,y)\,\bar{\Psi}_j^v(z), \quad \delta w = \Psi_i^w(x,y)\,\bar{\Psi}_j^w(z) \\
\delta\phi = \Psi_i^\phi(x,y)\,\bar{\Psi}_j^\phi(z), \quad \delta\psi = \Psi_i^\psi(x,y)\,\bar{\Psi}_j^\psi(z)
\end{aligned}
\tag{12}
$$

By assuming periodic motion, substituting these approximations into the weak form, and collecting the coefficients of the variations of the displacements and placing the results in matrix form, the system can be written as:

$$\begin{bmatrix} [M^{11}] & [0] & [0] & [0] & [0] \\ [0] & [M^{22}] & [0] & [0] & [0] \\ [0] & [0] & [M^{33}] & [0] & [0] \\ [0] & [0] & [0] & [0] & [0] \\ [0] & [0] & [0] & [0] & [0] \end{bmatrix} \begin{Bmatrix} \{U\} \\ \{V\} \\ \{W\} \\ \{\Phi\} \\ \{\Psi\} \end{Bmatrix} \rho\omega^2 +$$

$$\begin{bmatrix} [K^{11}] & [K^{12}] & [K^{13}] & [K^{14}] & [K^{15}] \\ [K^{21}] & [K^{22}] & [K^{23}] & [K^{24}] & [K^{25}] \\ [K^{31}] & [K^{32}] & [K^{33}] & [K^{34}] & [K^{35}] \\ [K^{41}] & [K^{42}] & [K^{43}] & [K^{44}] & [K^{45}] \\ [K^{51}] & [K^{52}] & [K^{53}] & [K^{54}] & [K^{55}] \end{bmatrix} \begin{Bmatrix} \{U\} \\ \{V\} \\ \{W\} \\ \{\Phi\} \\ \{\Psi\} \end{Bmatrix} = \begin{Bmatrix} \{0\} \\ \{0\} \\ \{0\} \\ \{0\} \\ \{0\} \end{Bmatrix} \tag{13}$$

The submatrices here are related to the materials' characteristics that include the elastic stiffnesses, piezoelectric coefficients, piezomagnetic coefficients or shape functions. These matrices are given in the Appendix A.

The DL model is based on separating the field variables in the thickness direction and within the plane of the plate. This can effectively reduce the computational effort. Since there is a break in the gradients of displacement in the z direction, one-dimensional Lagrangian polynomials are sufficient to describe these displacements in the thickness direction. The in-plane functions are generated depending on the various lateral boundary conditions. These are described below.

2.3 Boundary Conditions

The following classes of boundary conditions are discussed:

1. SSSS: simply supported around all edges

Srinivas [18] solved this problem using an exact method . The in-plane approximation functions are treated as harmonic functions as by Heyliger [11] to determine the fundamental in-plane modes.

For the simple supported condition:

$$w = \sigma_{xx} = \sigma_{xy} = \phi = \psi = 0 \quad at \quad x = 0, a \tag{14}$$

$$w = \sigma_{xy} = \sigma_{yy} = \phi = \psi = 0 \quad at \quad y = 0, b \tag{15}$$

To satify the essential boundary conditions on w, ϕ, and ψ, Fourier series are selected. The in-plane approximations can be written as:

$$\Psi_i^u(x,y) = cos\frac{m\pi x}{a} sin\frac{n\pi y}{b}$$
$$\Psi_i^v(x,y) = sin\frac{m\pi x}{a} cos\frac{n\pi y}{b}$$
$$\Psi_i^w(x,y) = sin\frac{m\pi x}{a} sin\frac{n\pi y}{b}$$

Here ϕ and ψ have the same expression as w, and each individual pair of (m,n) contain a different value of i.

[18] S. Srinivas, C.V. Joga Rao, and A.K. Rao, *Some Results From an Exact Analysis of Thick Laminates in Vibration and Buckling*, J. Appl. Mech. 37, 868-870(1970).

2. CCCC: clamped around all edges

$$u = v = w = \phi = \psi = 0 \quad at \quad x = 0, a \quad and \quad at \quad y = 0, b \tag{16}$$

Since displacements are zero at the domain endpoints, it is convenient to give the approximations along (x, y) directions written in "parent" domain (ξ, η) which allows computations in terms of coordinate origins. Chen *et al.* [8] used this approximation for the all clamped condition and compared their results with frequencies from a FEM approach. The coordinate, ξ and η are introduced as $\xi = \frac{2x}{a}$ and $\eta = \frac{2y}{b}$ and varying from -1 to 1, with ξ_i and η_i the equally spaced locations within (-1, 1). For example, within the ξ domain the displacements are expressed as following:

$$When \quad i = 1, \quad f_x = (1 - \xi)(1 + \xi)$$

$$When \quad i = 2, \quad f_x = (1 - \xi)\,\xi\,(1 + \xi)$$

$$When \quad i = 3, \quad f_x = (1 - \xi)\left(\frac{1}{3} - \xi\right)\left(\frac{1}{3} + \xi\right)(1 + \xi)$$

3. FCFC: Here two opposite sides of the plate are "free" (in that all components of the stress-traction vector are 0, as are the electric displacement and normal flux), and the others are clamped. In this case it is assumed that the plate is clamped along the x direction, while the y direction is free. Therefore the appropriate boundary conditions are:

$$u = v = w = \phi = \psi = 0 \quad at \quad x = 0, a \tag{17}$$

$$\sigma_{yy} = \sigma_{xy} = \sigma_{yz} = D_y = B_y = 0 \quad at \quad y = 0, b \tag{18}$$

Demarest [9] showed that group theory can be used to simplify vibration analysis. He used cubic Legendre polynomials which give accurate results. The approximate functions are given in the even/odd terms. The lowest three terms in the even group are 1, $(3x^2-1)/2$, and $(35x^4-30x^2+3)/8$, while for the odd functions are shown as x, $(5x^3-3x)/2$, and $(63x^5-70x^3+15x)/8$ [19].

4. CFFF: only one edge is clamped, the others are free. This is also know as the cantilever plate.

$$u = v = w = \phi = \psi = 0 \quad at \qquad x = 0 \tag{19}$$

$$\sigma_{xx} = \sigma_{xy} = \sigma_{xz} = D_x = B_x = 0 \quad at \qquad x = a \tag{20}$$

$$\sigma_{yy} = \sigma_{xy} = \sigma_{yz} = D_y = B_y = 0 \quad at \qquad y = 0, b \tag{21}$$

Here, to match the displacements at x=0, we use power series of at least first order along the x direction and maintain the Legendre polynomials in the y direction.

5. CCFF: two adjacent edges are clamped, while the others are free

$$u = v = w = \phi = \psi = 0 \quad at \qquad x = 0, \quad y = 0 \tag{22}$$

$$\sigma_{xx} = \sigma_{xy} = \sigma_{xz} = D_x = B_x = 0 \quad at \qquad x = a \tag{23}$$

$$\sigma_{yy} = \sigma_{xy} = \sigma_{yz} = D_y = B_y = 0 \quad at \qquad y = b \tag{24}$$

The displacements and potential along x and y directions are extended as power series in a manner similar to the cantilever plate.

[19] M. Abromowitz, I.A. Stegun, Handbook of Mathematical Functions, Dover, New York, 1965.

6. SFSF: two opposite sides are simply supported and the others are free

$$w = \sigma_{xx} = \sigma_{xy} = \phi = \psi = 0 \quad at \quad x = 0, a \tag{25}$$

$$\sigma_{yy} = \sigma_{xy} = \sigma_{yz} = D_y = B_y = 0 \quad at \quad y = 0, b \tag{26}$$

Fourier series are used in the x direction. The only difference is specified terms for approximate function, as m and n are either 2i+1 or 2i. The approximation functions in u and v are coupled with the displacement in w. And the modes are separated into two groups (odd and even) according to these groupings. For example, the first term in odd group are: $\Psi_1^u(x,y) = cos\frac{\pi x}{a} sin\frac{\pi y}{b}$, $\Psi_1^v(x,y) = sin\frac{\pi x}{a} cos\frac{\pi y}{b}$, and $\Psi_1^w(x,y) = sin\frac{\pi x}{a} sin\frac{\pi y}{b}$. The first terms in the even group are given as: $\Psi_2^u(x,y) = cos\frac{2\pi x}{a} sin\frac{2\pi y}{b}$, $\Psi_2^v(x,y) = sin\frac{2\pi x}{a} cos\frac{2\pi y}{b}$, and $\Psi_2^w(x,y) = sin\frac{2\pi x}{a} sin\frac{2\pi y}{b}$.

2.4 General Group Theories

Because of symmetries about the middle lines of the plate, the eigenvalue problem achieved from the governing equations can be separated into different groups. This allows a significant computational effort reduction. In general, this separation can be represented by the following sums:

$$\begin{aligned} \Psi_i^u(x,y,z) &= \sum_{i=1}^{m}\sum_{j=1}^{n} \Psi_i^u(x,y)\bar{\Psi}_j^u(z) \\ &= \sum_{k=1}^{n}\sum_{i=1}^{m} \Psi_{ik}^u(x)\Psi_{ik}^u(y) \sum_{j=1}^{n} \bar{\Psi}_j^u(z) \end{aligned} \tag{27}$$

$$
\begin{aligned}
&\sum_{k=1}^{n}\sum_{i=1}^{m}\Psi_{ik}^{u}(x)\Psi_{ik}^{u}(y) \\
= &\underbrace{\sum_{k=1,3,5\ldots}^{N_1}\sum_{i=1,3,5\ldots}^{N_1}\Psi_{ik}^{u}(x)\Psi_{ik}^{u}(y)}_{N_O(x)N_O(y)} + \underbrace{\sum_{k=1,3,5\ldots}^{N_1}\sum_{i=2,4,6\ldots}^{N_2}\Psi_{ik}^{u}(x)\Psi_{ik}^{u}(y))}_{N_O(x)N_E(y)} \\
&+ \underbrace{\sum_{k=2,4,6\ldots}^{N_2}\sum_{i=1,3,5\ldots}^{N_1}\Psi_{ik}^{u}(x)\Psi_{ik}^{u}(y)}_{N_E(x)N_O(y)} + \underbrace{\sum_{k=2,4,6\ldots}^{N_2}\sum_{i=2,4,6\ldots}^{N_2}\Psi_{ik}^{u}(x)\Psi_{ik}^{u}(y)}_{N_E(x)N_E(y)} \\
= &\underbrace{N_O(x)N_O(y)}_{group1} + \underbrace{N_O(x)N_E(y)}_{group2} + \underbrace{N_E(x)N_O(y)}_{group3} + \underbrace{N_E(x)N_E(y)}_{group4}
\end{aligned}
\tag{28}
$$

For simply supported plates, there is no deflection in z direction at the supports. The first four mode shapes of each direction as shown as follows. Each shape of deflection will fall into the combination of these, as shown in Figure 2.

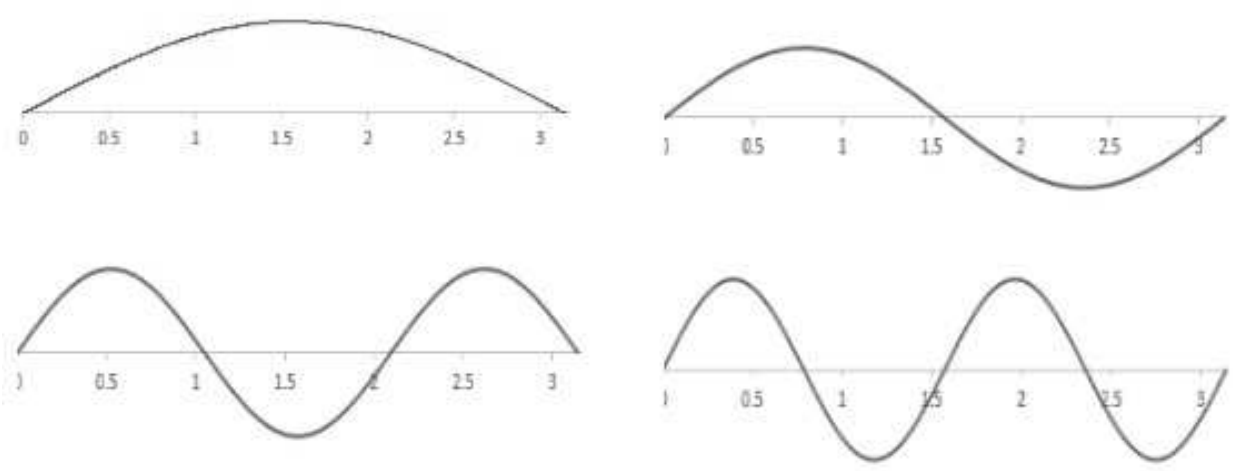

Figure 2: The first four modes for the simply supported condtion

For the all clamped and clamped and free on the opposite sides conditions, due to the symmetry of the center groups of displacement field can be written as in Table 1, where the

designations OD, EX, and so on were introduced by Ohno [20]. Therefore, instead of solving the entire problem, 4 reduced eigenvalueproblems can be solved.

Group	displacment	x	y	Group	displacemnet	x	y
OD,EZ	u	O	E	OX,EY	u	O	O
	v	E	O		v	E	E
	w	E	E		w	E	O
	ψ	E	E		ψ	E	O
	ϕ	E	E		ϕ	E	O
EX,OY	u	E	E	EV,OZ	u	E	O
	v	O	O		v	O	E
	w	O	E		w	O	O
	ψ	O	E		ψ	O	O
	ϕ	O	E		ϕ	O	O

Table 1: Group theory for CCCC and FCFC conditions

[20] I. Ohno, Free Vibration of a Rectangular Papallelepiped Crystal and its Application to Determination of Elastic Constants of Orthorhombic Crystals, *J. Phys. Earth.* 24, (1976) 355-379

CHAPTER 3 ISOTROPIC BEAMS

Beams are one of the most basic elements in the engineering field and are frequently used to model framed structures. Since the deflected shape of the beam can be caused by loads or support motion, especially those associated with wind and earthquakes, beam response can have a strong correlation to the natural frequency of vibration. Although the DL model is mainly used for plates in this thesis, it can also be used to represent beam response as the out-of-plane lateral dimension becomes small. To assess the accuracy and test the limitations of the DL model, a series of comparisons with Euler-Bernoulli (EB) beam theory [12] is provided in this section. The EB beam theory is the simplest theory for calculating the deflection characteristics of beams and gives the most accurate results for beams where the length is much larger than the other dimensions. As is the case for the plate, it is of interest to determine the level of accuracy of the elementary EB kinematic model as the length of the beam decreases, which is known as slenderness or thickness effect as following.

Except for the deflection, the elongation along the longitudianl direction is another significant charateristic of beams. Bar theory is the simplyest theory to detect the vibration of longitudinal direction. Since Kirchhoff's beam theory assumes that the cross section of the beam originally plane stay plane after deformation [12]. As beams become longer, the effect of the cross section can be neglected. The longitudinal vibration of beams is closer to the vibration of bars. Hence, axial frequencies are also inspected in this section.

Three types of beam boundary conditions are considered here that are among those most frequently encountered: simply supported, fixed-fixed and cantilever beams. The completely isotropic homogeneous beam is chosen first to study comparisons with the DL model. All

variables are assumed to be independent of the out-of-plane coordinate y in the examples that follow. Discrete layers of equal thickness are used. There are two convergence behaviors that are studied here: the number of axial terms with the layers fixed, and the number of layers with the axial terms fixed. Two different isotropic materials are considered with Poisson ratios: $\nu = 0$ and $\nu = 0.3$. The dimensionless frequency parameter used is $\varpi = \omega\sqrt{\rho h/G}$, and all frequencies are reported using this quantity. The cross section of the beam is square with b=h, where b is the width in the y-direction. Two values of length to thickness ratio are initially used: a/h=10 and a/h=20, respectively, to assess the influence of slendeness.

3.1 Free Vibrations of Simply Supported Isotropic Beams

3.1.1 Frequency Comparison with EB/ Axial/ Torsion Theory

The dimensionless frequencies for the representative beams are given in Tables 2 and 3. Several observations can be made. First, a single axial term can provide excellent results depending on the boundary conditions, as in the case of simple support. Other conditions may require at least two or more functions. Second, the axial frequency for $\nu = 0$ has excellent agreement with bar theory for all conditions considered here. However, when the beam is constrained in a Poisson sense, higher frequencies are achieved using the DL model. Third, in general, the bending frequencies for zero Poisson ratio are in excellent agreement with the EB result for a/h=20, but the agreement is not as good for a/h=10 when shear is more likely to influence the results. In every case, however, accounting for a non-zero Poisson ratio tends to increase the frequencies by about 18 percent.

Table 4 shows the dimensionless frequencies as a function of the number of axial terms. Maintaining five axial terms, the DL model can give relatively good results even with relatively few layers.

Table 2: Dimensionless frequencies of simply supported beams(a/h=20) with 8 layers

Isotropic materials	Terms in x	DL Model			
		1st bending	2nd bending	3rd bending	1st axial
Terms ($\nu = 0$)	1	1.0038e-2	3.9749e-2	———	0.2221
	2-6	1.0038e-2	3.9749e-2	8.7990e-2	0.2221
Terms ($\nu = 0.3$)	1	1.2009e-2	4.7430e-2	———	0.2655
	2-6	1.2009e-2	4.7430e-2	0.1046	0.2655
EB/Bar		1.0073e-2	4.0293e-2	9.0658e-2	0.2221

Table 3: Dimensionless frequencies of simply supported beams(a/h=10) with 8 layers

Isotropic materials	Terms in x	DL Model			
		1st bending	2nd bending	3rd bending	1st axial
Terms ($\nu = 0$)	1	3.9749e-2	0.1531	———	0.4443
	2-6	3.9749e-2	0.1531	0.3258	0.4443
Terms ($\nu = 0.3$)	1	4.7430e-2	0.1810	———	0.5306
	2-6	4.7430e-2	0.1810	0.3809	0.5306
EB/Bar		4.0293e-2	0.1612	0.3626	0.4442

Table 4: Dimensionless frequencies of discrete isotropic beams under simply supported condition(a/h=20) with five axial terms and $\nu = 0$

Layers	DL Model			
	1st bending	2nd bending	3rd bending	1st axial
1	1.0042e-2	3.9807e-2	8.8269e-2	0.2221
2	1.0042e-2	3.9807e-2	8.8269e-2	0.2221
4	1.0039e-2	3.9763e-2	8.8056e-2	0.2221
8	1.0038e-2	3.9749e-2	8.7990e-2	0.2221
16	1.0038e-2	3.9745e-2	8.7972e-2	0.2221
32	1.0038e-2	3.9744e-2	8.7968e-2	0.2221

3.1.2 Comparison with Other Theories

Natural frequencies of an isotropic beam under simply supported condition have been studied by Karin *et al.* [21] using what they called the Enhanced Continuum Mechanics Based Formulation (CMF) and Structural Mechanics Based Formulation (SMF). The dimensions of their beam were taken to be: a=2 m and b=h=0.4 m. The material properties are considered as follows: $\rho = 7850kg/m^3$, $E = 1 \times 10^9 N/m^2$ and $\nu = 0.3$. This problem is treated here using a 8-layer discretization through the thickness. Results are calculated by 5 terms in x and 3 terms in y. The comparisons are shown in Table 5.

Table 5: Frequencies for simply supported beams(rad/s)

Theory	1st bending	2nd bending	1st torsional	1st axial	1st shear	2nd shear
CMF	95.6340	332.235	319.346	560.642	1766.99	1878.87
SMF	95.6341	332.236	319.347	560.642	1766.99	1878.87
Timoshenko	95.6340	332.235	319.350	560.642	1766.99	1878.87
Present	96.8729	337.132	320.575	641.714	1749.63	1856.65

As opposed to the DL model of the pin-pin beam, Karin *et al.* treat their simply-supported beam as a fixed-roller condition. Therefore, for the axial frequencies, their results are closer to the frequencies of cantilever beams, which is shown as $w = \frac{(2n-1)\pi}{2L}\sqrt{E/\rho}$ (n=1,2,3,...) [12]. To compare with frequency given by $w = \frac{n\pi}{L}\sqrt{E/\rho}$ (n=1,2,3,...) [12], we double the 1st axial values. In Karin *et al*'s paper, they define the shear modes, which we call the transverse shear modes, meaning that there is only shear deformation in the xz plane. By comparing the possible mode shapes given by Karin *et al.* to these values, the corresponding 1st shear and 2nd shear mode shapes calculated by the DL model are plotted

[21] K. Nachbagauer, P. Gruber, and J. Gerstmayr, A 3D Shear Deformable Finite Element Based on the Absolute Nodal Coordinate Formulation, *Multibody Dynamics*, Springer Netherlands, (2013) pp 77-96.

in Figure 3. As the DL model uses a piecewise linear function through the thickness, results are slightly lower than Karin*et al*'s calculations. The remaining frequencies are in excellent agreement.

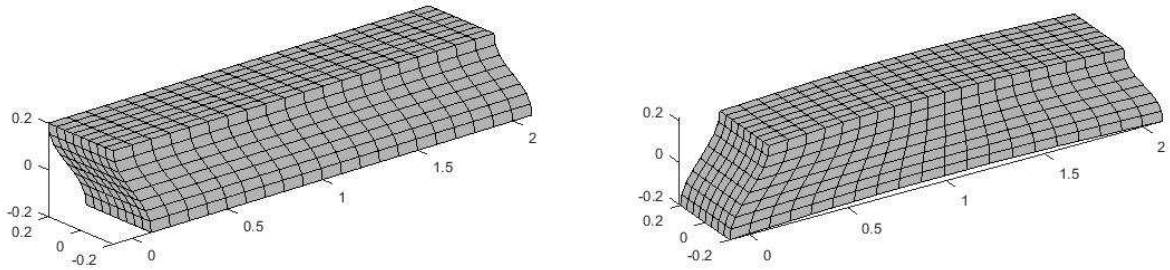

1st shear mode shape 2nd shear mode shape

Figure 3: The first two tranverse shear mode shapes of simply supported beams with a/h=5

3.1.3 Influence of a/h

Using 8 layers, 5 terms in x and 3 terms in y, Figures 4 and 5 show the differences between the DL and elementary beam/bar results for different Poisson ratios. Here, ω_A stands for the EB beam theory, St. Venant torsion theory, or the one-dimensional axial bar theory values. The analytical value for the torsional frequency is given by $\bar{\omega} = \sqrt{Gk_t/\rho L^2}$ [21], where k_t is 0.846 in this case. The corresponding ratios with respect to each a/h point are listed in Tables 6 and 7. It is clearly seen that with zero Poisson ratio and a length to the thickness ratio that is relatively large, the lower frequencies from the DL model are in nearly perfect agreement with the classical results. As the EB beam theory is kinematically stiff, the differences are larger for the higher modes. For most length-to-thickness ratios, there are only small differences for the axial and torsional frequencies.

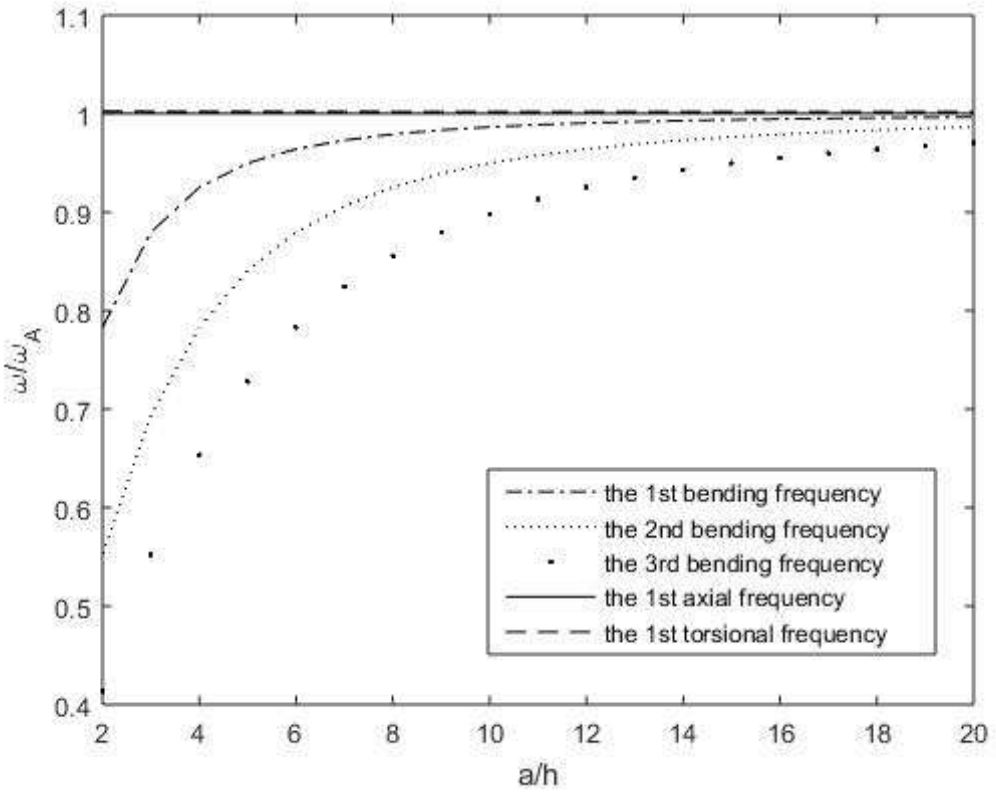

Figure 4: Differences between the DL model and the analytical values with $\nu = 0$ as a function of a/h ratio

Table 6: Ratios between the DL model and the analytical values with $\nu = 0$

a/h	1	2	3	4	5	6	7	8	9	10
1	0.5521	0.7830	0.8796	0.9252	0.9499	0.9641	0.9732	0.9792	0.9834	0.9865
2	0.3272	0.5521	0.6937	0.7831	0.8409	0.8796	0.9063	0.9254	0.9393	0.9498
3	0.2283	0.4137	0.5521	0.6536	0.7280	0.7830	0.8242	0.8555	0.8796	0.8984
4	1.0002	1.0002	1.0002	1.0002	1.0002	1.0002	1.0002	1.0002	1.0002	1.0002
5	1.0043	1.0027	1.0034	1.0023	1.0022	1.0022	1.0022	1.0022	1.0022	1.0022
a/h	11	12	13	14	15	16	17	18	19	20
1	0.9888	0.9905	0.9919	0.9930	0.9939	0.9946	0.9952	0.9958	0.9962	0.9966
2	0.9578	0.9641	0.9691	0.9732	0.9765	0.9792	0.9815	0.9834	0.9851	0.9865
3	0.9134	0.9254	0.9351	0.9431	0.9498	0.9554	0.9601	0.9641	0.9676	0.9706
4	1.0002	1.0002	1.0002	1.0002	1.0002	1.0002	1.0002	1.0002	1.0002	1.0002
5	1.0021	1.0021	1.0021	1.0021	1.0021	1.0021	1.0021	1.0021	1.0021	1.0021

1: the 1st bending frequency 2: the 2nd bending frequency 3: the 3rd bending frequency
4: the 1st axial frequency 5: the 1st torsional frequency

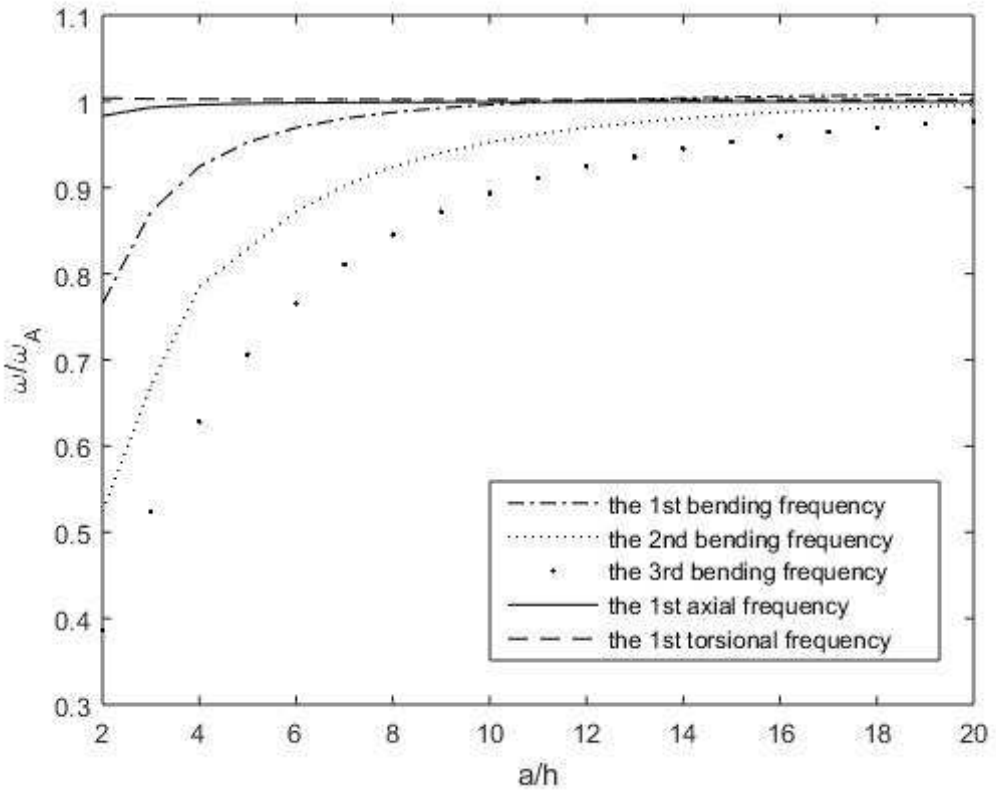

Figure 5: Differences between the DL model and the analytical values with $\nu = 0.3$ as a function of a/h ratio

Table 7: Ratios between the DL model and the analytical values with $\nu = 0.3$

a/h	1	2	3	4	5	6	7	8	9	10
1	0.5241	0.7654	0.8722	0.9244	0.9527	0.9695	0.9802	0.9874	0.9924	0.9961
2	0.3036	0.5241	0.6700	0.7848	0.8289	0.8722	0.9025	0.9244	0.9405	0.9527
3	0.2108	0.3867	0.5241	0.6281	0.7063	0.7654	0.8104	0.8451	0.8722	0.8935
4	0.8832	0.9832	0.9930	0.9962	0.9976	0.9983	0.9988	0.9991	0.9993	0.9994
5	1.0087	1.0040	1.0030	1.0026	1.0024	1.0023	1.0023	1.0022	1.0022	1.0022
a/h	11	12	13	14	15	16	17	18	19	20
1	0.9988	1.0009	1.0026	1.0039	1.0050	1.0058	1.0066	1.0072	1.0077	1.0081
2	0.9621	0.9695	0.9754	0.9802	0.9841	0.9874	0.9901	0.9924	0.9944	0.9961
3	0.9106	0.9244	0.9356	0.9449	0.9527	0.9592	0.9648	0.9695	0.9736	0.9771
4	0.9995	0.9996	0.9996	0.9997	0.9997	0.9998	0.9998	0.9998	0.9998	0.9999
5	1.0022	1.0022	1.0022	1.0022	1.0022	1.0022	1.0022	1.0022	1.0021	1.0021

1: the 1st bending frequency 2: the 2nd bending frequency 3: the 3rd bending frequency
4: the 1st axial frequency 5: the 1st torsional frequency

There is a Poisson end effect that results in a relatively large difference in axial frequency for smaller a/h ratios as shown in Figure 5. This effect can be observed with the side view of the middle surfaces in Figure 6. This demonstrates the proportion of end effects over the entire beam under simply supported conditions. It can be seen that as the a/h ratio increases the influence of end effects are decreased. Since torsional frequencies only vary with shear modulus, there is virtually no change for torsional frequencies.

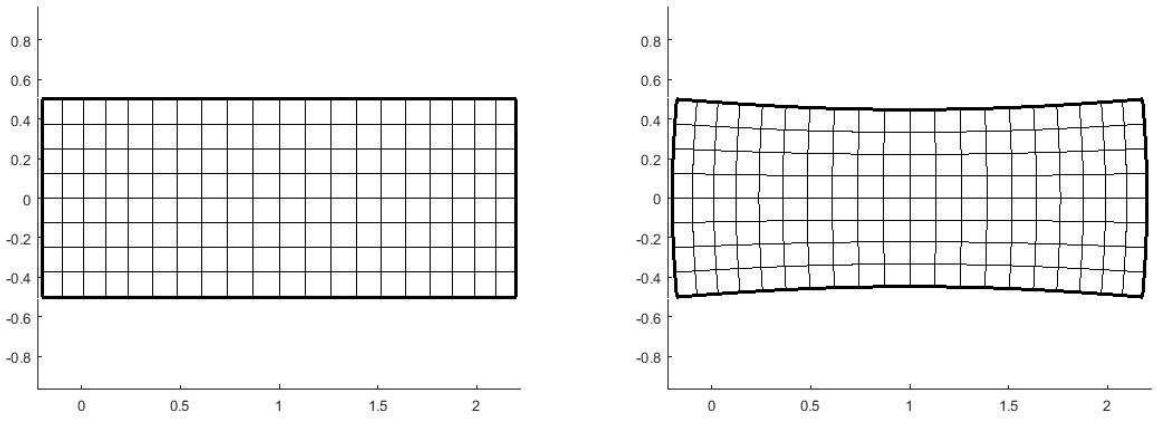

a/h=2 with ν=0 a/h=2 with ν=0.3

Figure 6: Poisson effects of simply supported beams in axial motion for Mode 1

3.1.4 Mode Shapes

For a non-zero Poisson ratio of $\nu = 0.3$ and fixed length-to-thickness ratio of 10, the first nine mode shapes for the simply-supported beam are illustrated in Figure 7. As layers are discreted in the thickness direction, beams are easier bended within xz plane. Bending mode shapes are repeated in xz and yz planes. Here, only show bending deflection in the transverse direction. The lengths are frequently exaggerated in these plots because of the scale factors used to visualized the modes.

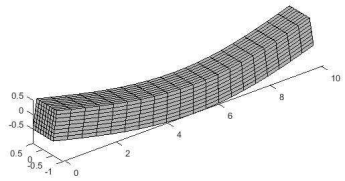

Mode 1: 1st bending

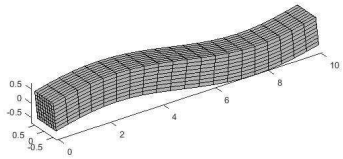

Mode 2: 2nd bending

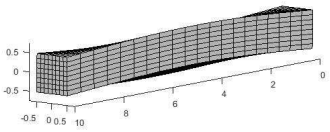

Mode 3: 1st torsional

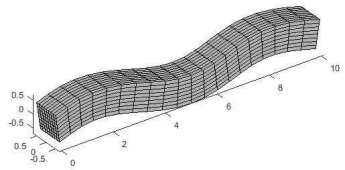

Mode 4: 3rd bending

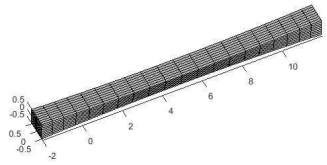

Mode 5: 1st axial

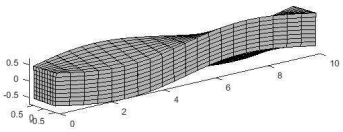

Mode 6: 2nd torsional

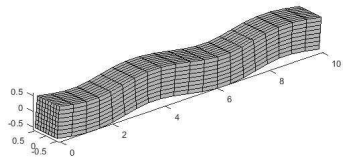

Mode 7: 4th bending

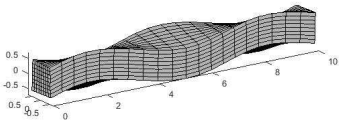

Mode 8: 3rd torsional

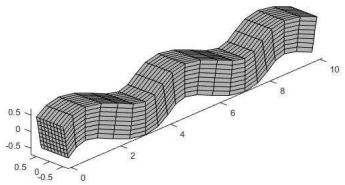

Mode 9: 4th bending

Figure 7: First nine mode shapes of simply supported beams

3.1.5 Slenderness

The first eleven nondimensional frequencies of simply supported beams composed of this isotropic materials are plotted as a function of a/h ratio in Figure 8. Frequencies are normalized by $\Omega = \bar{\omega}a^2\sqrt{\rho h/C_{max}}$, where C_{max} is the maximum value in the stiffness matrix (C_{ij}). The full curved lines represent the transverse bending modes. The curved lines represent the in-plane bending modes, and the torsional or axial mode shapes are displayed by straight dashed lines. The capital letters near lines are abbreviations of the corresponding

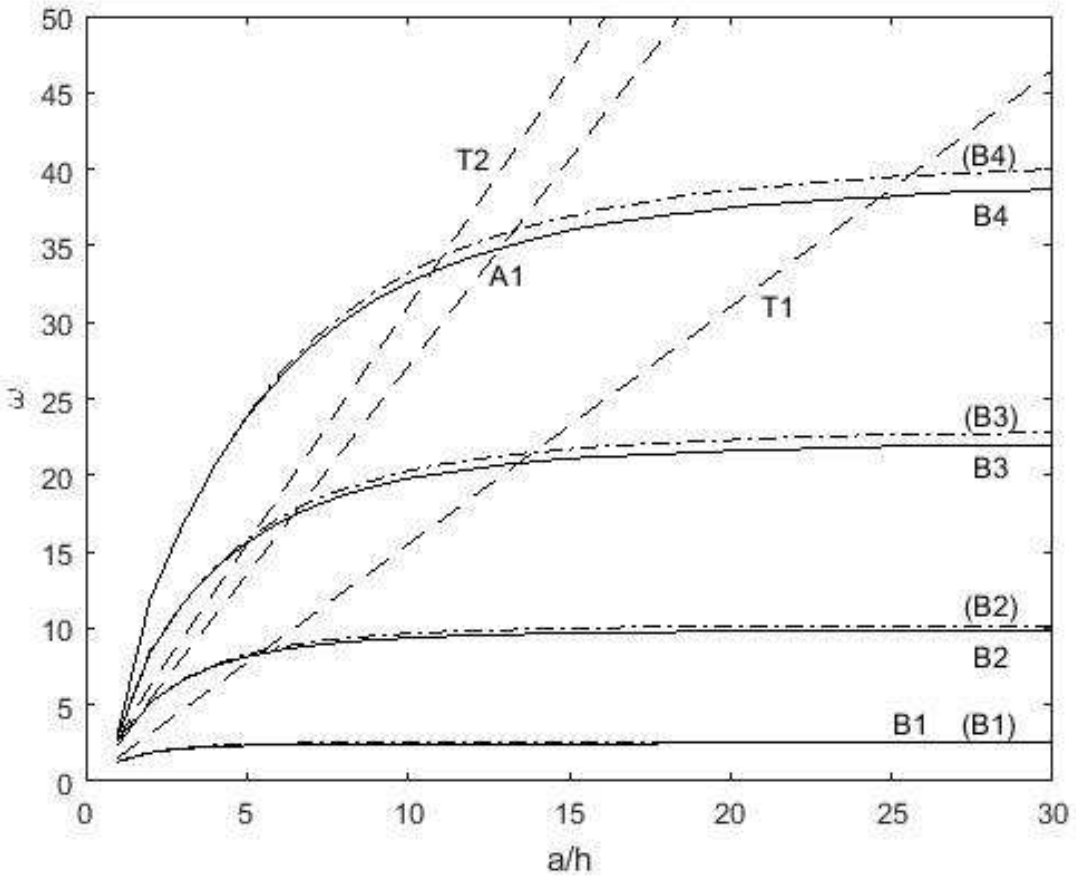

Figure 8: The first eleven frequencies for simply supported beams with $\nu = 0.3$ as a function of a/h ratio

mode type: B= bending, A= axial, and T= torsional. The labels given in the bracket indicate the in-plane bending modes. The nature of the mode was identified by monitoring the motion of the vertical straight lines perpendicular the x axis. The label in the figure shows the corresponding mode shapes as a/h ratio is equal to 10 in sequence. One special case needs to be mentioned. At the intersection of two lines of different mode types, two mode patterns can occur together. Hence the freqencies are the same but the modal response is of a different type.

3.2 Free Vibrations of Fixed-fixed Isotropic Beams

3.2.1 Frequency Comparion with EB/ Axial/ Torsion Theory

As in the case of simply supported beams, the out-of-plane terms are eliminated to test the convergence of the DL model for the fixed-fixed case. The dimensionless frequencies of fixed-fixed beams at ratio of a/h=20 and a/h=10 are shown in Tables 8 and 9. With higher values of approximation in x, the convergence is apparent for this boundary condition. Results from the DL model are close to the classical EB and bar results for zero Poisson ratio but the differences are again higher when this value is non-zero. From Table 10, there is little difference in frequency as the number of layers increases beyond 8.

Table 8: Dimensionless frequencies of fixed-fixed beams(a/h=20) with 8 layers

Isotropic materials	Terms in x	DL Model			
		1st bending	2nd bending	3rd bending	1st axial
Terms ($\nu = 0$)	1	0.1581	———	———	0.2236
	2	8.8256e-2	0.2957	———	0.2236
	3	2.2615e-2	0.1921	0.4583	0.2221
	4	2.2599e-2	6.2247e-2	0.3268	0.2221
	5	2.2537e-2	6.2028e-2	0.1230	0.2221
	6	2.2536e-2	6.1088e-2	0.1218	0.2221
Terms ($\nu = 0.3$)	1	0.1581	———	———	0.2958
	2	8.9394e-2	0.2958	———	0.2761
	3	2.7894e-2	0.1953	0.4587	0.2703
	4	2.7790e-2	7.6207e-2	0.3331	0.2681
	5	2.7233e-2	7.5446e-2	0.1494	0.2679
	6	2.7214e-2	7.3141e-2	0.1464	0.2671
EB/Bar		2.2834e-2	6.2944e-2	0.1234	0.2221

Table 9: Dimensionless frequencies of fixed-fixed beams(a/h=10) with 8 layers

Isotropic materials	Terms in x	DL Model			
		1st bending	2nd bending	3rd bending	1st axial
Terms ($\nu = 0$)	1	0.3162	———	———	0.4472
	2	0.1853	0.5909	———	0.4472
	3	8.7170e-2	0.4083	0.9165	0.4443
	4	8.7003e-2	0.2293	0.6974	0.4443
	5	8.6858e-2	0.2276	0.4289	0.4443
	6	8.6842e-2	0.2256	0.4217	0.4443
Terms ($\nu = 0.3$)	1	0.3162	———	———	0.5916
	2	0.1927	0.5914	———	0.5523
	3	0.1059	0.4254	0.9196	0.5405
	4	0.1050	0.2725	0.7258	0.5364
	5	0.1036	0.2679	0.4987	0.5358
	6	0.1035	0.2639	0.4857	0.5346
EB/Bar		9.1337e-2	0.2518	0.4936	0.4442

Table 10: Dimensionless frequencies of discrete isotropic beams under fixed-fixed condition(a/h=20) with five axial terms and $\nu = 0$

Layers	DL Model			
	1st bending	2nd bending	3rd bending	1st axial
1	2.2575e-2	6.2306e-2	0.1238	0.2221
2	2.2575e-2	6.2306e-2	0.1238	0.2221
4	2.2546e-2	6.2094e-2	0.1231	0.2221
8	2.2537e-2	6.2028e-2	0.1230	0.2221
16	2.2535e-2	6.2011e-2	0.1229	0.2221
32	2.2534e-2	6.2006e-2	0.1229	0.2221

3.2.2 Influence of a/h

From Figures 9-10, it is clear that the frequency reduction for fixed-fixed beams is larger than those under the simply supported condition at lower a/h ratios for the DL model compared to the simply-supported condition. The fundamental frequency from the classical result is nearly 10 percent different when a/h is less than 6. Additionally, the non-zero Poisson ratio gives a much higher axial frequency for small length-to-thickness ratios. This is likely because of the additional end restraint.

3.2.3 Mode Shapes

The lateral views of the first nine modes of the fixed-fixed beam are shown in Figure 11. The mode types are similar to those of the beam under simply supported conditions.

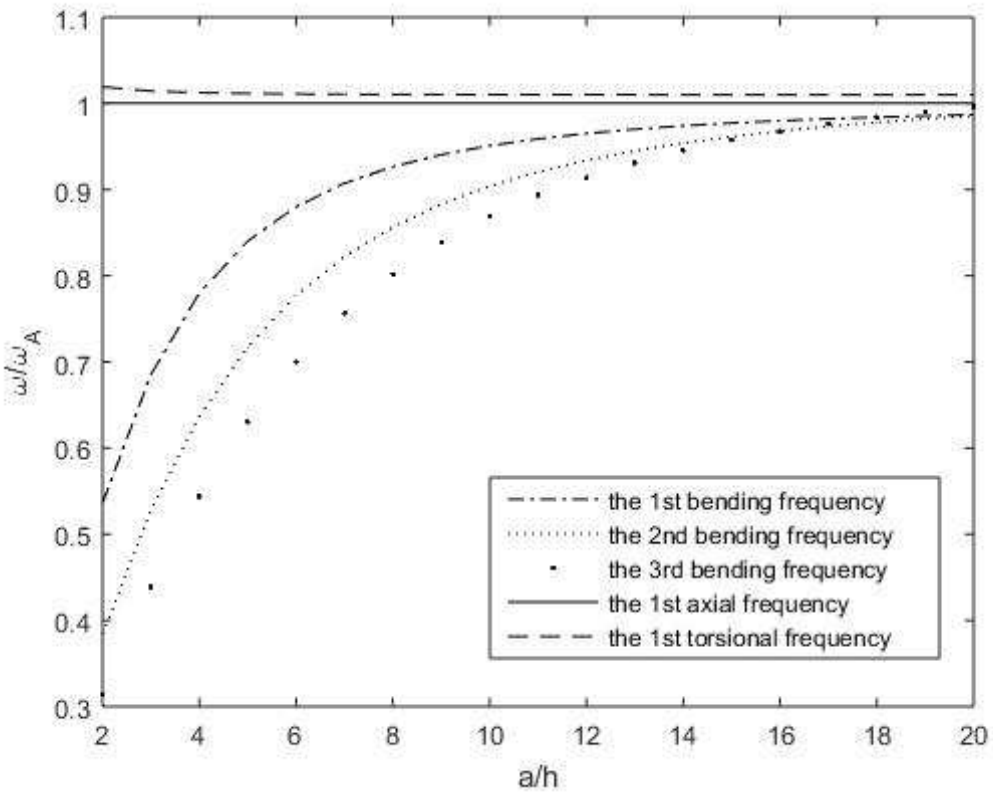

Figure 9: Differences between the DL model and the analytical values with $\nu = 0$ as a function of a/h ratio

Table 11: Ratios between the DL model and the analytical values with $\nu = 0$

a/h	1	2	3	4	5	6	7	8	9	10
1	0.3087	0.5358	0.6852	0.7797	0.8403	0.8802	0.9074	0.9266	0.9405	0.9510
2	0.1945	0.3833	0.5281	0.6367	0.7172	0.7771	0.8222	0.8565	0.8830	0.9039
3	0.1683	0.3140	0.4390	0.5439	0.6301	0.6999	0.7563	0.8018	0.8388	0.8689
4	1.0002	1.0002	1.0002	1.0002	1.0002	1.0002	1.0002	1.0002	1.0002	1.0002
5	1.0346	1.0192	1.0144	1.0125	1.0115	1.0110	1.0107	1.0105	1.0103	1.0102
a/h	11	12	13	14	15	16	17	18	19	20
1	0.9589	0.9651	0.9700	0.9740	0.9772	0.9799	0.9821	0.9840	0.9856	0.9870
2	0.9205	0.9339	0.9449	0.9540	0.9615	0.9679	0.9733	0.9780	0.9820	0.9854
3	0.8936	0.9140	0.9311	0.9453	0.9574	0.9677	0.9765	0.9841	0.9907	0.9964
4	1.0002	1.0002	1.0002	1.0002	1.0002	1.0002	1.0002	1.0002	1.0002	1.0002
5	1.0102	1.0101	1.0101	1.0100	1.0100	1.0100	1.0100	1.0099	1.0099	1.0099

1: the 1st bending frequency 2: the 2nd bending frequency 3: the 3rd bending frequency
4: the 1st axial frequency 5: the 1st torsional frequency

Table 12: Ratios between the DL model and the analytical values with $\nu = 0.3$

a/h	1	2	3	4	5	6	7	8	9	10
1	0.2793	0.4998	0.6566	0.7623	0.8332	0.8815	0.9152	0.9394	0.9573	0.9707
2	0.1869	0.3551	0.4957	0.6086	0.6973	0.7666	0.8208	0.8635	0.8976	0.9251
3	0.1570	0.2913	0.4091	0.5123	0.6015	0.6774	0.7414	0.7952	0.8402	0.8780
4	1.0373	1.0263	1.0224	1.0203	1.0191	1.0184	1.0180	1.0178	1.0176	1.0175
5	1.0436	1.0242	1.0175	1.0145	1.0129	1.0120	1.0114	1.0111	1.0108	1.0106
a/h	11	12	13	14	15	16	17	18	19	20
1	0.9810	0.9891	0.9956	1.0008	1.0051	1.0086	1.0116	1.0141	1.0162	1.0181
2	0.9475	0.9660	0.9814	0.9943	1.0053	1.0147	1.0228	1.0298	1.0359	1.0413
3	0.9098	0.9367	0.9595	0.9789	0.9956	1.0099	1.0223	1.0331	1.0425	1.0508
4	1.0174	1.0173	1.0173	1.0173	1.0172	1.0172	1.0172	1.0172	1.0171	1.0171
5	1.0105	1.0104	1.0103	1.0102	1.0102	1.0101	1.0101	1.0101	1.0100	1.0100

1: the 1st bending frequency 2: the 2nd bending frequency 3: the 3rd bending frequency
4: the 1st axial frequency 5: the 1st torsional frequency

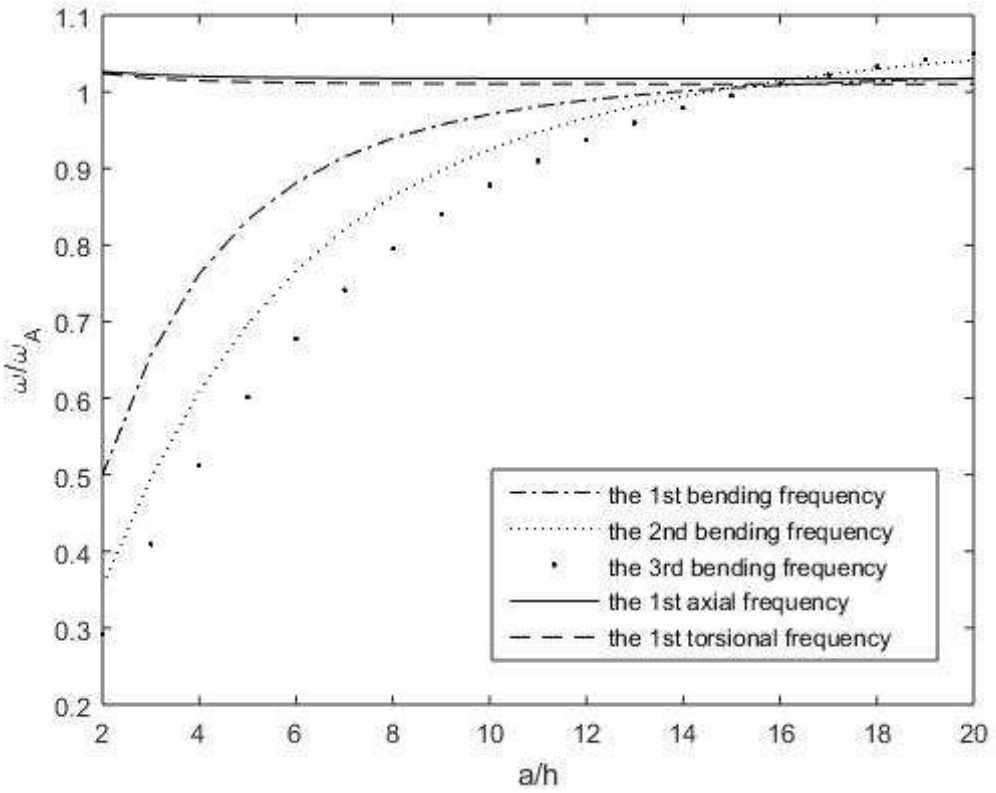

Figure 10: Differences between the DL model and the analytical values with $\nu = 0.3$ as a function of a/h ratio

3.2.4 Slenderness

Figure 12 illustrates the influence of a/h for first eleven dimensionless frequencies for isotropic beams under fixed-fixed conditions. Same notation as the previous condition. The full curved lines indicate the transverse bending modes. The curved dash lines represent the in-plane bending modes. Since only polynomials are used in y direction, the beams are kinematically stiffer deformed in the xy plane. Also, due to different approximation terms used in the x and y directions, the bending modes are quite different for the higher frequencies. Under this condition, more axial and torsional mode shapes appear between each of the bending modes. Compared with the simply supported condition, axial and torsional

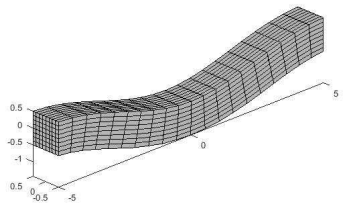

Mode 1: 1st bending

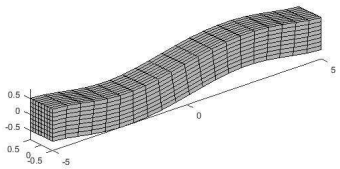

Mode 2: 2nd bending

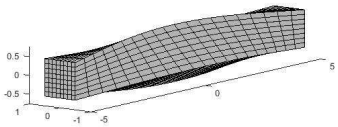

Mode 3: 1st torsional

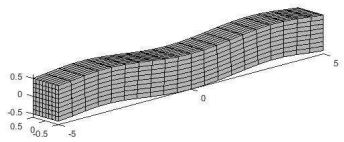

Mode 4: 3rd bending

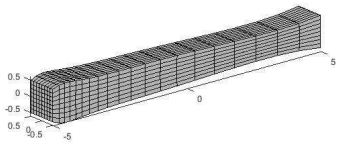

Mode 5: 1st axial

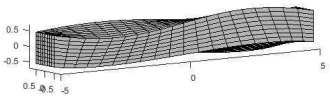

Mode 6: 2nd torsional

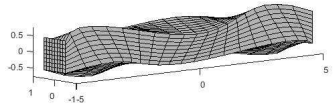

Mode 7: 3rd torsional

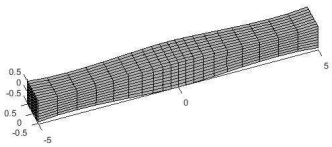

Mode 8: 2nd axial

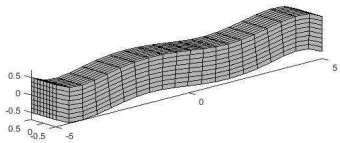

Mode 9: 4th bending

Figure 11: First nine mode shapes of fixed-fixed beams

modes change sides for higher frequencies under this boundary condition.

3.3 Free vibrations of Cantilever Isotropic Beams

3.3.1 Frequency Comparsion with EB/ Axial/ Torsion Theory

The natural frequencies at the ratio of a/h=20 and a/h=10 for the two different isotropic cantilever beams are shown in Tables 13 and 14. Due to the small number of degrees of freedom, some frequencies do not appear for small numbers of terms in the approximation. From the tables, as the number of terms is increased, the better convergence

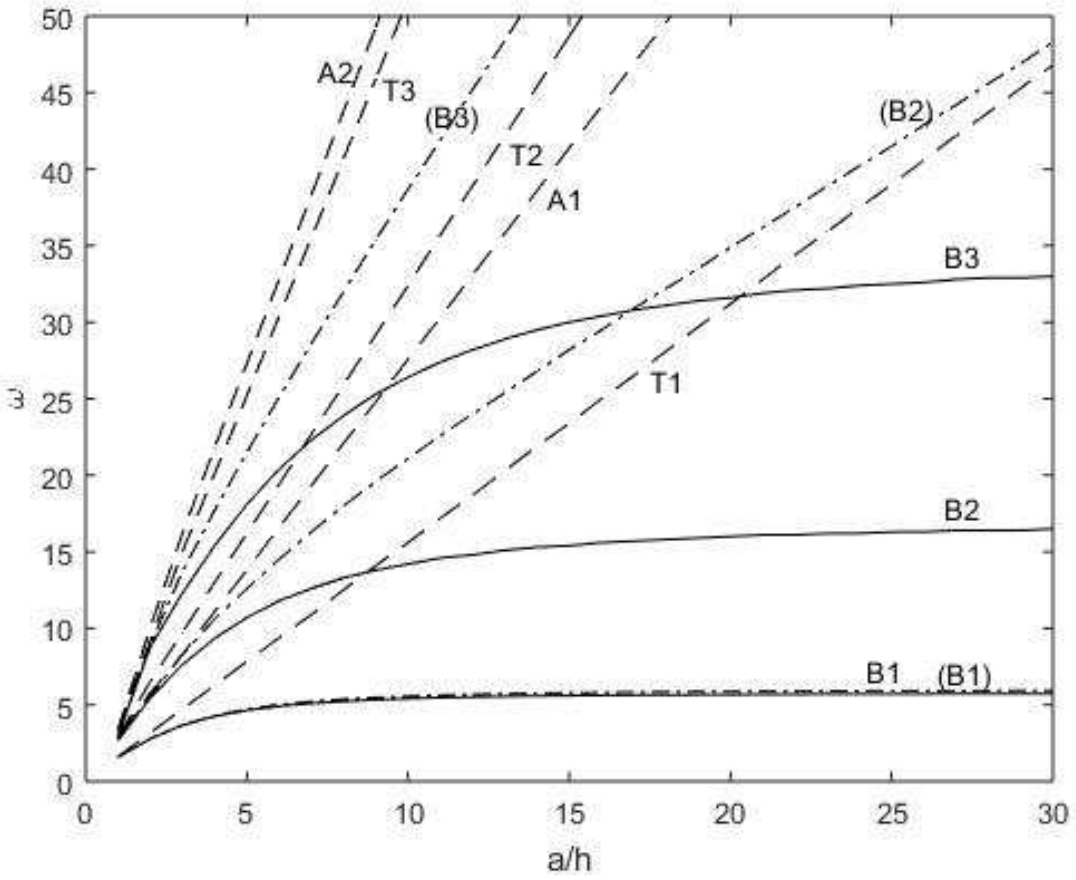

Figure 12: The first eleven frequencies for fixed-fixed beams with $\nu = 0.3$ as a function of a/h ratio

appears to be obtained.

3.3.2 Influence of a/h

Figures 13 and 14 represent frequencies as a function of the a/h ratio. Similar tendencies are achieved as for the fixed-fixed beams, except that the precent reduction for this condition is much smaller than that under the fixed-fixed case. For example, a 10 percent reduction for the fundamental frequency occurs when the length-to-thickness ratio is nearly 3, which is the half length of beams under that condition for fixed-fixed beams. Additionally, the torsional frequency is consistantly 4 percent higher than the analytical values. This is

Table 13: Dimensionless frequencies of cantilever beams(a/h=20) with 8 layers

Isotropic materials	Terms in x	DL Model			
		1st bending	2nd bending	3rd bending	1st axial
Terms ($\nu = 0$)	1	4.3372e-3	———	———	0.1225
	2	4.5247e-3	0.1167	———	0.1115
	3	3.5988e-3	3.3951e-2	0.2240	0.1111
	4	3.5837e-3	2.2430e-2	0.1084	0.1111
	5	3.5827e-3	2.2340e-2	6.2845e-2	0.1111
Terms ($\nu = 0.3$)	1	4.3413e-3	———	———	0.1504
	2	5.4700e-3	0.1173	———	0.1376
	3	4.4078e-3	4.0227e-2	0.2276	0.1345
	4	4.3633e-3	2.7265e-2	0.1260	0.1338
	5	4.3355e-3	2.7026e-2	7.6099e-2	0.1335
EB/Bar		3.5885e-3	2.2489e-2	6.2968e-2	0.1111

most likely because of warping restraint at the fixed end.

3.3.3 Mode Shapes

For an a/h ratio of 10, the first nine mode shapes are plotted in Figure 15.

3.3.4 Slenderness

Figure 16 demonstrates the lowest frequencies for cantilever beams as a function of a/h. The trends are similar to those for the fixed-fixed beams. However, the angles between the lines representing the torsional and axial modes are more uniformly distributed for this condition. The sequence of these two modes appear alternatively.

Table 14: Dimensionless frequencies of cantilever beams(a/h=10) with 8 layers

Isotropic materials	Terms in x	DL Model			
		1st bending	2nd bending	3rd bending	1st axial
Terms ($\nu = 0$)	1	8.7165e-2	———	———	0.2449
	2	1.7676e-2	0.2401	———	0.2230
	3	1.4318e-2	0.1219	0.4841	0.2221
	4	1.4265e-2	8.6821e-2	0.3490	0.2221
	5	1.4262e-2	8.6422e-2	0.2340	0.2221
	6	1.4269e-2	8.6189e-2	0.2316	0.2221
Terms ($\nu = 0.3$)	1	8.7490e-2	———	———	0.3008
	2	2.1253e-2	0.2446	———	0.2751
	3	1.7517e-2	0.1411	0.5044	0.2690
	4	1.7331e-2	0.1046	0.3915	0.2676
	5	1.7232e-2	0.1034	0.2775	0.2670
	6	1.7181e-2	0.1027	0.2727	0.2667
EB/Bar		1.4354e-2	8.9956e-2	0.2519	0.2221

Table 15: Dimensionless frequencies of discrete isotropic beams under fixed-free condition(a/h=20) with five axial terms and $\nu = 0$

Layers	DL Model			
	1st bending	2nd bending	3rd bending	1st axial
1	3.5833e-3	2.2371e-2	6.3065e-2	0.1111
2	3.5833e-3	2.2371e-2	6.3065e-2	0.1111
4	3.5829e-3	2.2347e-2	6.2936e-2	0.1111
8	3.5827e-3	2.2340e-2	6.2845e-2	0.1111
32	3.5363e-3	2.2060e-2	6.2032e-2	0.1107

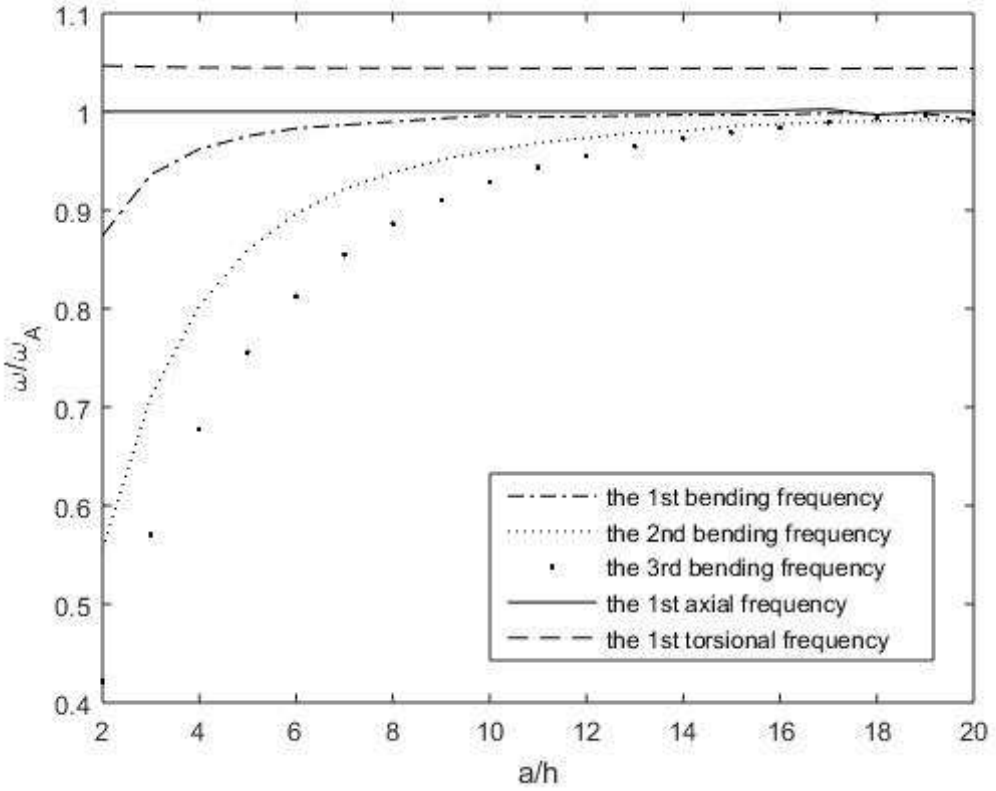

Figure 13: Differences between the DL model and the analytical values with $\nu = 0$ as a function of a/h ratio

Table 16: Ratios between the DL model and the analytical values with $\nu = 0$

a/h	1	2	3	4	5	6	7	8	9	10
1	0.6830	0.8741	0.9363	0.9620	0.9753	0.9831	0.9865	0.9898	0.9932	0.9962
2	0.2973	0.5555	0.7108	0.8030	0.8599	0.8966	0.9213	0.9387	0.9513	0.9605
3	0.1925	0.4215	0.5704	0.6779	0.7558	0.8127	0.8547	0.8862	0.9103	0.9289
4	1.0002	1.0002	1.0002	1.0002	1.0002	1.0002	1.0002	1.0002	1.0002	1.0002
5	1.0501	1.0468	1.0456	1.0450	1.0447	1.0445	1.0444	1.0444	1.0443	1.0443
a/h	11	12	13	14	15	16	17	18	19	20
1	0.9947	0.9952	0.9961	0.9968	0.9969	0.9970	0.9986	0.9977	0.9982	0.9911
2	0.9685	0.9733	0.9788	0.9805	0.9855	0.9875	0.9895	0.9905	0.9921	0.9893
3	0.9436	0.9553	0.9648	0.9726	0.9790	0.9839	0.9891	0.9931	0.9960	0.9978
4	1.0002	1.0002	1.0002	1.0002	1.0002	1.0013	1.0027	0.9968	1.0002	1.0002
5	1.0442	1.0442	1.0442	1.0442	1.0442	1.0443	1.0437	1.0440	1.0441	1.0441

1: the 1st bending frequency 2: the 2nd bending frequency 3: the 3rd bending frequency
4: the 1st axial frequency 5: the 1st torsional frequency

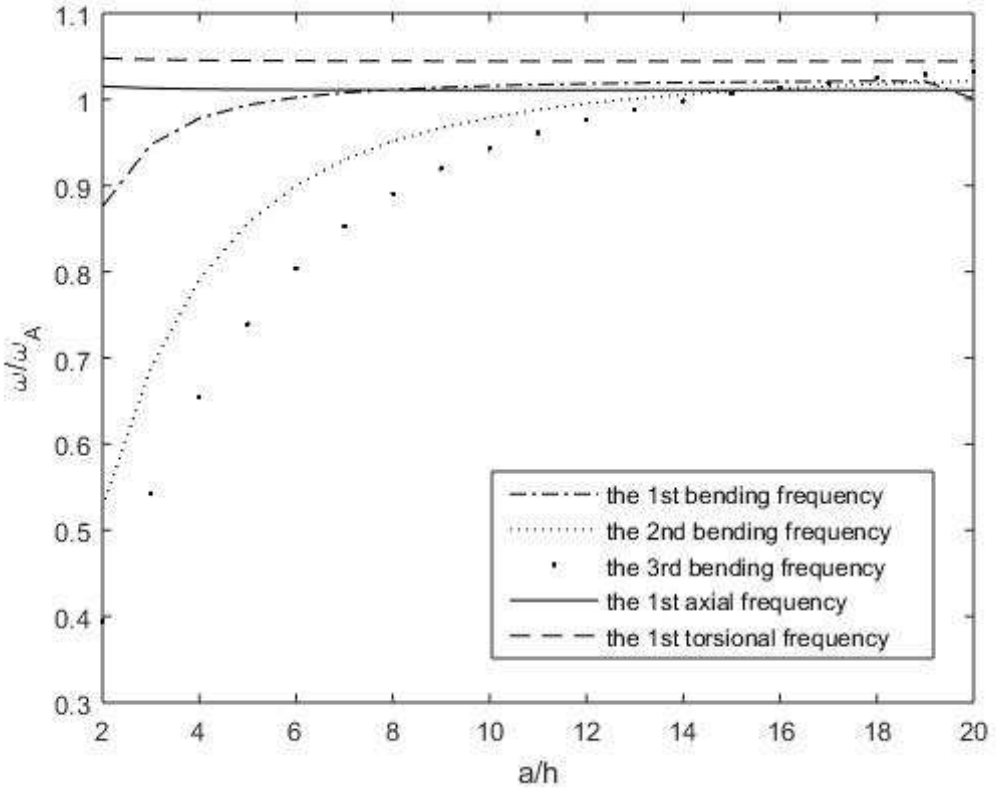

Figure 14: Differences between the DL model and the analytical values with $\nu = 0.3$ as a function of a/h ratio

Table 17: Ratios between the DL model and the analytical values with $\nu = 0.3$

a/h	1	2	3	4	5	6	7	8	9	10
1	0.6643	0.8758	0.9475	0.9781	0.9935	1.0023	1.0078	1.0114	1.0139	1.0157
2	0.2797	0.5268	0.6888	0.7911	0.8566	0.9001	0.9301	0.9514	0.9671	0.9789
3	0.1600	0.3944	0.5428	0.6543	0.7391	0.8035	0.8527	0.8904	0.9198	0.9430
4	1.0207	1.0152	1.0129	1.0120	1.0115	1.0112	1.0111	1.0109	1.0109	1.0108
5	1.0524	1.0479	1.0463	1.0455	1.0451	1.0448	1.0446	1.0445	1.0444	1.0444
a/h	11	12	13	14	15	16	17	18	19	20
1	1.0171	1.0182	1.0190	1.0196	1.0202	1.0205	1.0210	1.0213	1.0210	1.0008
2	0.9880	0.9952	1.0009	1.0057	1.0095	1.0127	1.0151	1.0177	1.0195	1.0216
3	0.9614	0.9762	0.9883	0.9983	1.0066	1.0136	1.0187	1.0245	1.0289	1.0328
4	1.0108	1.0108	1.0107	1.0107	1.0107	1.0107	1.0107	1.0107	1.0107	1.0107
5	1.0443	1.0443	1.0443	1.0443	1.0442	1.0442	1.0442	1.0442	1.0442	1.0442

1: the 1st bending frequency 2: the 2nd bending frequency 3: the 3rd bending frequency
4: the 1st axial frequency 5: the 1st torsional frequency

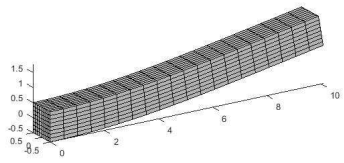

Mode 1: 1st bending

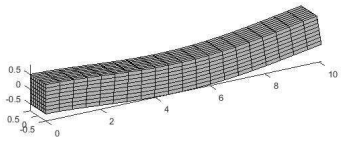

Mode 2: 2nd bending

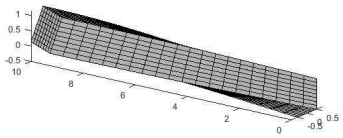

Mode 3: 1st torsional

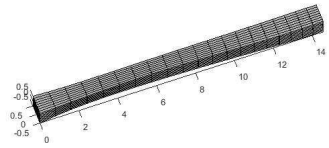

Mode 4: 1st axial

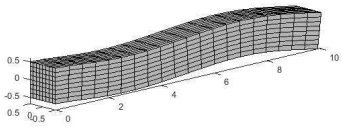

Mode 5: 3rd bending

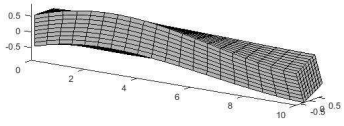

Mode 6: 2nd torsional

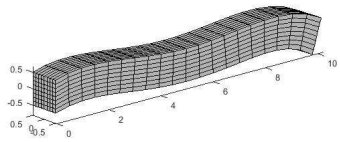

Mode 7: 4th bending

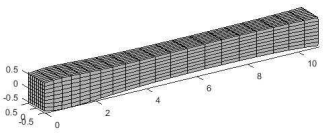

Mode 8: 2nd axial

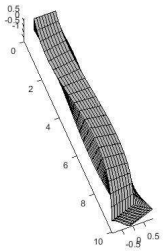

Mode 9: 3rd torsional

Figure 15: First nine mode shapes of cantilever beams

3.4 Characteristics of Isotropic Beams

By examining behaviors of free vibration of isotropic beams under three basic boundary conditions using the DL model, results are useful and can also be used as a reference for the studying of sandwiched MEE plates. Hence, a brief summary of isotropic beams is presented as following:

1. Because of Poisson end effects, using results calculated by the classical beam theories causes relatively large differences for the bending and axial frequencies with small

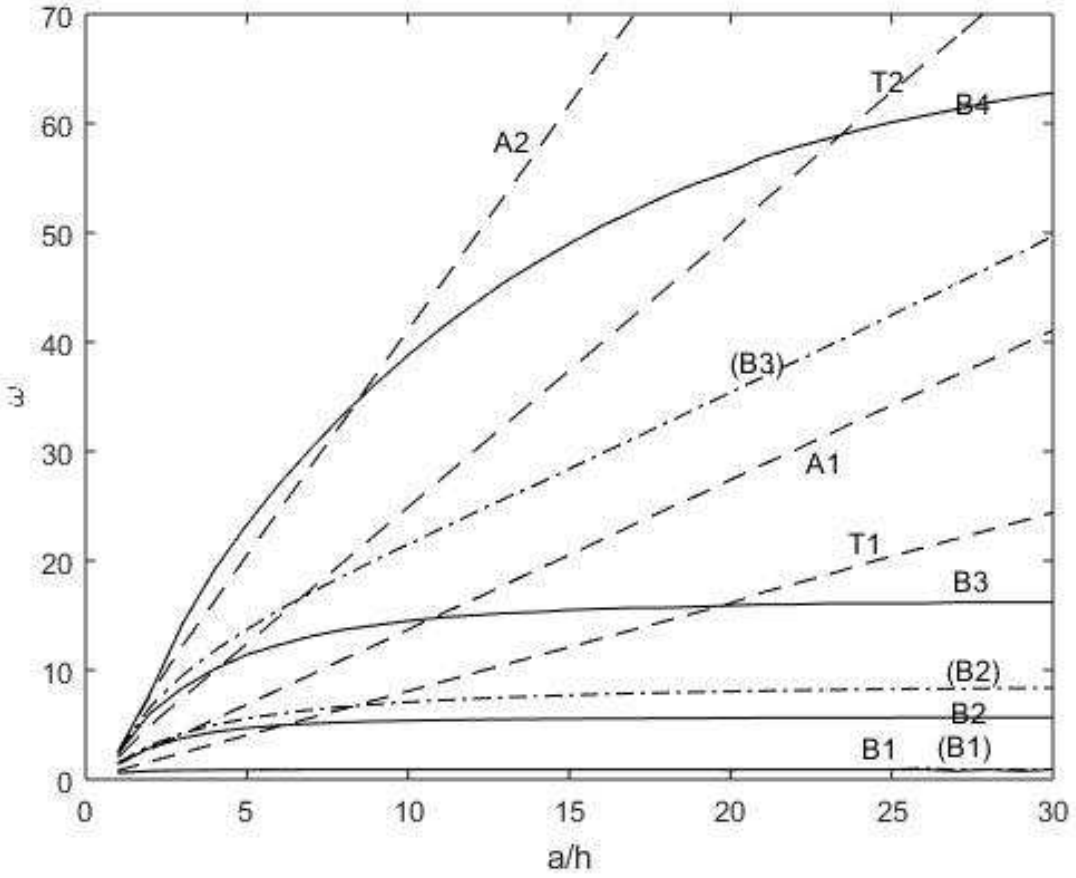

Figure 16: The first eleven frequencies for cantilever beams with $\nu = 0.3$ as a function of a/h ratio

length-to-thickness ratios.

2. Due to te end restriction, the non-zero Poisson ratio gives higher axial frequencies for small slenderness ratios under fixed-fixed and fixed-free conditions.

3. When frequencies are calculated by $\bar{\omega} = \omega a\sqrt{\rho_{max}/C_{max}}$ and plotted with equation $\Omega = \bar{\omega}a^2\sqrt{\rho h/C_{max}}$, the configurations of bending frequencies as a function of a/h ratio are demonstrated as curved lines, while the lines of axial and torsional frequencies are straight. The intersections of two lines indicate the occurance of coupled mode shapes.

CHAPTER 4 COMPOSITE MEE BEAMS

Using regularities found in isotropic beams detect frequencies as a function of slenderness of composite MEE beams under the similar boundary conditions. The following section contains results for hexagonal and MEE composite beams. Four stacking sequences of MEE beams are considered here: BBB, FFF, BFB and FBF, where B stands for $BaTiO_3$ and F stands for $CoFe_2O_4$ material. Properties of these materials are listed in Appendix B.

4.1 Characteristics of Composite MEE Beams

Composite beams frequently possess discontinuity of gradients of the displacements through the thickness direction. An example of this is shown in Figure 17. This plot represents the normalized u displacement component across the thickness of the beam with a/h=2 and b=h=0.3 at the corner for the fundamental mode under simply supported condition. The beam is made of BGB materials, where G stands for the Graphite-polymer materials. Properties of G material are listed in Table 18. The dashed lines represent the intersurface between each layers. Kinks in the curves are caused by the linear approximate function in z direction.

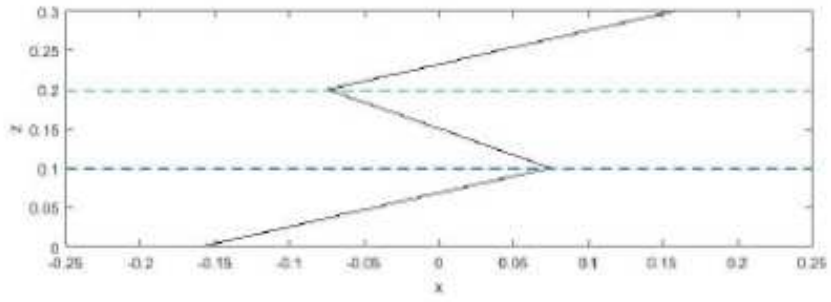

x	z
-0.1590	0
0.0747	0.1
-0.0747	0.2
0.1590	0.3

Figure 17: Through-thickness modal distribution of u at corner of bimaterial

Table 18: Properties of Graphite-polymer materials

material coefficients of Graphite-polymer materials					
E_1	$12.1(10^9)$ Pa	ν_{23}	0.248	G_{23}	$4.4(10^9)$ Pa
E_2	$155.0(10^9)$ Pa	ν_{13}	0.458	G_{13}	$3.2(10^9)$ Pa
E_3	$12.1(10^9)$ Pa	ν_{21}	0.248	G_{12}	$4.4(10^9)$ Pa

The dimensions of the cross section are b=h=0.3. The frequencies are calculated according to the dimensionless parameter $\bar{\omega} = \omega h\sqrt{\rho_{max}/C_{max}}$ and plotted by $\Omega = \bar{\omega}a^2\sqrt{\rho_{max}h/C_{max}}$. Here, ρ_{max} and C_{max} are the maximum values within beams of the densities and elastic stiffness tensor components.

4.2 Simply Supported Condition

The DL model gives good convergence for isotropic beams with lower terms. Hence, 12 layers and 3 terms in x and y are used in this case.

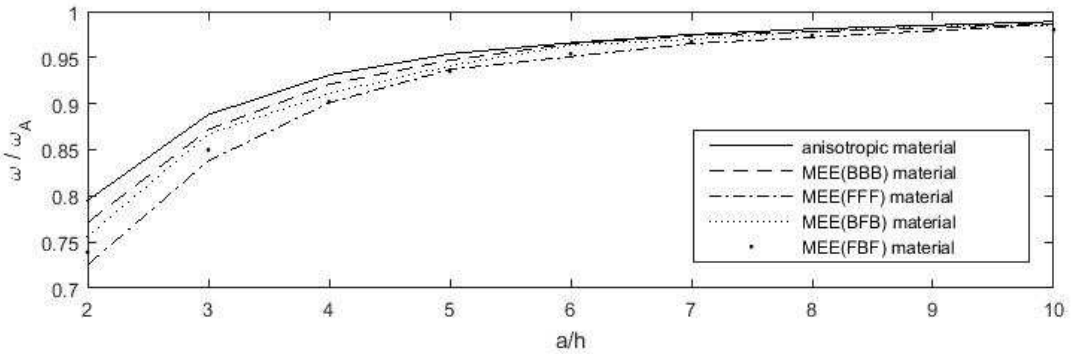

Figure 18: Differences of the fundamental frequency with five stacking sequences under simply supported conditions

The fundamental frequency variation with thickness ratio for five different material combinations is shown in Figure 18. ω_A is taken as the value at a/h=30 with respect to each stacking. From Figure 18, the differences between beams are quite small for the first bending frequency.

Figures 19-23 illustrate the influence of slenderness for the first eleven frequencies for the five stacking sequences. The same notation is used as for the simply supported beams composed of isotropic materials. The horizontal dashed lines give the a/h=30 value of each transverse bending mode to show the influence of slenderness.

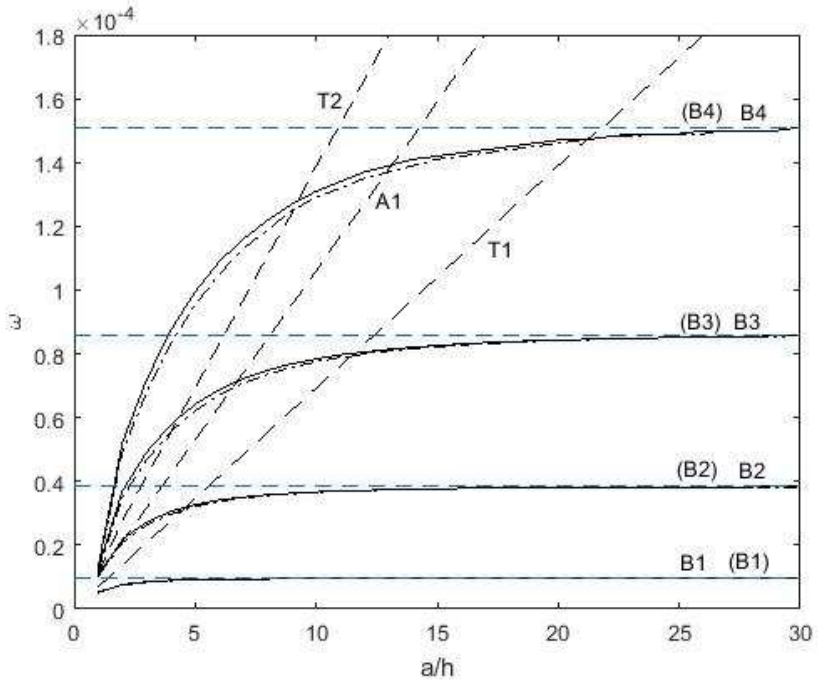

Figure 19: The influence of slenderness for the first eleven frequencies for beams with anisotropic materials under simply supported conditions

Frequencies for the other beams are shown through Figure 26-29. The anisotropic beams are controlled by in-plane bending modes at lower a/h ratios. This trait is especially obvious for higher frequencies. With the increasing length over thickness ratios, the in-plane bending and the corresponding transverse bending frequencies are nearly identical. This is because of the trigonometic function used in the K matrix which is shown in the appendix. As the length increases, the length square is in the denominator. After integration those terms become small. Then when the frequencies are computed, the same number nearly gets.

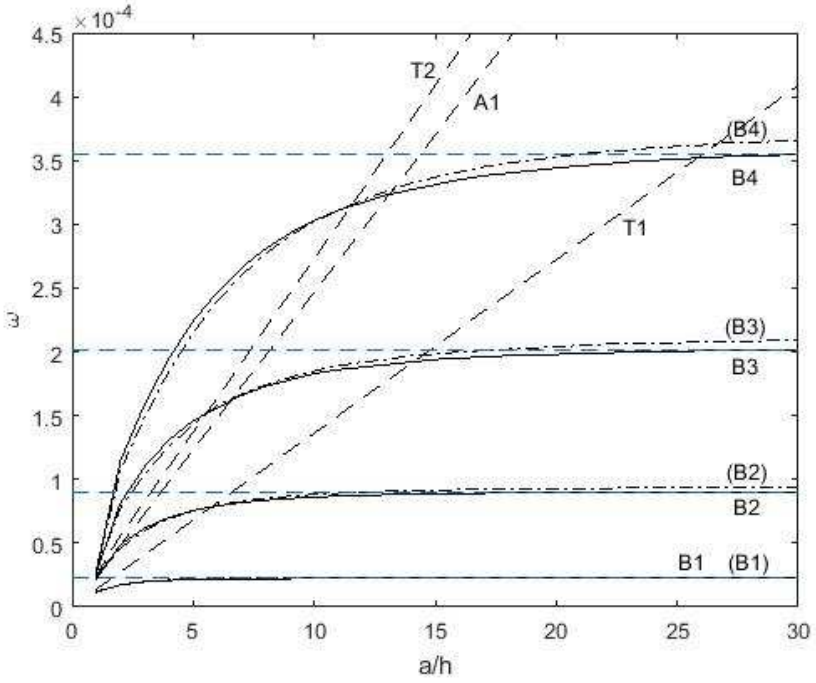

Figure 20: The influence of slenderness for the first eleven frequencies for beams with BBB materials under simply supported conditions

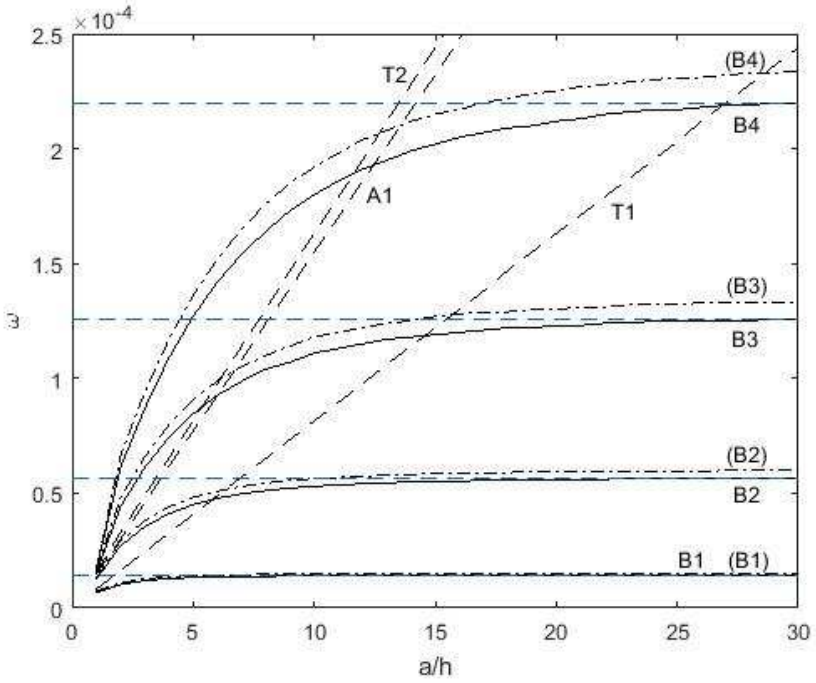

Figure 21: The influence of slenderness for the first eleven frequencies for beams with FFF materials under simply supported conditions

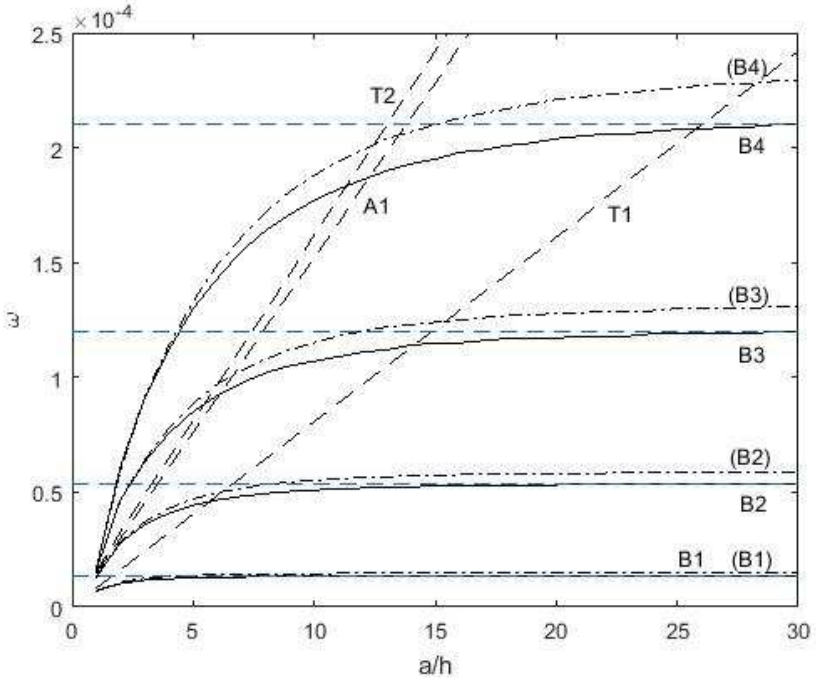

Figure 22: The influence of slenderness for the first eleven frequencies for beams with BFB materials under simply supported conditions

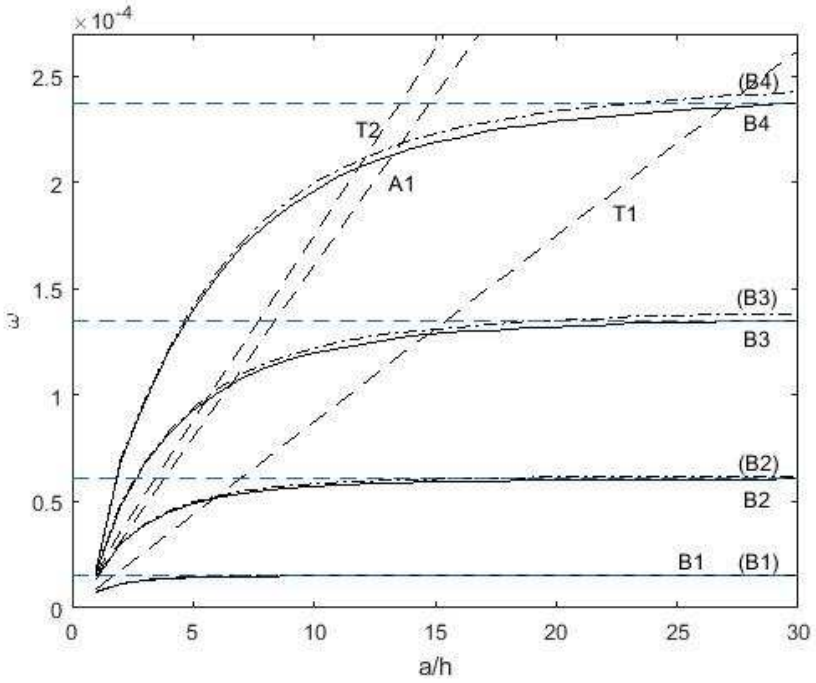

Figure 23: The influence of slenderness for the first eleven frequencies for beams with FBF materials under simply supported conditions

For MEE composite beams, it is shown that with large slenderness, beams are easily bended in the transverse direction. This phenomenon is especially clear as increasing the component of F material, even for lower a/h ratios. The differences between in-plane and transverse bending frequencies increase with slenderness ratio.

Tables 19 and 20 list the first eleven frequencies according to each stacking sequences at a/h ratio of 10 and 20. And Table 21 gives the bending frequency for the first four modes.

Results for all beams with a/h=10 and a/h=20 are listed in Table 22. Due to the asymptote chosen as a/h=30, percent differences shown here are slightly lower than the actual results for higher bending frequencies, such as the 4th bending frequency. An incremental increase of F material, reductions tread higher under this lateral boundary condition. As the amount of F material increases, the reductions also increase. For example, at a/h=10, for the 3rd bending frequency, 11.9(FFF)>11.11(FBF)>10.83(BFB)>9.41(BBB).

Table 19: Frequencies for simply supported beams composed of five stacking sequences at a/h=10

Mode	Hex	BBB	FFF	BFB	FBF
1	9.51E-6	2.24E-5	1.40E-5	1.33E-5	1.50E-5
2	9.52E-6	2.32E-5	1.48E-5	1.45E-5	1.54E-5
3	3.66E-5	8.61E-5	5.30E-5	5.09E-5	5.72E-5
4	3.67E-5	8.82E-5	5.63E-5	5.52E-5	5.84E-5
5	6.93E-5	1.36E-4	8.14E-5	8.07E-5	8.75E-5
6	7.75E-5	1.83E-4	1.11E-4	1.07E-4	1.20E-4
7	7.84E-5	1.85E-4	1.18E-4	1.15E-4	1.22E-4
8	1.06E-4	2.47E-4	1.55E-4	1.52E-4	1.61E-4
9	1.29E-4	2.73E-4	1.63E-4	1.62E-4	1.75E-4
10	1.31E-4	3.02E-4	1.80E-4	1.77E-4	1.96E-4
11	1.39E-4	3.03E-4	1.92E-4	1.88E-4	2.00E-4

Table 20: Frequencies for simply supported beams composed of five stacking sequences at a/h=20

Mode	Hex	BBB	FFF	BFB	FBF
1	9.60E-6	2.27E-5	1.42E-5	1.35E-5	1.52E-5
2	9.62E-6	2.35E-5	1.50E-5	1.47E-5	1.56E-5
3	3.80E-5	8.96E-5	5.59E-5	5.34E-5	6.01E-5
4	3.80E-5	9.29E-5	5.94E-5	5.81E-5	6.15E-5
5	1.39E-4	2.72E-4	1.63E-4	1.61E-4	1.75E-4
6	8.41E-5	1.98E-4	1.23E-4	1.17E-4	1.32E-4
7	8.43E-5	2.04E-4	1.31E-4	1.28E-4	1.35E-4
8	2.12E-4	4.94E-4	3.10E-4	3.05E-4	3.22E-4
9	1.46E-4	5.45E-4	3.26E-4	3.23E-4	3.50E-4
10	1.47E-4	3.53E-4	2.12E-4	2.04E-4	2.29E-4
11	2.77E-4	3.44E-4	2.25E-4	2.21E-4	2.34E-4

Table 21: Bending frequencies for simply supported beams composed of five stacking sequences at a/h=30

Bending Mode	Hex	BBB	FFF	BFB	FBF
1	9.62E-6	2.27E-5	1.42E-5	1.35E-5	1.53E-5
2	3.84E-5	9.04E-5	5.65E-5	5.37E-5	6.07E-5
3	8.57E-5	2.02E-4	1.26E-4	1.20E-4	1.35E-4
4	1.51E-4	3.55E-4	2.20E-4	2.10E-4	2.37E-4

This phenomenon may be caused by the influence of piezoelectric and piezomagnetic constants. From these properties, the F material is stiffer than B material in bending. Two possible conditions may cause this. First, the piezomagnetic coefficients are relatively large. This parameter represents the ability of magnetic potential energy transfer to mechanic energy which is associated with the deformation. Second, the coupling between displacements

Table 22: Differences for simply supported beams composed of five stacking sequences

a/h	Bending frequency	% Differences below a/h=30 $\bar{\omega}$				
		Hexagonal	BBB	FFF	BFB	FBF
10	1	1.14	1.32	1.41	1.48	1.96
	2	4.43	4.76	6.19	5.21	5.77
	3	8.52	9.41	11.90	10.83	11.11
	4	13.25	14.65	18.18	15.71	17.30
20	1	0.21	0.00	0.00	0.00	0.65
	2	1.04	0.77	1.06	0.93	0.99
	3	1.63	1.98	2.38	2.50	2.22
	4	2.65	3.10	3.64	2.86	3.38

caused by strain energy and magnectic field is stronger than that caused by strain energy and electric field.

4.3 Fixed-fixed Condition

As observed from the case of isotropic beams, a large number of terms are required to satisfy convergence for the fixed-fixed case. Frequencies are calculated using 12 layers and 4 axial terms. Figure 24 presents the difference of fundamental frequency as a function of a/h ratio. Compared with the simply-supported case, the differences are significantly larger.

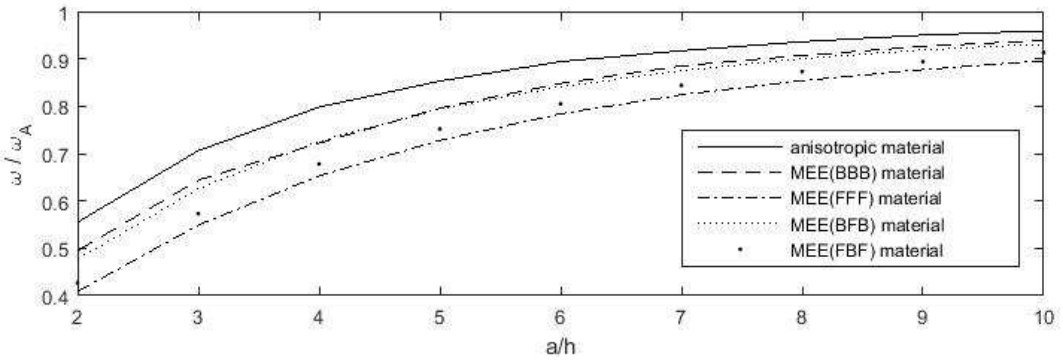

Figure 24: Differences of the fundamental frequency with five stacking sequences under fixed-fixed conditions

Figures 25-29 give the effect of a/h ratio for the first eleven frequencies under fixed-fixed conditions. For purely piezoelectric beams, the in-plane bending frequencies are slightly lower than the transverse bending frequencies. This phenomenon is more obvious for the third bending frequency in Figure 26. However, for purely piezomagnetic materials, the lines are switched.

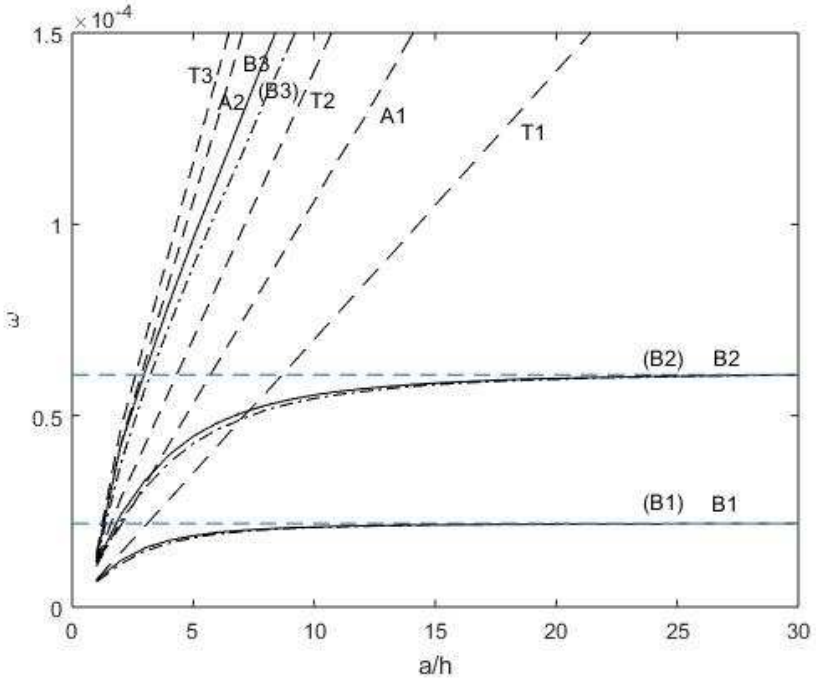

Figure 25: The influence of slenderness for the first eleven frequencies for beams with anisotropic materials under fixed-fixed conditions

Tables 23 and 24 show the first eleven frequencies for five stacking sequences at a/h ratios of 10 and 20, respectively.

Table 25 gives the values of the first three bending frequencies with length-to-thickness ratio is 30. The corresponding percent difference of the first two frequencies at slenderness of 10 and 20 respect below these values are listed in Table 26. When the a/h ratio is equal to 10, the reduction in frequency is relatively large. As the a/h ratio increases to 20, the

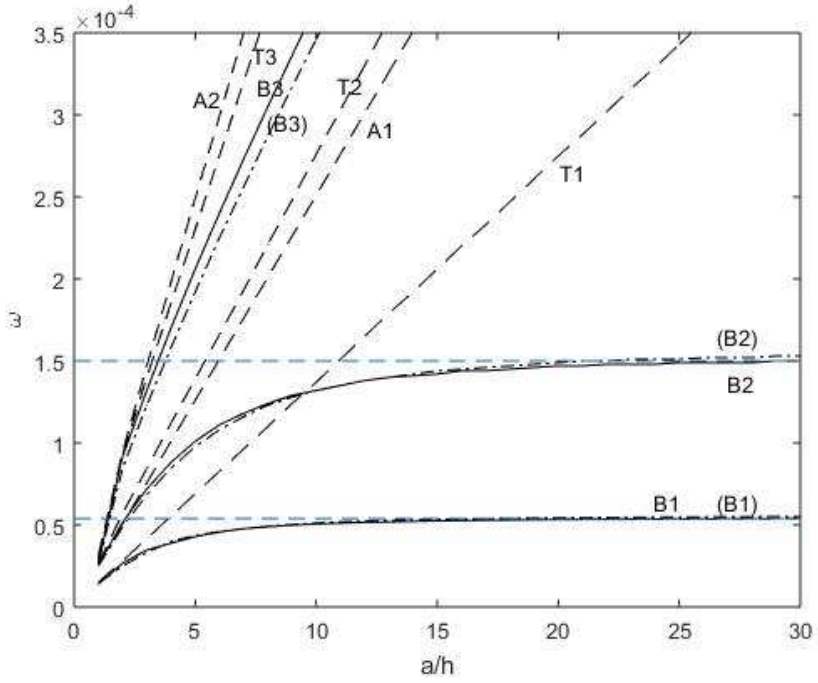

Figure 26: The influence of slenderness for the first eleven frequencies for beams with BBB materials under fixed-fixed conditions

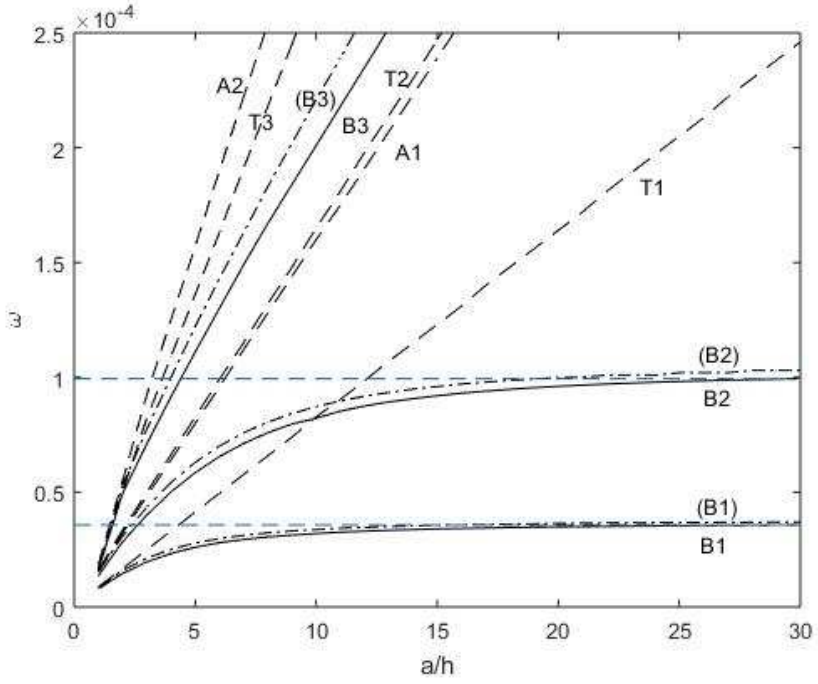

Figure 27: The influence of slenderness for the first eleven frequencies for beams with FFF materials under fixed-fixed conditions

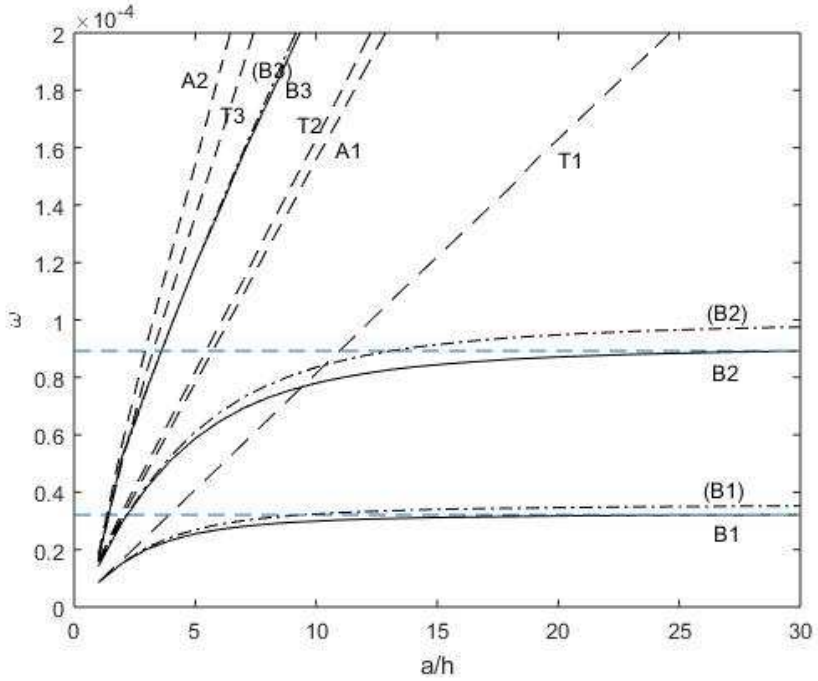

Figure 28: The influence of slenderness for the first eleven frequencies for beams with BFB materials under fixed-fixed conditions

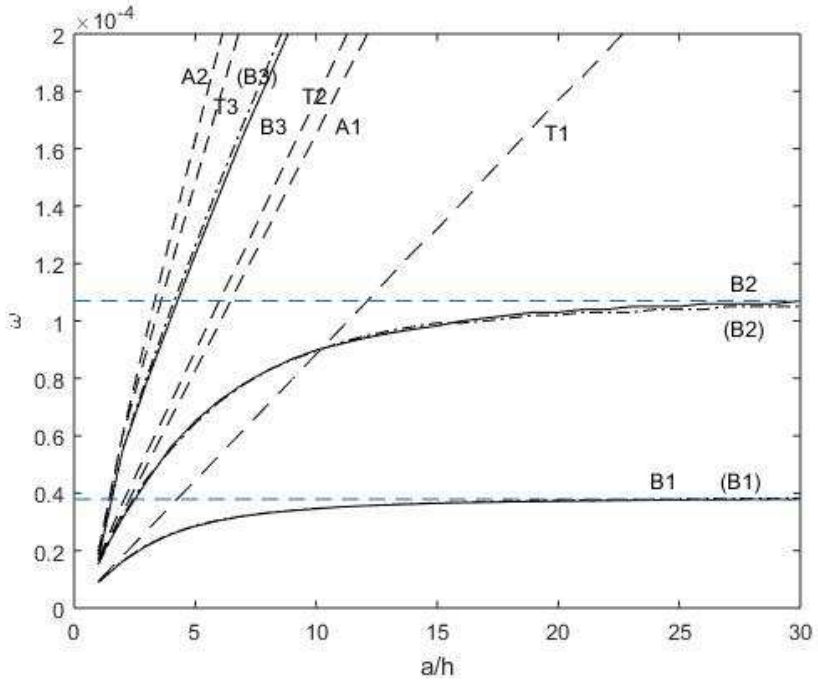

Figure 29: The influence of slenderness for the first eleven frequencies for beams with FBF materials under fixed-fixed conditions

Table 23: Frequencies for fixed-fixed beams composed of five stacking sequences at a/h=10

Mode	Hex	BBB	FFF	BFB	FBF
1	2.07E-5	5.06E-5	3.20E-5	2.99E-5	3.46E-5
2	2.09E-5	5.12E-5	3.38E-5	3.24E-5	3.47E-5
3	5.45E-5	1.32E-4	8.22E-5	7.80E-5	8.84E-5
4	5.54E-5	1.32E-4	8.28E-5	8.14E-5	8.95E-5
5	6.99E-5	1.37E-4	8.73E-5	8.35E-5	8.99E-5
6	1.06E-4	2.51E-4	1.60E-4	1.56E-4	1.65E-4
7	1.40E-4	2.76E-4	1.65E-4	1.63E-4	1.77E-4
8	1.61E-4	3.46E-4	2.01E-4	2.12E-4	2.22E-4
9	1.75E-4	3.67E-4	2.21E-4	2.15E-4	2.28E-4
10	2.12E-4	4.56E-4	2.72E-4	2.69E-4	2.93E-4
11	2.31E-4	5.01E-4	3.17E-4	3.11E-4	3.29E-4

Table 24: Frequencies for fixed-fixed beams composed of five stacking sequences at a/h=20

Mode	Hex	BBB	FFF	BFB	FBF
1	2.16E-5	5.32E-5	3.49E-5	3.17E-5	3.75E-5
2	2.16E-5	5.43E-5	3.63E-5	3.46E-5	3.72E-5
3	5.95E-5	1.49E-4	1.64E-4	8.71E-5	1.77E-4
4	5.98E-5	1.47E-4	9.61E-5	1.63E-4	1.02E-4
5	1.40E-4	2.75E-4	9.99E-5	9.48E-5	1.03E-4
6	2.12E-4	5.01E-4	3.19E-4	3.11E-4	3.30E-4
7	2.80E-4	5.50E-4	3.29E-4	3.26E-4	3.54E-4
8	3.00E-4	6.35E-4	3.66E-4	3.88E-4	4.00E-4
9	3.29E-4	6.64E-4	4.03E-4	3.94E-4	4.17E-4
10	4.25E-4	9.07E-4	5.43E-4	5.37E-4	5.85E-4
11	4.62E-4	1.00E-3	6.36E-4	6.22E-4	6.59E-4

Table 25: Bending frequencies for fixed-fixed beams composed of five stacking sequences at a/h=30

Bending Mode	Hex	BBB	FFF	BFB	FBF
1	2.18E-5	5.39E-5	3.57E-5	3.21E-5	3.79E-5
2	6.07E-5	1.50E-4	9.94E-5	8.92E-5	1.07E-4
3	4.86E-4	9.66E-4	5.29E-4	5.65E-4	5.76E-4

Table 26: Differences for fixed-fixed beams composed of five stacking sequences

a/h	Bending frequency	% Differences below a/h=30 $\bar{\omega}$				
		Hexagonal	BBB	FFF	BFB	FBF
10	1	4.13	6.12	10.36	6.85	8.71
	2	8.73	12.00	17.30	12.56	15.98
20	1	0.46	1.11	2.24	1.25	1.85
	2	1.65	2.00	3.32	2.35	3.74

difference is reduced to within 5 percent.

4.4 Fixed-free Condition

A total of 4 terms in x and y directions accompanied with 3 discrete layers through the thickness are used for this boundary condition. The difference of the fundamental frequency are plotted in Figure 30. These lines are similar to beams with the simply supported boundary condition.

Figures 31-35 demonstrate the first eleven frequencies influenced by slenderness for cantilever beams. There is a litte difference between each in-plane bending and transverse bending frequences. It is caused by two conditions. First, the plate is layered through the thickness; therefore, the plate is slightly stiffer for the in-plane bending. Second, different approximate terms are used for the y and z directions. Hence, as the length increases, this

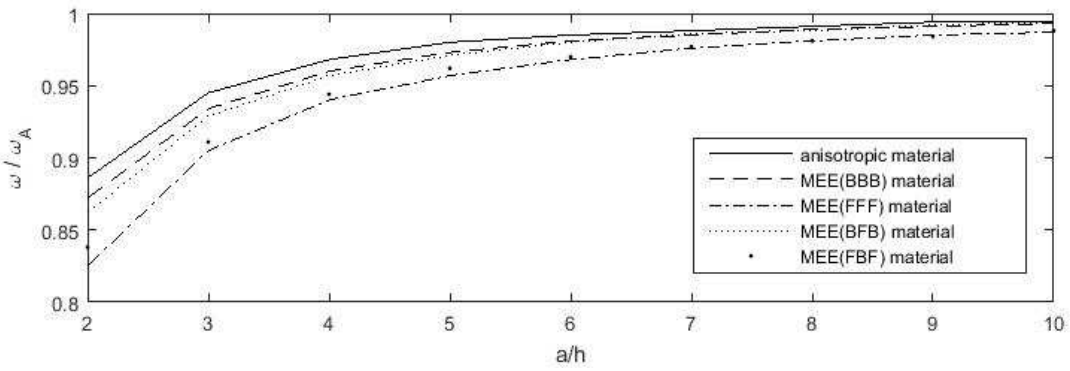

Figure 30: Differences of the fundamental frequency with five stacking sequences under fixed-free conditions

difference increases quickly with the integration of the K matix.

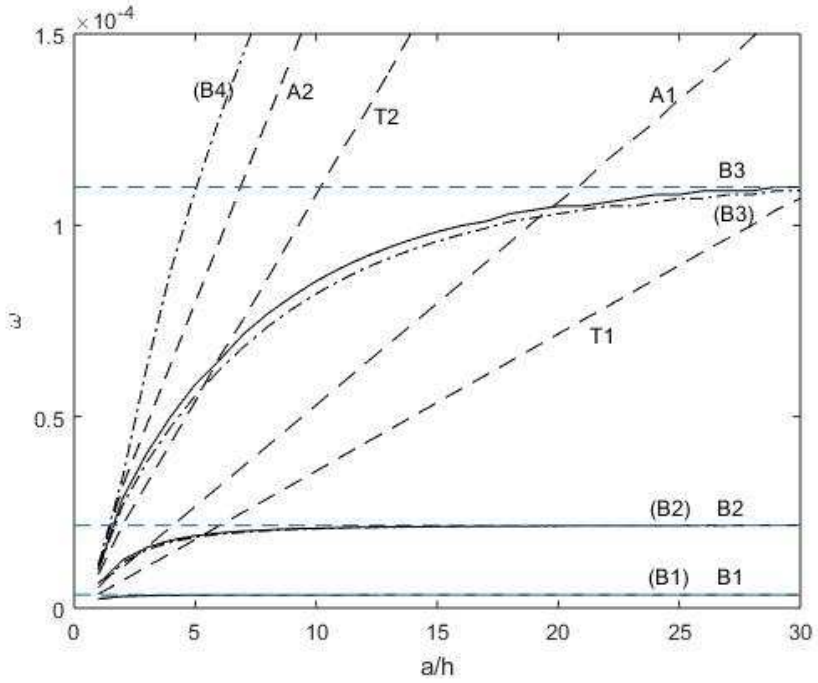

Figure 31: The influence of slenderness for the first eleven frequencies for beams with anisotropic materials under fixed-free conditions

Tables 27 and 28 give the first eleven frequencies of five stacking sequencies under cantilever condition at a/h=10 and a/h=20.

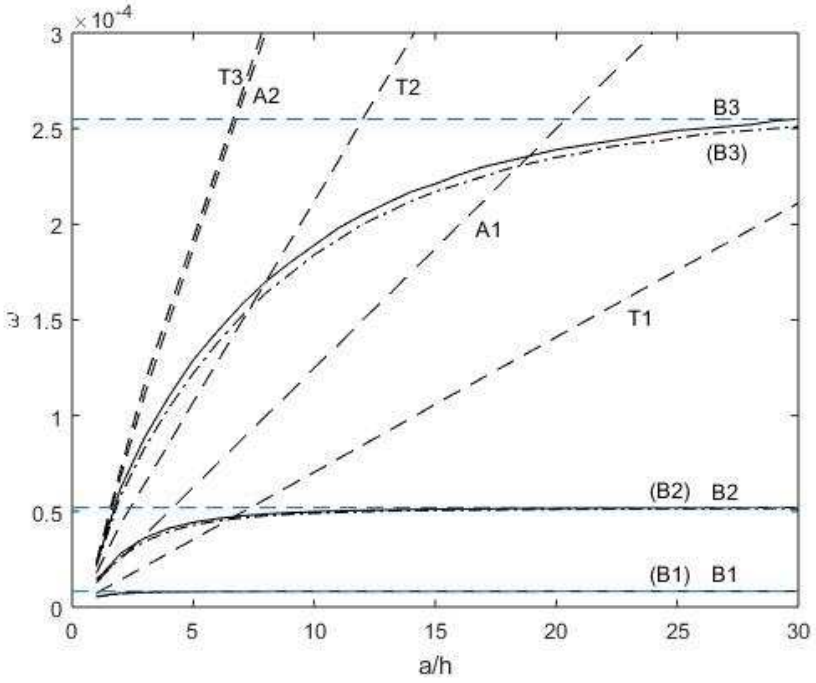

Figure 32: The influence of slenderness for the first eleven frequencies for beams with BBB materials under fixed-free conditions

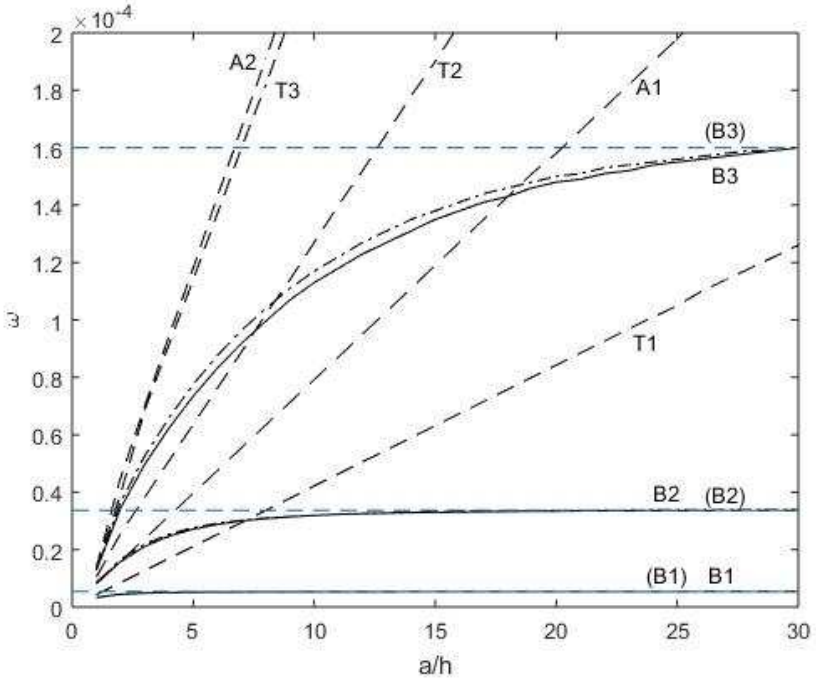

Figure 33: The influence of slenderness for the first eleven frequencies for beams with FFF materials under fixed-free conditions

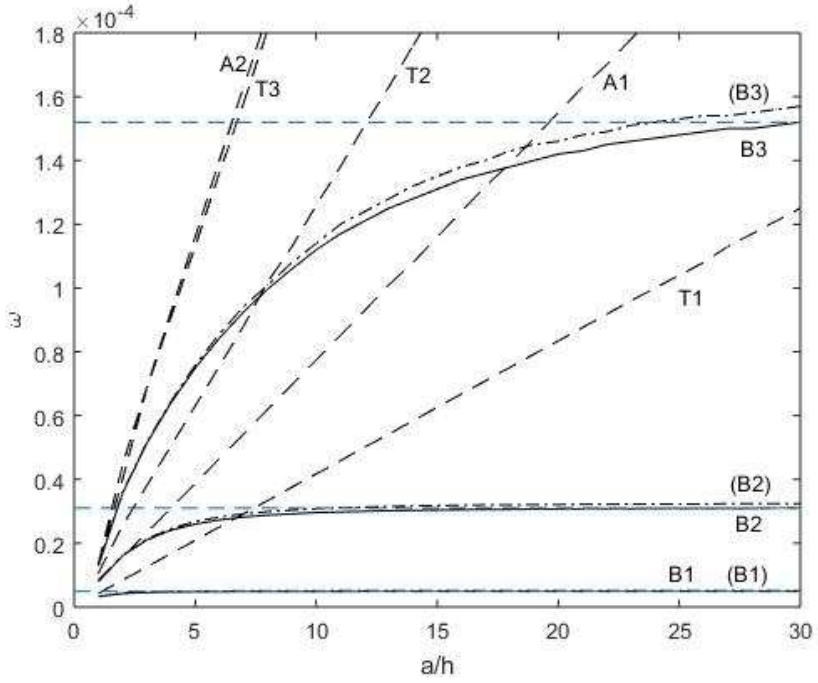

Figure 34: The influence of slenderness for the first eleven frequencies for beams with BFB materials under fixed-free conditions

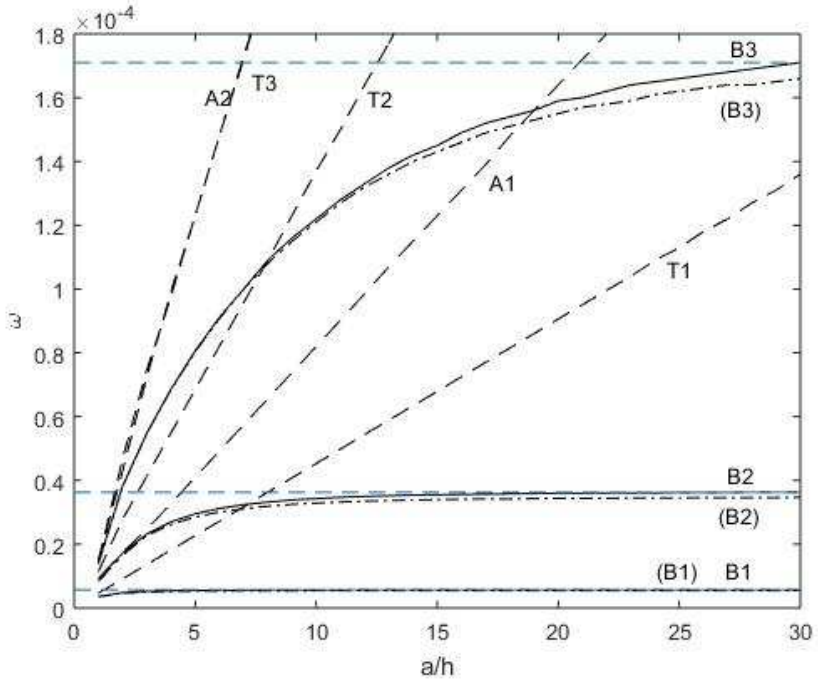

Figure 35: The influence of slenderness for the first eleven frequencies for beams with FBF materials under fixed-free conditions

Table 27: Frequencies for fixed-free beams composed of five stacking sequences at a/h=10

Mode	Hex	BBB	FFF	BFB	FBF
1	3.41E-6	8.09E-6	5.25E-6	4.88E-6	5.42E-6
2	3.41E-6	8.17E-6	5.29E-6	5.08E-6	5.66E-6
3	2.07E-5	4.90E-5	3.19E-5	2.96E-5	3.29E-5
4	2.08E-5	4.98E-5	3.19E-5	3.08E-5	3.43E-5
5	3.58E-5	7.04E-5	4.22E-5	4.17E-5	4.53E-5
6	5.30E-5	1.25E-4	7.92E-5	7.74E-5	8.20E-5
7	8.21E-5	1.84E-4	1.13E-4	1.12E-4	1.21E-4
8	8.54E-5	1.89E-4	1.17E-4	1.14E-4	1.22E-4
9	1.08E-4	2.12E-4	1.27E-4	1.26E-4	1.37E-4
10	1.60E-4	3.76E-4	2.28E-4	2.26E-4	2.46E-4
11	1.91E-4	3.81E-4	2.39E-4	2.33E-4	2.47E-4

Table 28: Frequencies for fixed-free beams composed of five stacking sequences at a/h=20

Mode	Hex	BBB	FFF	BFB	FBF
1	3.42E-6	8.15E-6	5.30E-6	4.91E-6	5.46E-6
2	3.43E-6	8.22E-6	5.35E-6	5.12E-6	5.71E-6
3	2.14E-5	5.10E-5	3.36E-5	3.07E-5	3.44E-5
4	2.15E-5	5.15E-5	3.34E-5	3.21E-5	3.60E-5
5	7.16E-5	1.41E-4	8.43E-5	8.34E-5	9.06E-5
6	1.06E-4	2.50E-4	1.58E-4	1.55E-4	1.64E-4
7	1.03E-4	2.35E-4	1.48E-4	1.42E-4	1.55E-4
8	1.05E-4	2.39E-4	1.50E-4	1.46E-4	1.59E-4
9	2.16E-4	4.24E-4	2.54E-4	2.51E-4	2.73E-4
10	3.19E-4	7.53E-4	4.56E-4	4.50E-4	4.91E-4
11	3.39E-4	7.61E-4	4.78E-4	4.67E-4	4.95E-4

Table 33 shows the difference for five stacking sequences, while the corresponding frequencies at a/h=30 are listed in Table 29. The percentages increase rapidly for the third bending frequency. For the a/h ratio of 20, the reduction is 5 percent or higher. For the first two frequencies, the differences are quite small.

Table 29: Bending frequencies for fixed-free beams composed of five stacking sequences at a/h=30

Bending Mode	Hex	BBB	FFF	BFB	FBF
1	3.43E-6	8.23E-6	5.36E-6	4.91E-6	5.73E-6
2	2.16E-5	5.19E-5	3.37E-5	3.10E-5	3.63E-5
3	1.10E-4	2.55E-4	1.60E-4	1.52E-4	1.71E-4

Table 30: Differences for fixed-free beams composed of five stacking sequences

a/h	Bending frequency	% Differences below a/h=30 $\bar{\omega}$				
		Hexagonal	BBB	FFF	BFB	FBF
10	1	0.58	0.73	1.31	0.61	1.22
	2	3.70	4.05	5.34	3.58	5.51
	3	22.36	25.88	29.38	26.32	28.65
20	1	0.00	0.12	0.19	0.00	0.35
	2	0.46	0.77	0.89	0.00	0.83
	3	4.55	6.27	7.50	6.58	7.02

CHAPTER 5 ISOTROPIC PLATES

One of the key issues in the use of plate theory is determining the limits of its accuracy as the plate thickness increases relative to the side dimensions. Before considering the case of the laminated MEE plate, it is instructive to consider the frequency of the reduced case of the isotropic square plate. This crucial topic has seen much discussion in recent years, and it provides a useful comparison for the elasticity/continuum solution presented in this study. We calculate the dimensionless frequencies for an isotropic square plate for six different lateral boundary condition combinations. The continuum theory results clearly depend on the a/h ratio of the plate, and we examine this influence by showing the frequencies calculated by the continuum theory and comparing with the analytical thin-plate results. The results show the limitations with the respect to the application of analytical thin isotropic plate theory. Several of the lowest modes have fairly large differences with classical plate theory results even when the plate has a fairly large a/h ratio. There has always been an element of uncertainty regarding acceptable values for the thickness ratio of plates for which the equations of thin plate theory will still apply, and this work attempts to further quantity those limits.

Starting from isotropic plate and moving on to MEE plate using the discrete-layer method, the non-dimensional vibration charateristics of individual plates with varied different thickness ratio a/h are presented and compared with the results available in the literature with respect to different kinds of boundary conditions. The limitations of classical thin plate theory and previously tabulated values for several frequencies in vibration are

discussed. The effects of the thickness ratio on each of the primary modal frequencies are also examined, and limitations of thin plate theory are finally presented.

5.1 Classical Isotropic Plates' Theories

Kirchhoff's assumptions [12] are the basic kinematic restrictions in thin plate theory under small deflection:

- Compared to the lateral dimensions of the plate, the thickness is much smaller.
- The mid-plane stays as the neutral plane after deformation.
- The deflection of the mid-plane is small while comparing to the thickness of the plate, which is also known as the small-deflection theory.
- Plane sections perpendicular to the mid-surface stay normal to the mid-surface after deflection. This assumption implies that the shear strains are zeros.
- The thickness of the plate does not change during a deflection. Thus, compared to the other components of stress the transverse normal stress is small and can be neglected.

Since it is assumed that the straight-line perpendicular to the middle surface stays normal to the middle surface without extension after the deformation of the plate, shear strains γ_{xz} and γ_{yz} are zeros for the plate. This assumption requires that the shear stress σ_{xz} and σ_{yz} must be recovered from equilibrium since they are zero using the constitutive law. As the thickness decreases, typically 10 times smaller than the laterial dimensions, thin plate theory can give relatively good results. By recovering the shear stresses directly from the strains, the Mindlin model provides some improvement and the results are more accurate [12] . Using the piecewise approximation through the thickness direction, the DL model is more flexible than the previous models. Lower and more accurate frequencies can be obtained.

As a number of references provide the results of the natural vibration of isotropic square plates, a variety of frequency comparison are presented below for specific sets of boundary conditions along the edges.

5.2 Simply Supported Condition

The convergence of the semi-analytical discrete layer model has been explored using the natural frequencies of a square isotropic plate. For the simply supported condition, the Navier solution gives an exact result for Kirchhoff's plate theory. The in-plane variations in transverse displacement are given as a single term in sine or cosine components of the expansion. Fixing a/b=1, a/h=10 and $\nu = 0.3$, the natural frequencies are compared with Srinivas's elasticity theory and Reddy's higher-order shear deformation theory (HSDPT) [22].

Equal thicknesses of each discrete layer were used. The results are presented in terms of the non-dimensional parameter $\bar{\omega} = \omega \left(\rho h^2/G\right)^{1/2}$. Using 6 terms in x and y directions, the results are shown in Table 31 as a function of the number of discrete layers (N). The highlights in bold indicate the in-plane modes for which the transverse displacement is zero.

Each frequency was computed using 36 in-plane terms and 8 sub-layers, with the corresponding mode shapes plotted using the plate mid-plane and 3D are shown in Figures 36 and 37. Since the transverse displacement is $w(x,y) = sin\frac{n\pi x}{a} sin\frac{m\pi y}{b}$, the numbers given in brackets are shown as Navier grouping function(m,n).

It is clear that because of the symmetric boundary condition for the plate, repeated frequencies appear in the mode shapes. All modes shown are bending modes with the exception of mode 7, which is an in-plane stretching mode that were not computed by

[22] J.N. Reddy and N.D. Phan, Stability and Vibraiton of Isotropic, Orthotropic and Laminted Plates according to a Higher-order Shear Deformation Theory, *Journal of Sound and Vibration* 98(2), 157-170 (1985).

Table 31: The first ten non-dimensional frequencies of an isotropic square plate under simply supported condition with $\nu = 0.3$ and $a/h = 10$, normalized by $\bar{\omega} = \omega \left(\rho h^2/G\right)^{1/2}$

Boundary conditions	Freq. number	Srinivas at al. [18]	HSDPT [22]	Present solution		
				N=4	N=8	N=16
SSSS	1	0.0932	0.0931	0.0939	0.0933	0.0932
	2,3	0.226	0.2222	0.2245	0.2231	0.2227
	4	0.3421	0.3411	0.3452	0.3429	0.3423
	5,6	0.4171	0.4158	0.4211	0.4182	0.4174
	7	——	——	**0.4443**	**0.4443**	**0.4443**
	8,9	0.5239	0.5221	0.5292	0.5253	0.5243
	10	——	0.6545	0.6642	0.6589	0.6575

Srinivas and Reddy. The displacement component w is quite small compared with the displacements in other direction, and we use the deformation of the in-plane mesh to show the deformed state as viewed from below.

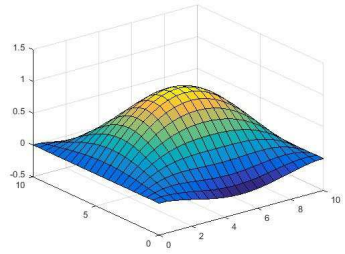

Mode 1: (1,1)

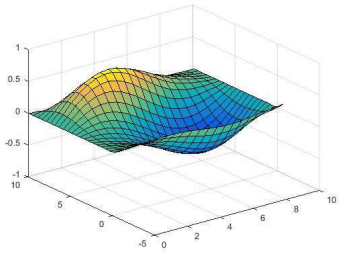

Mode 2: (1,2)

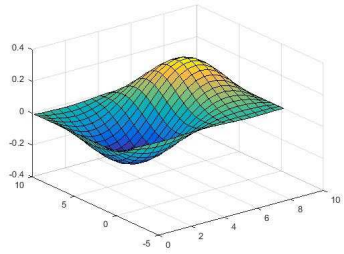

Mode 3: (2,1)

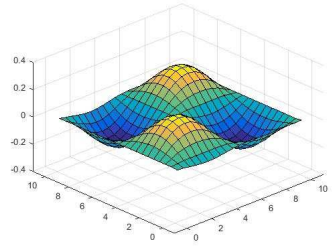

Mode 4: (2,2)

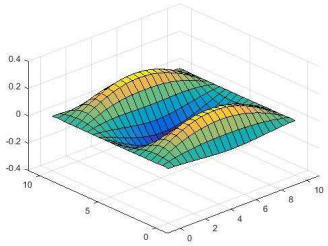

Mode 5: (1,3)

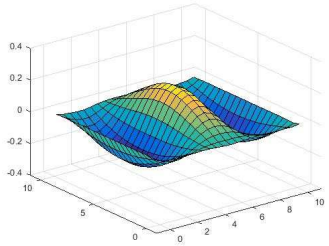

Mode 6: (3,1)

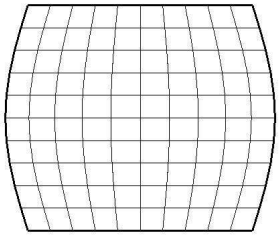

Mode 7

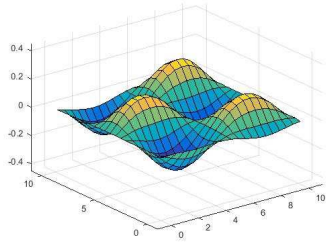

Mode 8: (2,3)

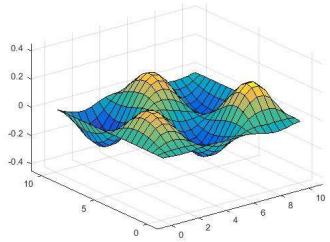

Mode 9: (3,2)

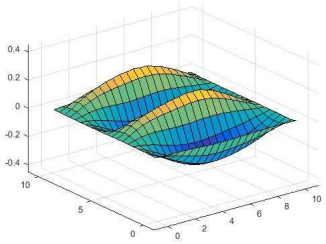

Mode 10: (1,4)

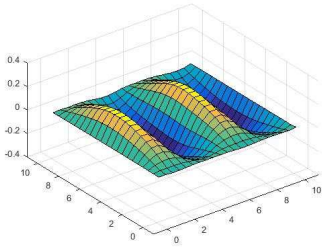

Mode 11: (4,1)

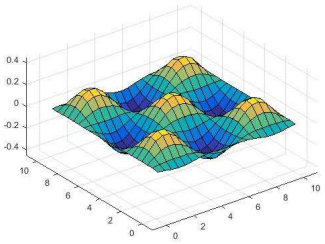

Mode 12: (3,3)

Figure 36: First twelve mode shapes for isotropic plates under simply supported condition plotted using the mid-plane

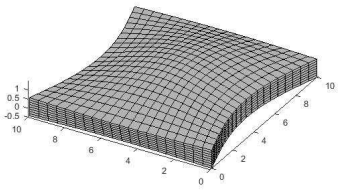

Mode 1: (1,1)

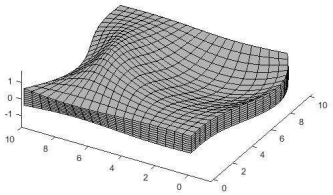

Mode 2: (1,2)

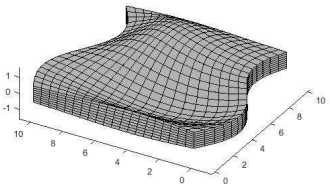

Mode 3: (2,1)

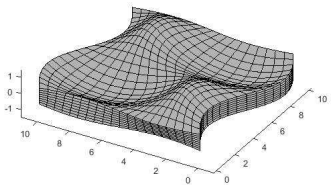

Mode 4: (2,2)

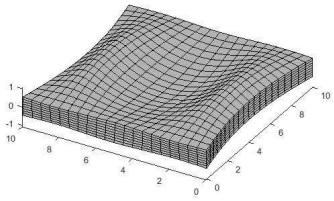

Mode 5: (1,3)

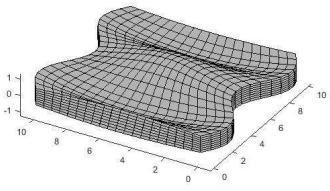

Mode 6: (3,1)

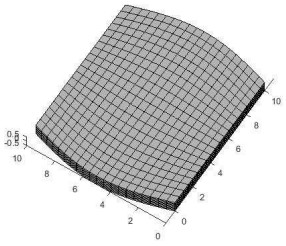

Mode 7

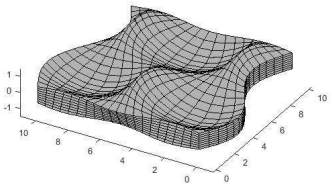

Mode 8: (2,3)

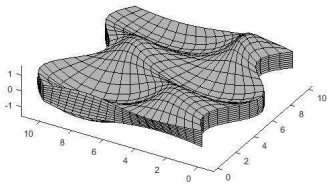

Mode 9: (3,2)

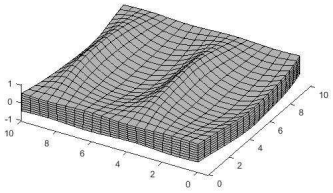

Mode 10: (1,4)

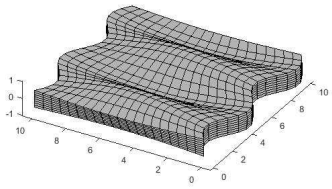

Mode 11: (4,1)

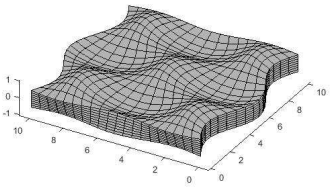

Mode 12: (3,3)

Figure 37: First twelve mode shapes for isotropic plates under simply supported condition plotted in 3D

5.3 All-Clamped Condition

The natural frequencies of an all clamped isotropic($\nu = 0.3$) plate have been computed by Liew *et al.*[23] using the Rayleigh-Ritz procedure solve the energy function derived from Mindlin's plate theory [23]. The frequency parameter was given as $\bar{\omega} = (\omega a^2/\pi^2)\sqrt{\rho h/D}$, where $D = Eh^3/[12(1-\nu^2)]$ and h is the total thickness. Using 36 in-plane terms with 8 layers, results are shown in Table 32 and the corresponding mode shapes shown in mid-surface and 3D are plotted in Figures 38 and 39.

Once again, the present model captures in-plane modes that were not considered by Liew *et al.*. It is clear that as the thickness increases, the in-plane frequencies are reduced and approach the lowest bending frequency given by simpler theories.

[23]K.M. Liew, Y.Xiang and S. Kitipornchai, Transverse vibration of thick rectangular plates-1. Comprehensive sets of boundary conditions,*Computers and Structures* 49(1) 1-29(1993).

Table 32: The first ten non-dimensional frequencies of an isotropic square plate under CCCC condition with $\nu = 0.3$, normalized by $\bar{\omega} = (\omega a^2/\pi^2)\sqrt{\rho h/D}$

Boundary conditions	Freq. number	a/h=10		a/h=5	
		Liew *et al.* [**?**]	Present	Liew *et al.* [**?**]	Present
CCCC	1	3.2954	3.3297	2.6875	2.7370
	2	6.2858	6.3633	4.6907	4.7940
	3	6.2858	6.3633	4.6907	4.7940
	4	8.8098	8.9295	——	**6.2751**
	5	10.3788	10.5316	——	**6.2751**
	6	10.4778	10.6316	6.2985	6.4484
	7	——-	**12.5221**	7.1767	7.3598
	8	——-	**12.5221**	——	**7.4371**
	9	12.5529	12.7474	7.2759	7.4621
	10	12.5529	12.7474	8.5155	8.7416

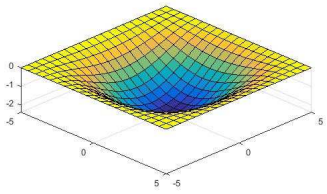

Mode 1

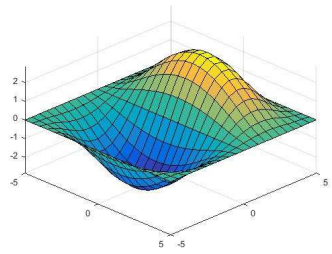

Mode 2

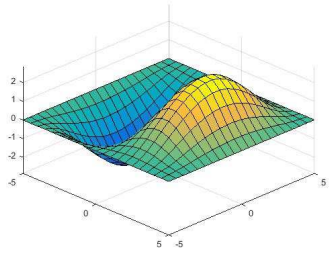

Mode 3

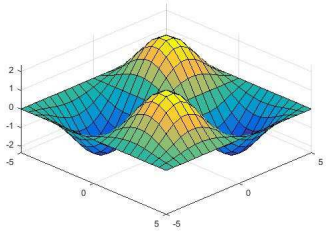

Mode 4

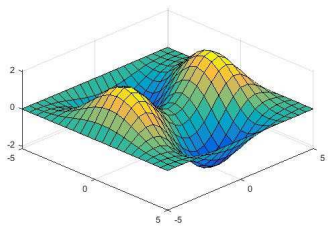

Mode 5

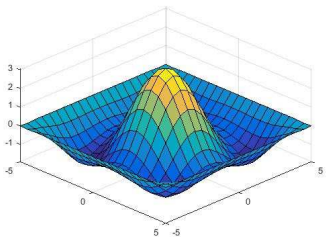

Mode 6

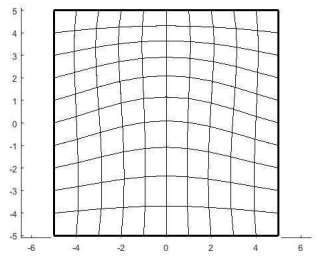

Mode 7

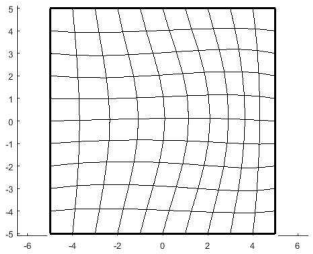

Mode 8

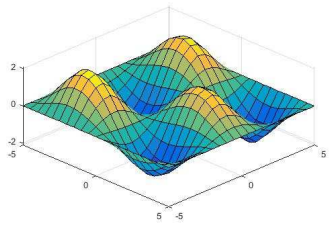

Mode 9

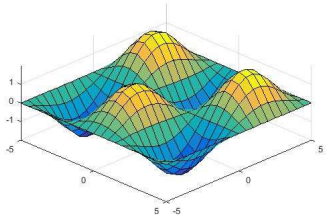

Mode 10

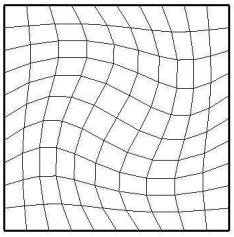

Mode 11

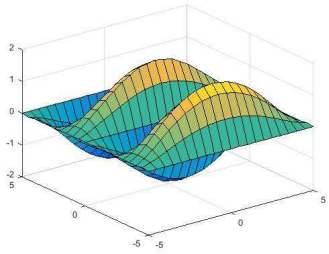

Mode 12

Figure 38: First twelve mode shapes of isotropic plates under CCCC condition plotted using the mid-plane

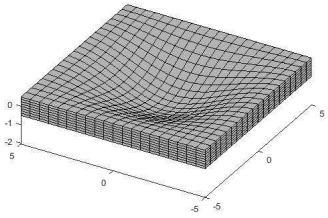

Mode 1

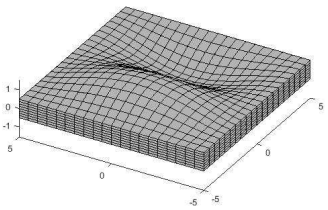

Mode 2

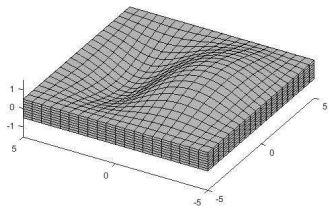

Mode 3

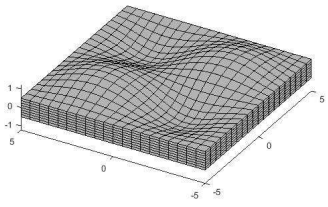

Mode 4

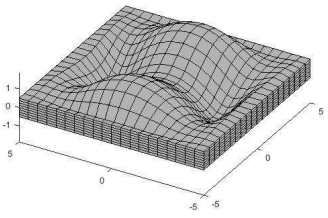

Mode 5

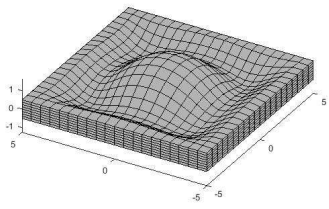

Mode 6

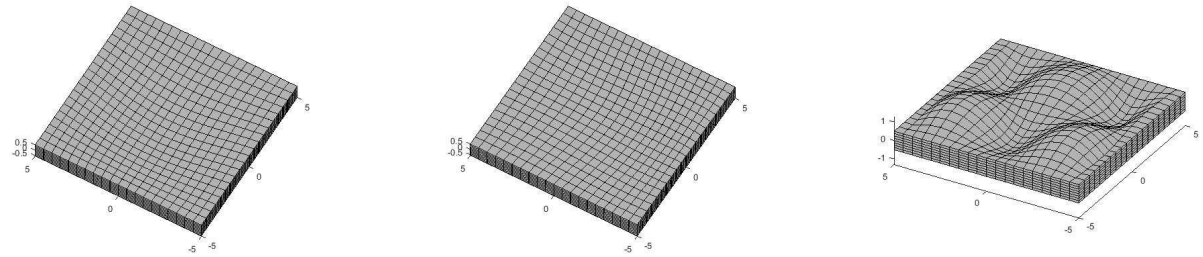

Mode 7 Mode 8 Mode 9

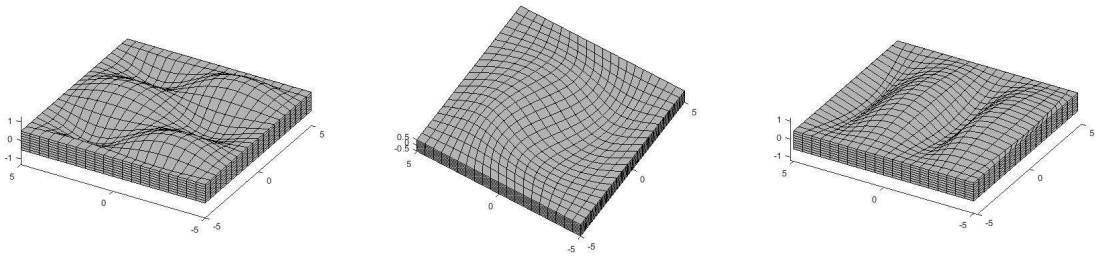

Mode 10 Mode 11 Mode 12

Figure 39: First twelve mode shapes of isotropic plates under CCCC condition plotted in 3D

5.4 FCFC Condition

Table 33 lists the first ten non-dimensional natural frequencies of isotropic square plates for the FCFC condition. This case was also considered by Liew *et al.* [23] . A total of 36 in-plane terms are used along with 8 layers in the thickness direction.

Figures 40 and 41 show the first twelve mode shapes of this kind of plates in mid-surface and 3D. Due to the Poisson effect, there are some extension in transverse direction at ends, like Mode 1. By making cut planes perpendicular to the y axis, it is possible to detect the deflection of bending modes. The opposite deflections of free sides indicate the torsional modes, for example Mode 2.

Table 33: The first ten non-dimensional frequencies of an isotropic square plate under FCFC condition with $\nu = 0.3$, normalized by $\bar{\omega} = (\omega a^2/\pi^2)\sqrt{\rho h/D}$

Boundary conditions	Freq. number	a/h=10		a/h=5	
		Liew at al. [23]	Present	Liew at al. [23]	Present
FCFC	1	2.0904	2.1094	1.7772	1.8061
	2	2.4342	2.4533	2.0151	2.0429
	3	3.9055	3.9312	—	**2.9771**
	4	5.3392	5.3996	3.1652	3.2004
	5	5.7811	5.8408	4.0413	4.1242
	6	——	**5.9501**	4.3472	4.4262
	7	6.9368	6.9834	—	**5.3326**
	8	7.3046	7.3757	—	**5.4493**
	9	9.6241	9.7567	5.3813	5.4827
	10	9.9989	10.0960	5.3813	5.4831

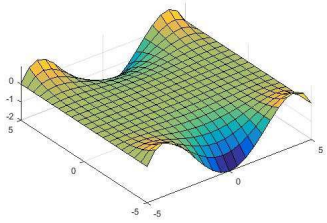

Mode 1

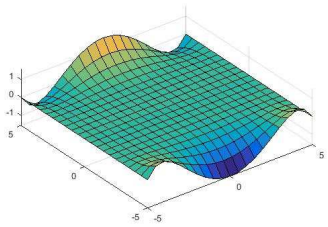

Mode 2

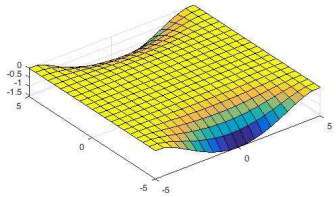

Mode 3

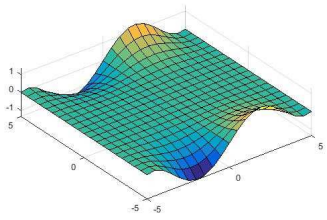

Mode 4

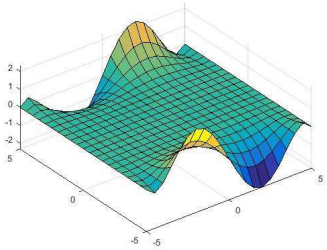

Mode 5

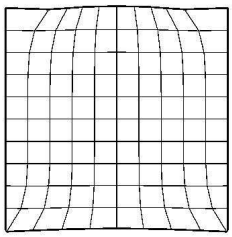

Mode 6

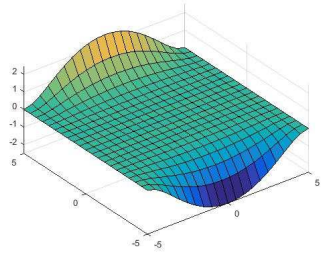

Mode 7

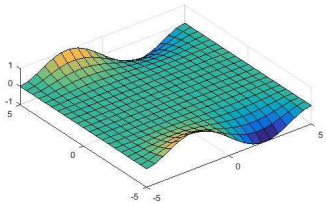

Mode 8

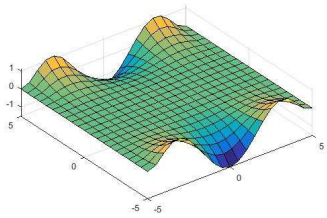

Mode 9

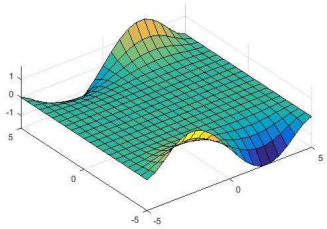

Mode 10

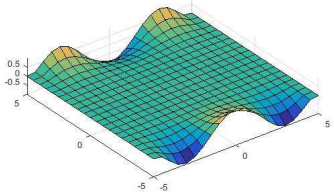

Mode 11

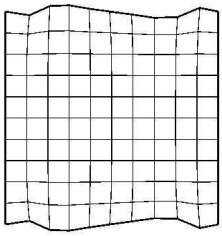

Mode 12

Figure 40: First twelve mode shapes of isotropic plates under FCFC condition

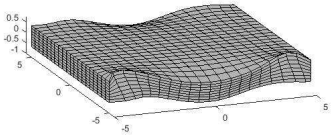

Mode 1

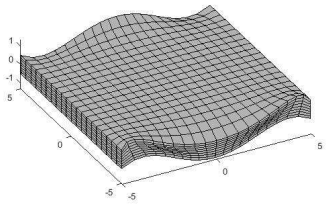

Mode 2

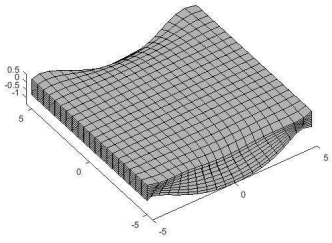

Mode 3

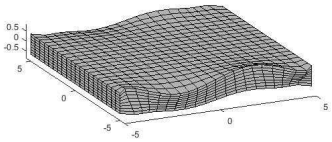

Mode 4

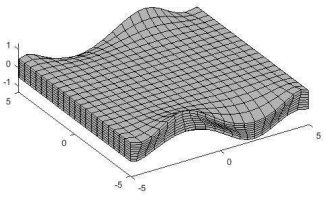

Mode 5

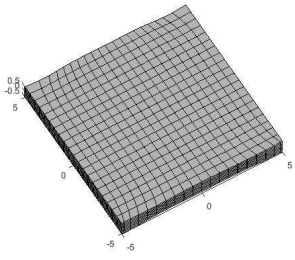

Mode 6

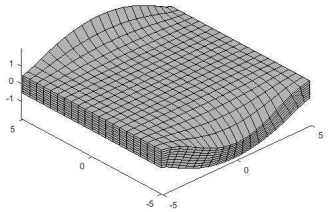

Mode 7

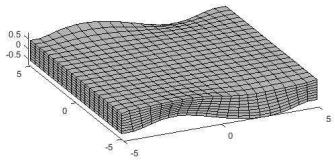

Mode 8

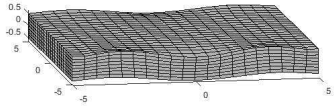

Mode 9

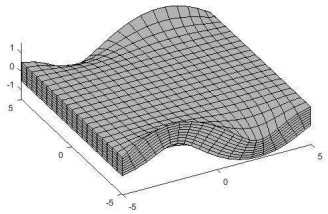

Mode 10

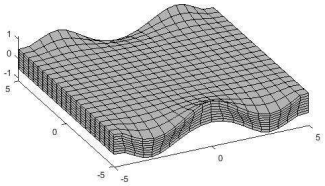

Mode 11

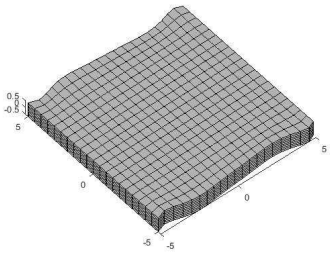

Mode 12

Figure 41: First twelve mode shapes of isotropic plates under FCFC condition plotted in 3D

5.5 CFFF Condition

The cantilever plate is an extremely important case that has numerous practical applications, ranging from balconies and sunshades in the daily life to touch spots in the cellphone. Liew *et al.* gave results without showing the mode shapes. Frequencies are compared respect to the approaching values in Table 34. The present model consistantly gives bending and torsional frequencies that are larger than those of the Mindlin results compared with Liew *et al.* [23] . The in-plane frequencies are normally smaller.

Using 16 in-plane terms together with 4 layers, Figures 42 and 43 demonstrates the corresponding mode shapes.

Table 34: The first ten non-dimensional frequencies of an isotropic square plate under CFFF condition with $\nu = 0.3$, normalized by $\bar{\omega} = (\omega a^2/\pi^2)\sqrt{\rho h/D}$

Boundary conditions	Freq. number	a/h=10		a/h=5	
		Liew at al. [23]	Present	Liew at al. [23]	Present
CFFF	1	0.3476	0.3573	0.3384	0.3471
	2	0.8168	0.8401	0.7445	0.7637
	3	2.0356	2.1111	——	**1.1181**
	4	2.5836	**2.2349**	1.7806	1.8451
	5	2.8620	2.9795	2.2765	2.5154
	6	4.8162	3.0007	2.4205	2.5742
	7	5.4834	**5.3357**	3.8851	**2.6689**
	8	5.7769	5.4769	4.3168	**2.9809**
	9	6.2381	**5.9619**	4.5996	4.3811
	10	7.9181	7.9682	4.8966	**4.8979**

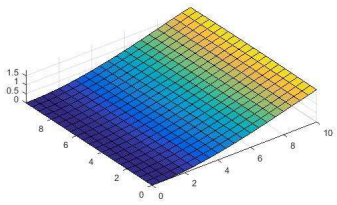

Mode 1

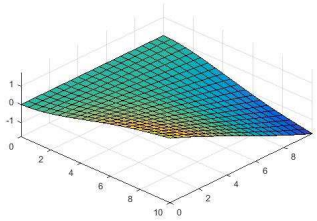

Mode 2

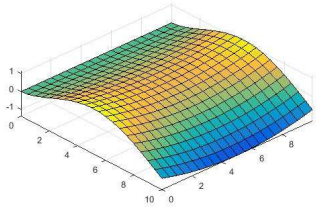

Mode 3

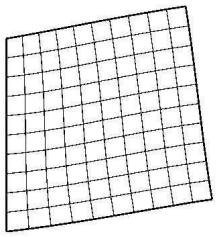

Mode 4

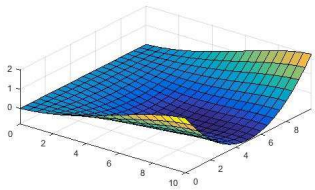

Mode 5

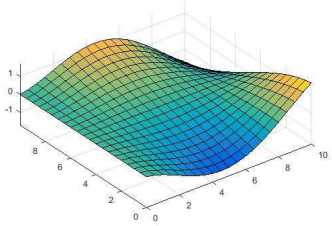

Mode 6

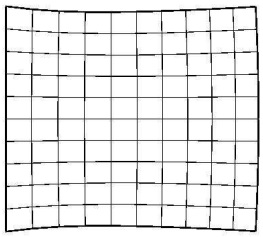

Mode 7

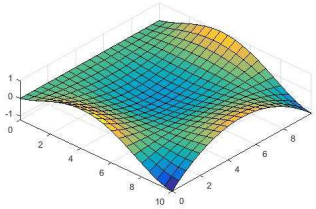

Mode 8

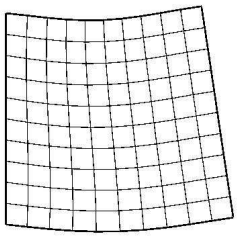

Mode 9

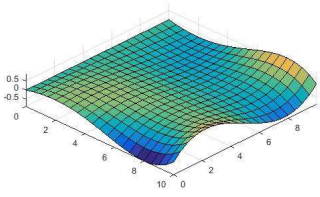

Mode 10

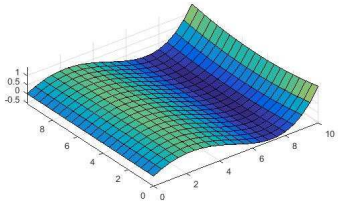

Mode 11

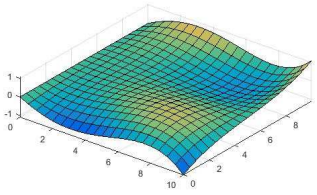

Mode 12

Figure 42: First twelve mode shapes of isotropic plates under CFFF condition plotted using the mid-plane

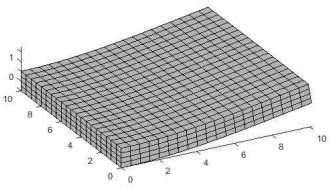

Mode 1

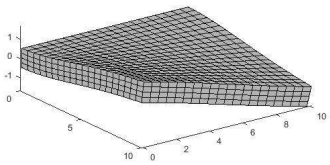

Mode 2

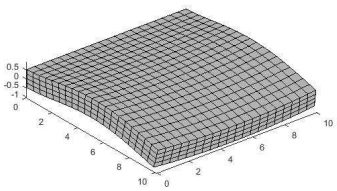

Mode 3

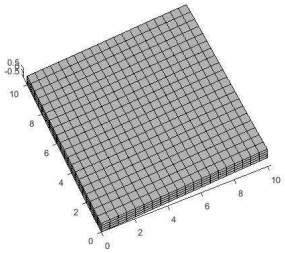

Mode 4

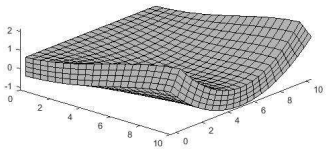

Mode 5

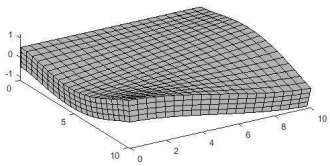

Mode 6

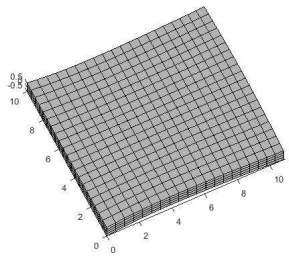

Mode 7

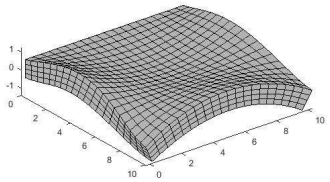

Mode 8

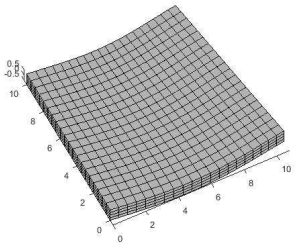

Mode 9

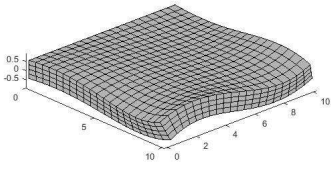

Mode 10

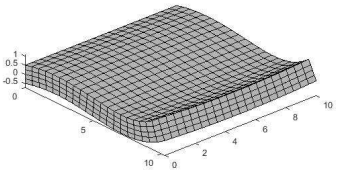

Mode 11

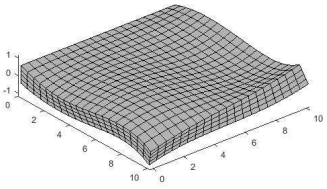

Mode 12

Figure 43: First twelve mode shapes of isotropic plates under CFFF condition plotted in 3D

5.6 CCFF Condition

Results for this case are computed using 4 terms in both x and y directions together with 4 layers. Comparison of frequencies is domenstrated in Table 35 and the corresponding mode shapes shown in 2D and 3D are plotted in Figures 44 and 45. Compared with Liew *et al.*'s results, frequencies calculated by Liew *et al.*'s might miss some in-plane values under this condition for the a/h=5 case.

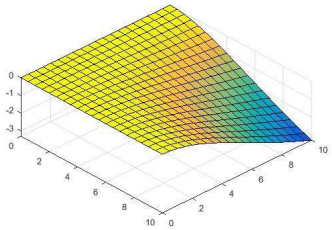

Mode 1

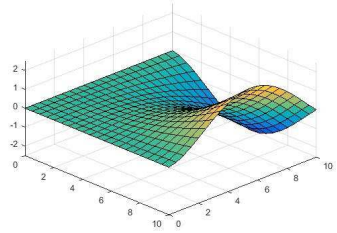

Mode 2

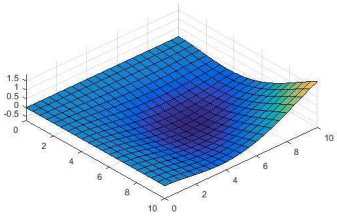

Mode 3

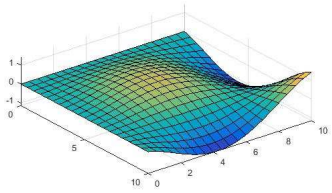

Mode 4

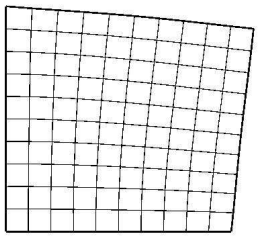

Mode 5

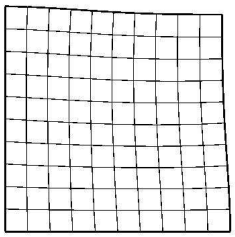

Mode 6

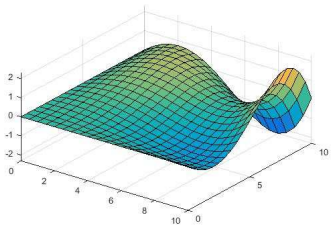

Mode 7

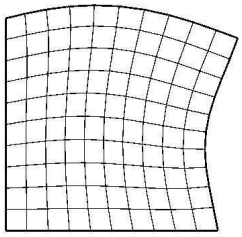

Mode 8

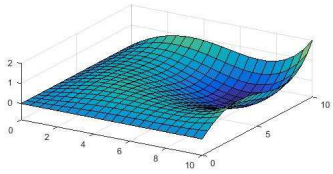

Mode 9

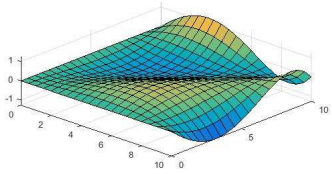

Mode 10

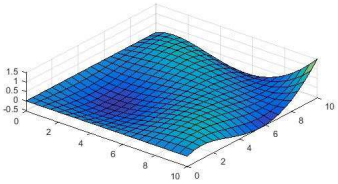

Mode 11

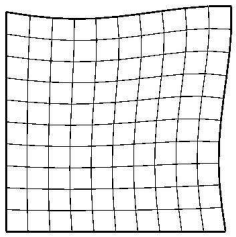

Mode 12

Figure 44: First twelve mode shapes of isotropic plates under CCFF condition plotted using the mid-plane

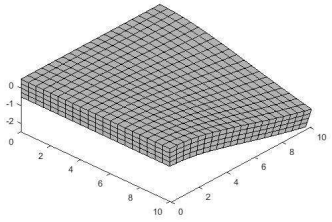

Mode 1

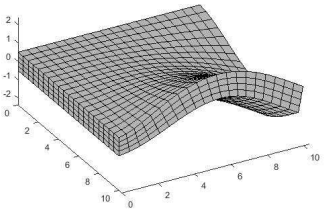

Mode 2

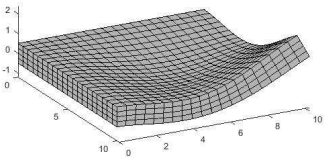

Mode 3

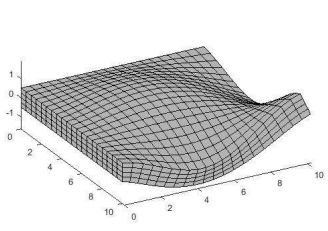

Mode 4

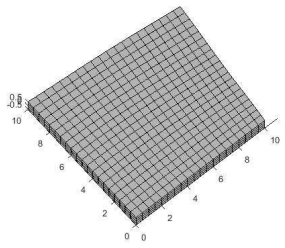

Mode 5

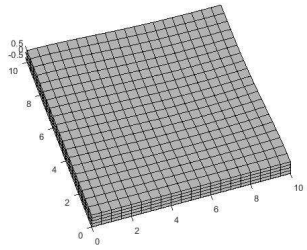

Mode 6

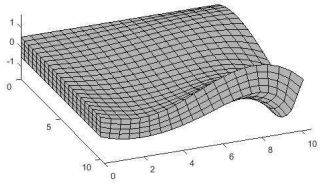

Mode 7

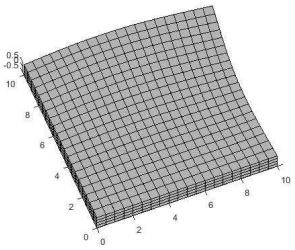

Mode 8

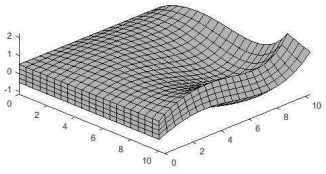

Mode 9

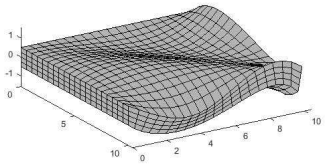

Mode 10

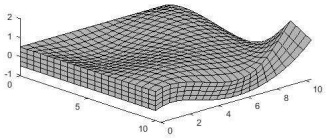

Mode 11

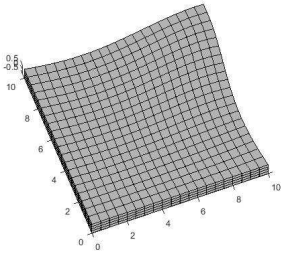

Mode 12

Figure 45: First twelve mode shapes of isotropic plates under CCFF condition plotted in 3D

5.7 SFSF Condition

Table 36 shows the comparison with Liew *et al.*'s results. It is clear that Liew *et al.*'s theory can only cover bending frequencies under SFSF condition. The corresponding mode shapes for a/h=10 are shown in Figures 46 and 47.

Table 35: The first ten non-dimensional frequencies of an isotropic square plate under CCFF condition with $\nu = 0.3$, normalized by $\bar{\omega} = (\omega a^2/\pi^2)\sqrt{\rho h/D}$

Boundary conditions	Freq. number	a/h=10		a/h=5	
		Liew at al. [23]	Present	Liew at al. [23]	Present
CCFF	1	0.6762	0.6946	0.6328	0.6489
	2	2.2438	2.3246	1.9221	1.9856
	3	2.5049	2.6055	2.1499	2.2313
	4	4.2557	4.5059	——	**2.6032**
	5	5.5633	**5.2043**	——	**3.3287**
	6	5.8188	**6.6564**	3.4217	3.5729
	7	7.2399	7.9353	4.3468	**3.9720**
	8	7.5055	**7.9449**	4.5533	5.3123
	9	9.9651	8.6372	5.4276	5.6800
	10	10.1661	9.5767	5.6539	**6.1263**

Table 36: The first ten non-dimensional frequencies of an isotropic square plate under SFSF condition with $\nu = 0.3$, normalized by $\bar{\omega} = (\omega a^2/\pi^2)\sqrt{\rho h/D}$

Boundary conditions	Freq. number	a/h=10		a/h=5	
		Liew at al. [23]	Present	Liew at al. [23]	Present
SFSF	1	0.9565	0.9593	0.9102	0.9139
	2	1.5593	1.5670	1.4280	1.4342
	3	3.4307	3.4808	——	**2.4697**
	4	3.6838	3.7036	2.9521	2.9845
	5	4.3358	4.3634	3.1684	3.1994
	6	——	**4.9400**	3.6435	3.6777
	7	6.2971	6.4010	——	**4.6127**
	8	6.7071	6.9051	5.0216	5.0994
	9	7.7648	7.8291	5.3173	5.4507
	10	8.3513	8.4230	——	**5.6993**

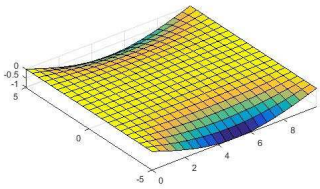

Mode 1

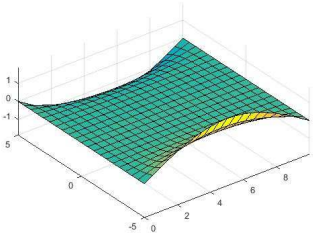

Mode 2

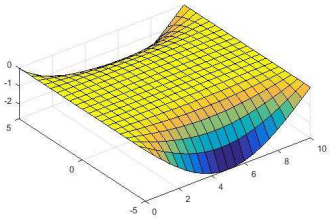

Mode 3

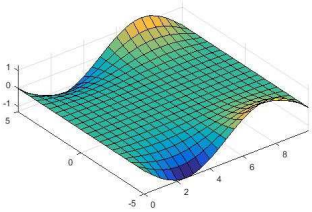

Mode 4

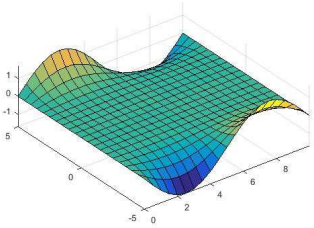

Mode 5

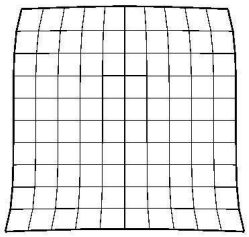

Mode 6

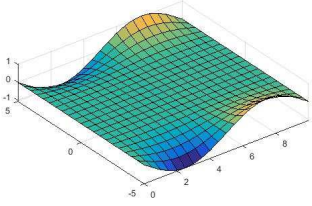

Mode 7

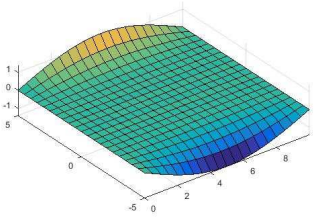

Mode 8

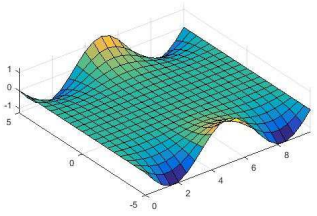

Mode 9

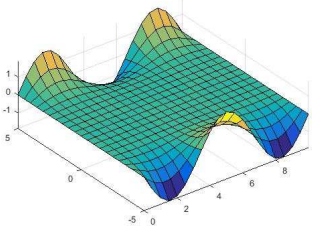

Mode 10

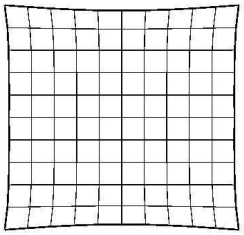

Mode 11

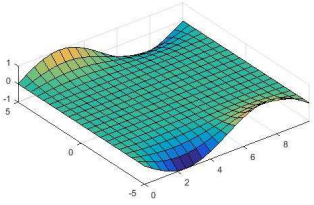

Mode 12

Figure 46: First twelve mode shapes of isotropic plates under SFSF condition plotted using the mid-plane

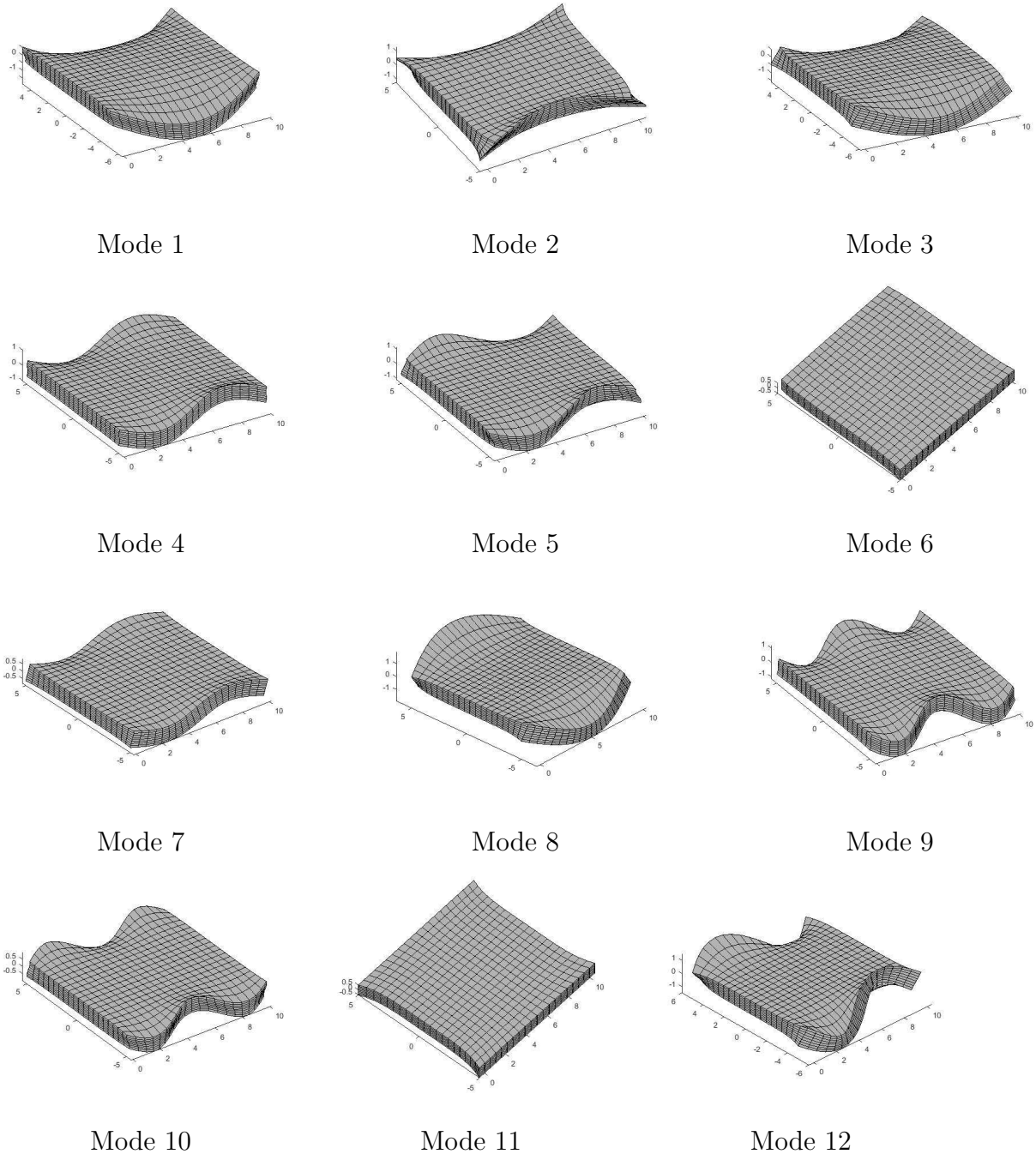

Mode 1 Mode 2 Mode 3

Mode 4 Mode 5 Mode 6

Mode 7 Mode 8 Mode 9

Mode 10 Mode 11 Mode 12

Figure 47: First twelve mode shapes of isotropic plates under SFSF condition plotted in 3D

6.1 Comparison with Existing Results

The free vibration of composite MEE plates under CCCC and FCFC conditions have already been studied by Chen, Heyliger and Pan [8] using the semi-analytical DL approach. To ensure that the present model works well under these conditions, choose the same coefficients used by Chen *et al.*. Using the same layers and number of in-plane terms, exactly same values were achieved for the hexagonal material under CCCC and FCFC conditions as shown in Table 37.

Table 37: The first six non-dimensional frequencies of an elastic square plate with hexagonal materials under CCCC & FCFC conditions, normalized by $\bar{\omega} = \omega h\sqrt{\rho/C_{11}}$

CCCC	Chen *et al.* [8]	Present	FCFC	Chen *et al.* [8]	Present
1	0.3332	0.3332	1	0.2193	0.2193
2	0.5987	0.5987	2	0.2572	0.2572
3	0.5987	0.5987	3	0.3798	0.3798
4	0.7459	0.7459	4	0.3967	0.3967
5	0.7459	0.7459	5	0.5182	0.5182
6	0.8138	0.8138	6	0.5656	0.5656

To verify the results for MEE materials, Table 38 lists the first six non-dimensional frequencies for homogeneous plates of BBB or FFF under CCCC condition. Good agreement can be found in each case.

Table 38: The first six non-dimensional frequencies of square plates composed of BBB & FFF materials under CCCC condition, normalized by $\bar{\omega} = \omega a\sqrt{\rho_{max}/C_{max}}$

	the B material		the F material	
	Chen *et al.* [8]	Present	Chen *et al.* [8]	Present
1	1.7817	1.7817	1.3667	1.3667
2	2.9486	2.9486	2.2311	2.2311
3	2.9486	2.9486	2.2311	2.2311
4	3.2195	3.2195	2.7905	2.7905
5	3.2195	3.2195	2.2311	2.2311
6	3.7120	3.7120	2.9345	2.9345

6.2 SSSS Condition

Fixing the total thickness as h=0.3, the non-dimensional frequencies are calculated by $\bar{\omega} = \omega h\sqrt{\rho_{max}/c_{max}}$ and plotted with $\Omega = \bar{\omega}a^2\sqrt{\rho_{max}h/c_{max}}$. Using 3 terms in x and y associated with 12 layers, the fundamental frequency various with thickness ratio respect to five different material combinations is displayed in Figure 48. The same notation as for MEE composite beams, where ω_A is the value of a/h=30 for each stacking. From the figure, when slenderness ratio is 5, the reductions of these five materials are close to 10 percent.

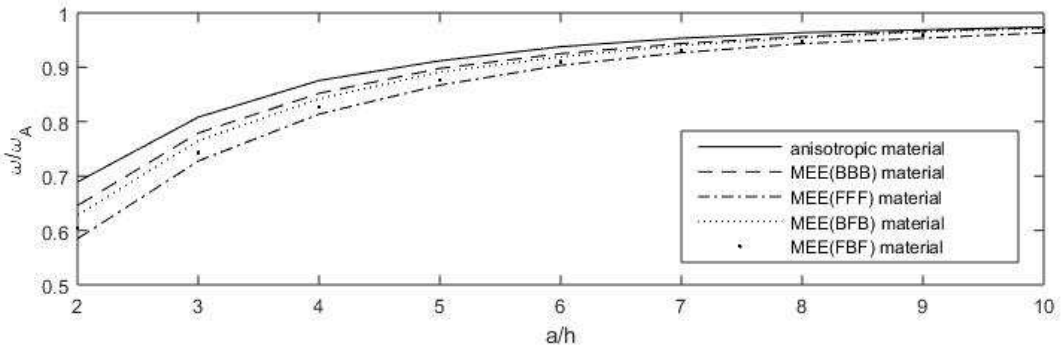

Figure 48: Differences of the fundamental frequency with five stacking sequences under SSSS conditions

According to the same slenderness, the order of the reduction ratio is FFF >FBF >BFB >BBB >Hex.

Figure 49 displays the influence of slenderness for the first six frequencies of hexagonal material and the corresponding mode shapes. The horizontal dashed lines indicate the asymptote of each frequency which is chozen as the value at a/h=30. Since the boundary condition is symmetric about the center, mode shapes are repeated(Mode 2: (2,1) & Mode 3: (1,2) and Mode 5: (1,3) & Mode 6: (3,1)) and the frequency lines are coincident for these modes. It is clear that the shape of each mode is similar to the same condition of isotropic plates.

Figures 50-53 show the frequency arrangement of the other four stacking sequences. The figurations are almost the same as the hexagonal material, except that the in-plane mode appears for the FBF sequence which is illustrated by a straight dashed line in Figure 53. By drawing a line perpendicular to the x axis, it is apparent that the appearance of order sequence is different for the FBF sequence. Using the same notation as mode shapes for isotropic plates, mode 6(3,1) comes after mode 7 which is a in-plane mode shape under this condition.

Tables 39-41 list the first six frequencies at a/h ratios of 10, 20 and 30, respectively. The corresponding difference percentages are given in Table 42. The same phenomenon occurs as shown in simply supported beams. With the increased amount of F material, the reductions also increase. For the a/h ratio larger than 20, the differences are within 3 percent.

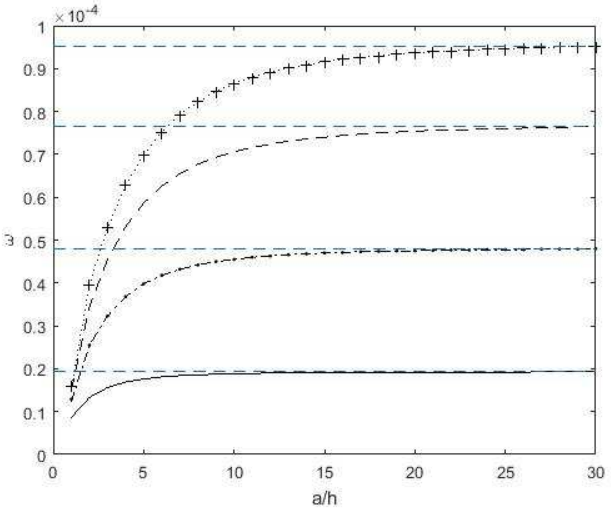

The influence of slenderness for the first six frequencies for plates with ansotropic materials under SSSS condition

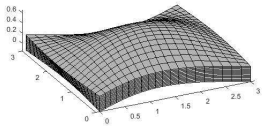

Mode 1

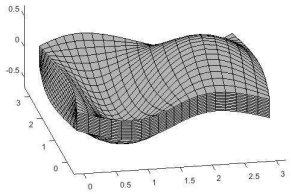

Mode 2

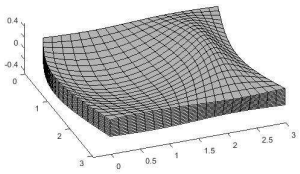

Mode 3

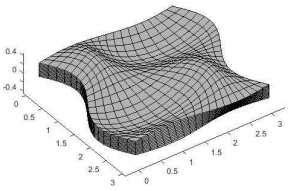

Mode 4

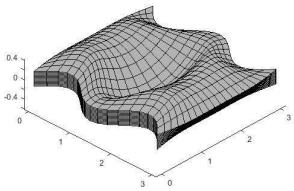

Mode 5

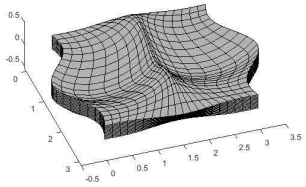

Mode 6

First six mode shapes for plates with ansotropic materials under SSSS condition

Figure 49: First six frequencies and mode shapes under SSSS condition

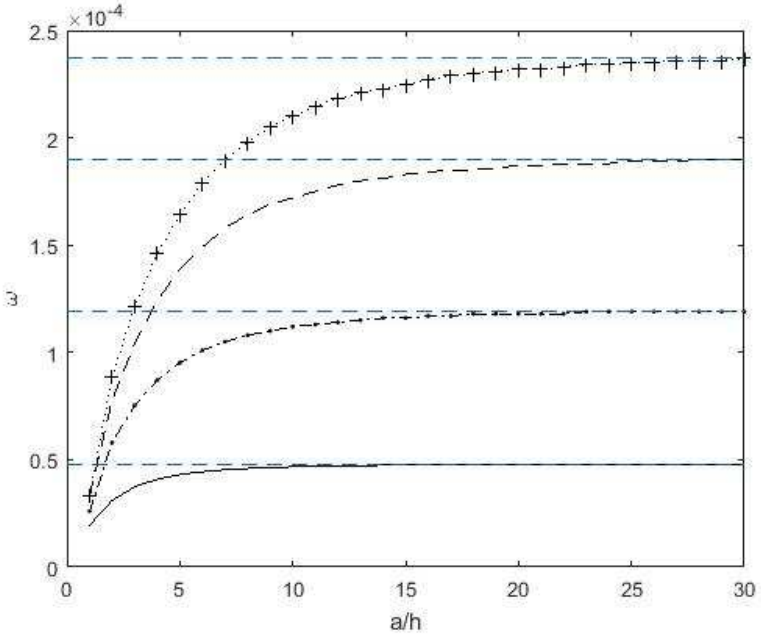

Figure 50: The influence of slenderness for the first six frequencies for plates with BBB materials under SSSS conditions

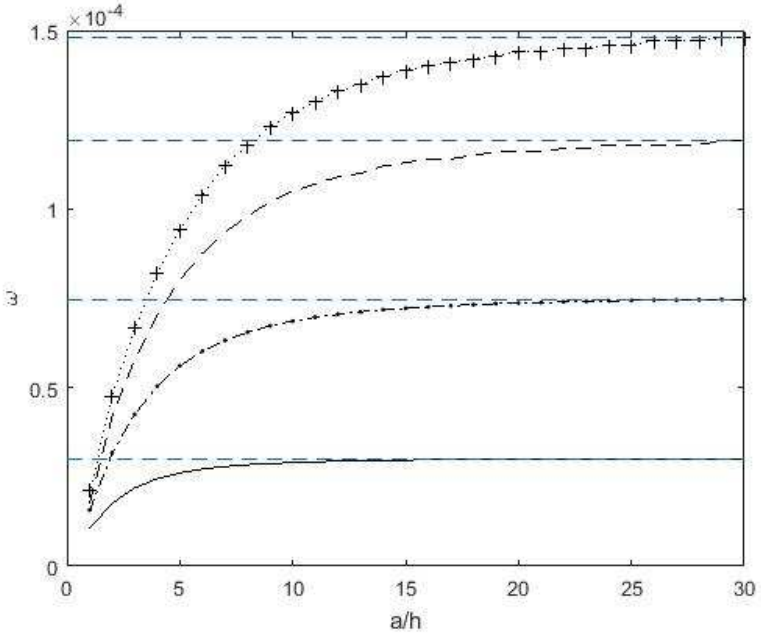

Figure 51: The influence of slenderness for the first six frequencies for plates with FFF materials under SSSS conditions

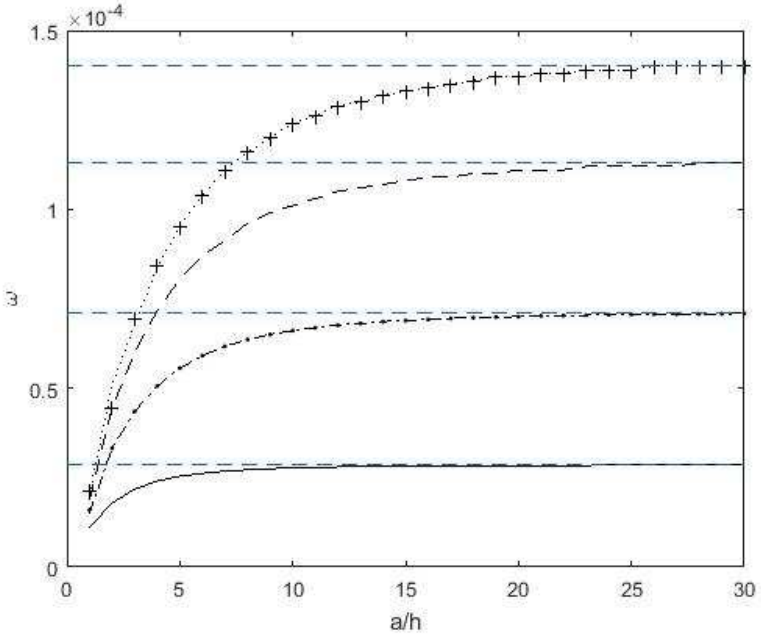

Figure 52: The influence of slenderness for the first six frequencies for plates with BFB materials under SSSS conditions

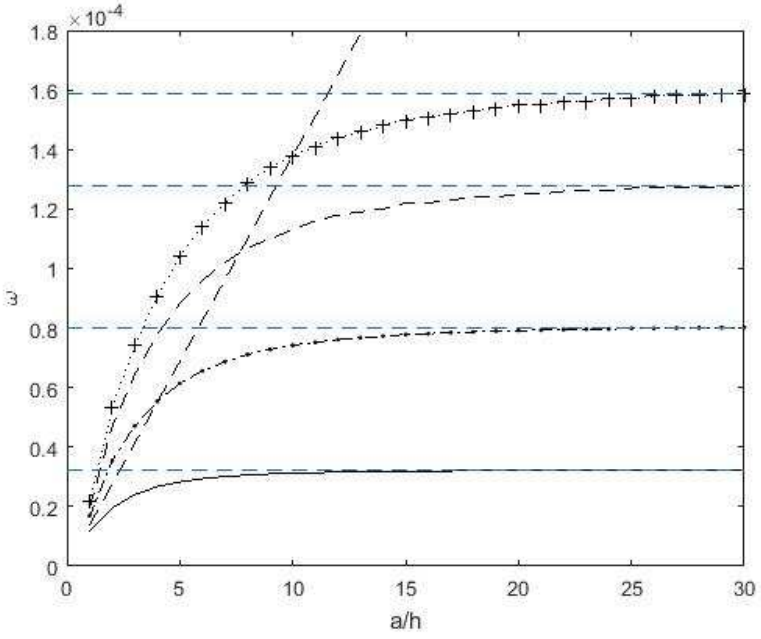

Figure 53: The influence of slenderness for the first seven frequencies for plates with FBF materials under SSSS conditions

Table 39: Frequencies for homogeneous plates composed of five stacking sequences under SSSS condition at a/h=10

Mode	Hex	BBB	FFF	BFB	FBF
1	1.88E-5	4.67E-5	2.90E-5	2.77E-5	3.12E-5
2	4.55E-5	1.12E-4	6.86E-5	6.61E-5	7.42E-5
3	4.55E-5	1.12E-4	6.86E-5	6.61E-5	7.42E-5
4	7.06E-5	1.72E-4	1.05E-4	1.01E-4	1.13E-4
5	8.65E-5	2.10E-4	1.27E-4	1.24E-4	1.38E-4
6	8.65E-5	2.10E-4	1.27E-4	1.24E-4	1.38E-4

Table 40: Frequencies for homogeneous plates composed of five stacking sequences under SSSS condition at a/h=20

Mode	Hex	BBB	FFF	BFB	FBF
1	1.92E-5	4.78E-5	2.99E-5	2.84E-5	3.21E-5
2	4.75E-5	1.18E-4	7.37E-5	7.00E-5	7.92E-5
3	4.75E-5	1.18E-4	7.37E-5	7.00E-5	7.92E-5
4	7.54E-5	1.87E-4	1.16E-4	1.11E-4	1.25E-4
5	9.37E-5	2.32E-4	1.44E-4	1.37E-4	1.55E-4
6	9.37E-5	2.32E-4	1.44E-4	1.37E-4	1.55E-4

Table 41: Frequencies for homogeneous plates composed of five stacking sequences under SSSS condition at a/h=30

Bending Mode	Hex	BBB	FFF	BFB	FBF
1	1.93E-5	4.80E-5	3.01E-5	2.85E-5	3.23E-5
2	4.80E-5	1.19E-4	7.47E-5	7.09E-5	8.02E-5
3	4.80E-5	1.19E-4	7.47E-5	7.09E-5	8.02E-5
4	7.64E-5	1.90E-4	1.19E-4	1.13E-4	1.28E-4
5	9.52E-5	2.37E-4	1.48E-4	1.40E-4	1.59E-4
6	9.52E-5	2.37E-4	1.48E-4	1.40E-4	1.59E-4

Table 42: Differences for homogeneous plates composed of five stacking sequences under SSSS condition

a/h	Bending frequency	% Differences below a/h=30 $\bar{\omega}$				
		Hexagonal	BBB	FFF	BFB	FBF
10	1	2.59	2.71	3.65	2.81	3.41
	2	5.21	5.88	8.17	6.77	7.48
	3	5.21	5.88	8.17	6.77	7.48
	4	7.59	9.47	11.76	10.62	11.72
	5	9.14	11.39	14.19	11.43	13.21
	6	9.14	11.39	14.19	11.43	13.21
20	1	0.52	0.42	0.66	0.35	0.62
	2	1.04	0.84	1.34	1.27	1.25
	3	1.04	0.84	1.34	1.27	1.25
	4	1.31	1.58	2.52	1.77	2.34
	5	1.58	2.11	2.70	2.14	2.52
	6	1.58	2.11	2.70	2.14	2.52

6.3 CCCC Condition

Group theory was used for this condition, with 4 terms used in both lateral directions with 12 sub-layer through the thickness. The differences of the first frequency with respect to the five stacking sequences are shown in Figure 54. The reductions are bigger than the all simply supported condition. Around slenderness of 10, differences can be less than 10 percent.

Figure 55 gives the first six frequencies as a function of a/h ratio and the corresponding mode shapes. It is clear that as the slenderness increases, the fifth and the sixth frequencies are identical.

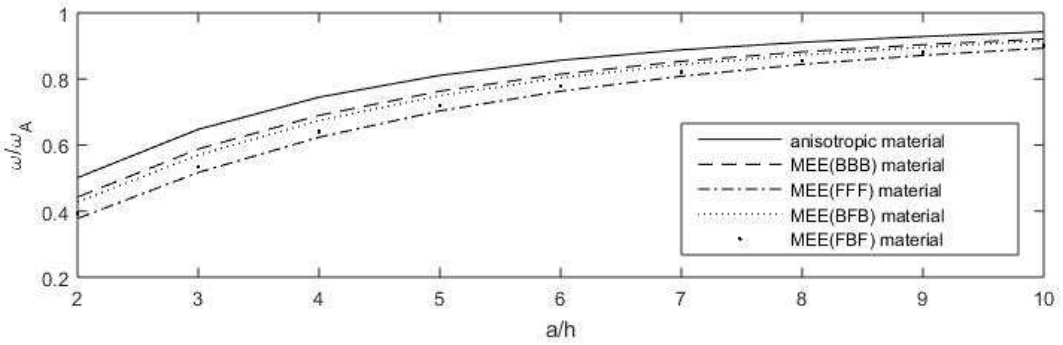

Figure 54: Differences of the fundamental frequency with five stacking sequences under CCCC conditions

Figures 56-59 show the effect of length-to-thickness ratio for the first six frequencies for other four stacking sequences under all-clamped conditions. The configuration of difference is similar to that of all simply supported condition. Frequencies are repeated and lines are coincident for mode 2 and 3. Otherwies, there is a litte difference for the fifth and sixth frequencies of the pure BBB and FFF materials. Hence, asymptotes of these two frequencies are slightly separated in Figures 56 and 57.

Tables 43-45 list the first six frequencies of the five stacking sequences under all-clamped condiiton with a/h are equal to 10, 20 and 30. Table 46 gives the percentage of difference according to five stacking sequences. The differences are larger for the higher frequencies at a/h=10. For the fifth frequency of FFF plates, the reduction is over 20 percent. Differences are reduced for the sixth frequency, which is quite apparent for the hexagonal material with a/h ratio of 20. It is caused by the occurrent order of mode shapes are changed for the higher frequencies at this point.

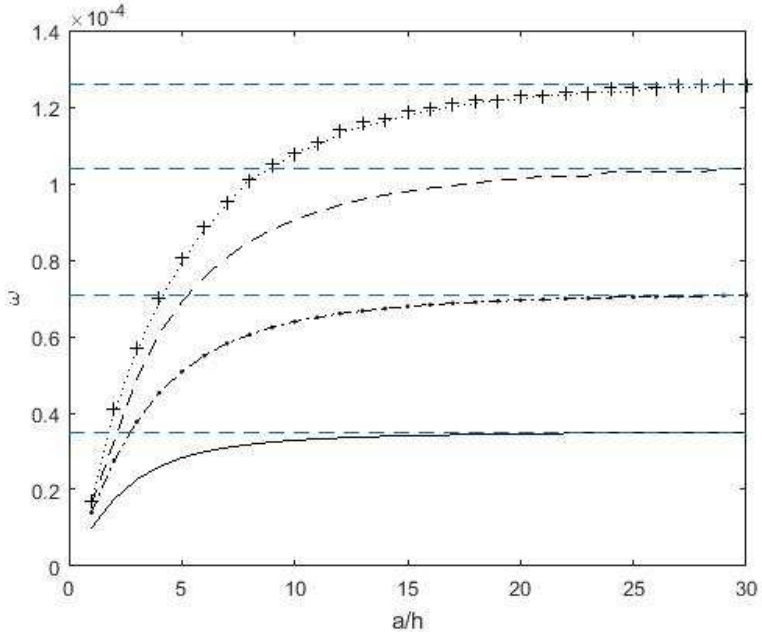

The influence of slenderness for the first six frequencies for plates with ansotropic materials under CCCC conditions

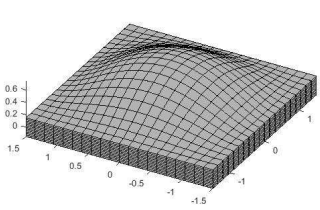

Mode 1

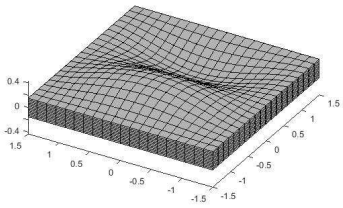

Mode 2

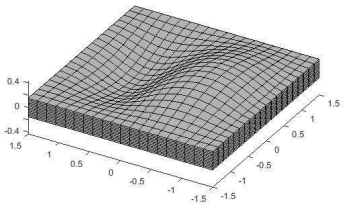

Mode 3

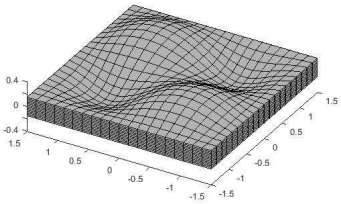

Mode 4

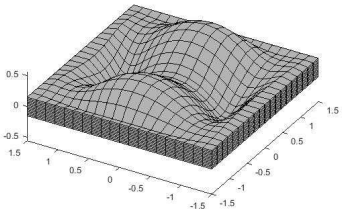

Mode 5

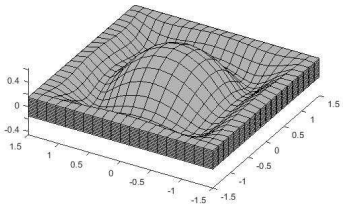

Mode 6

First six mode shapes for plates with ansotropic materials under CCCC conditions

Figure 55: First six frequencies and mode shapes under CCCC conditions

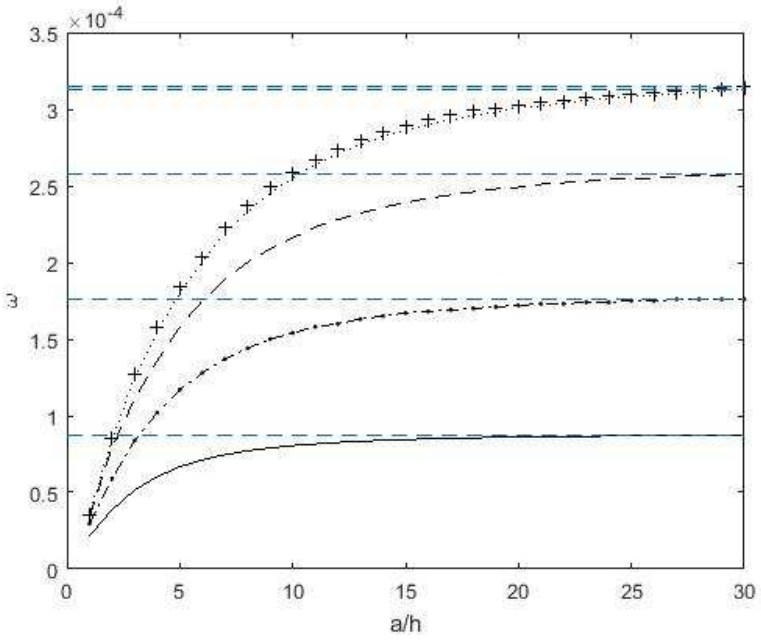

Figure 56: The influence of slenderness for the first six frequencies for plates with BBB materials under CCCC conditions

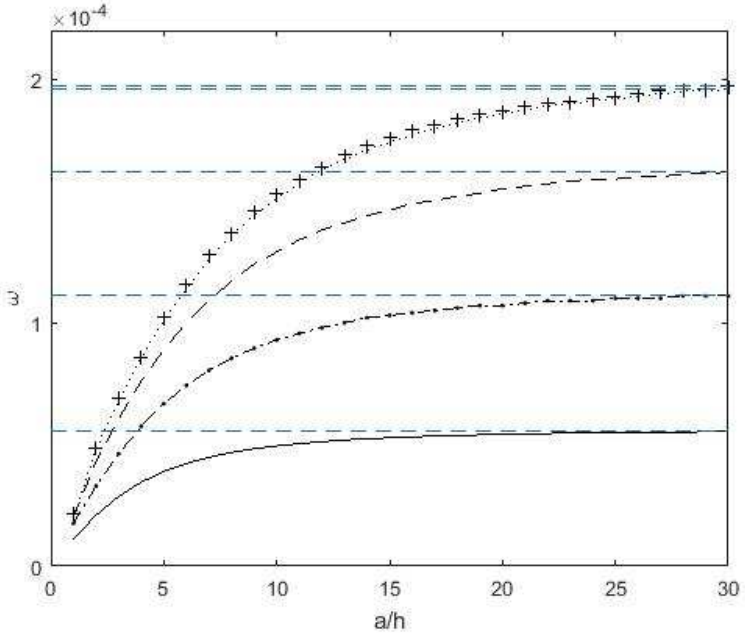

Figure 57: The influence of slenderness for the first six frequencies for plates with FFF materials under CCCC conditions

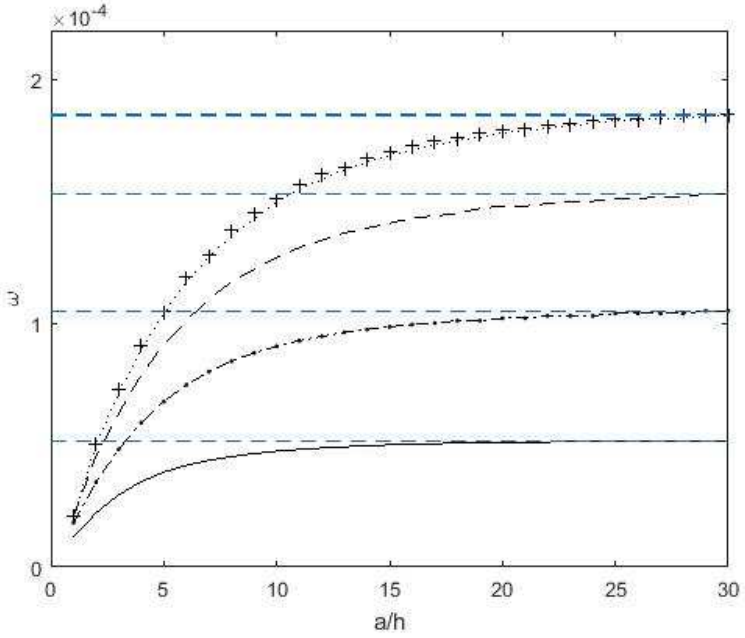

Figure 58: The influence of slenderness for the first six frequencies for plates with BFB materials under CCCC conditions

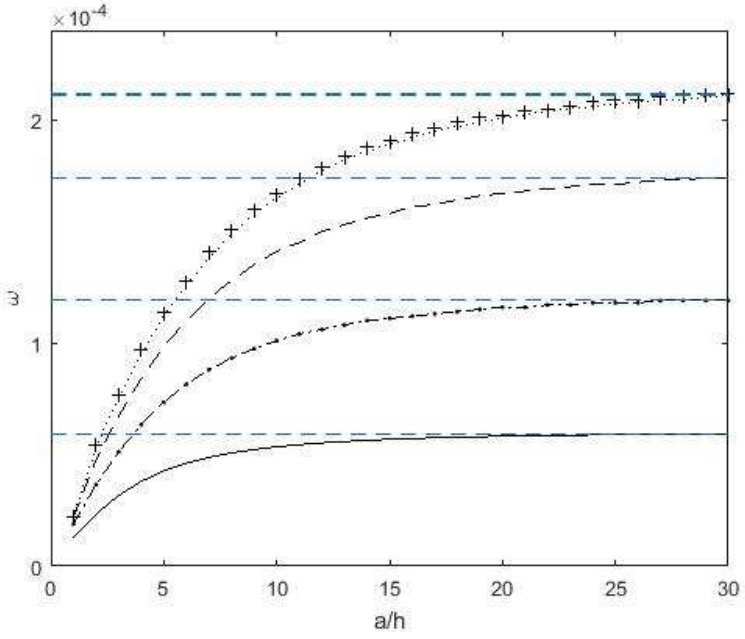

Figure 59: The influence of slenderness for the first six frequencies for plates with FBF materials under CCCC conditions

Table 43: Frequencies for homogeneous plates composed of five stacking sequences under CCCC condition at a/h=10

Mode	Hex	BBB	FFF	BFB	FBF
1	3.29E-5	8.05E-5	4.94E-5	4.75E-5	5.35E-5
2	6.39E-5	1.54E-4	9.29E-5	9.05E-5	1.01E-4
3	6.39E-5	1.54E-4	9.29E-5	9.05E-5	1.01E-4
4	9.05E-5	2.16E-4	1.29E-4	1.27E-4	1.41E-4
5	1.08E-4	2.55E-4	1.51E-4	1.50E-4	1.65E-4
6	1.08E-4	2.59E-4	1.53E-4	1.51E-4	1.67E-4

Table 44: Frequencies for homogeneous plates composed of five stacking sequences under CCCC condition at a/h=20

Mode	Hex	BBB	FFF	BFB	FBF
1	3.46E-5	8.61E-5	5.41E-5	5.11E-5	5.82E-5
2	6.95E-5	1.72E-4	1.07E-4	1.02E-4	1.16E-4
3	6.95E-5	1.72E-4	1.07E-4	1.02E-4	1.16E-4
4	1.01E-4	2.49E-4	1.55E-4	1.48E-4	1.67E-4
5	1.22E-4	3.01E-4	1.86E-4	1.78E-4	2.01E-4
6	1.23E-4	3.03E-4	1.87E-4	1.79E-4	2.02E-4

Table 45: Frequencies for homogeneous plates composed of five stacking sequences under CCCC condition at a/h=30

Bending Mode	Hex	BBB	FFF	BFB	FBF
1	3.49E-5	8.74E-5	5.53E-5	5.19E-5	5.93E-5
2	7.08E-5	1.76E-4	1.11E-4	1.05E-4	1.19E-4
3	7.08E-5	1.76E-4	1.11E-4	1.05E-4	1.19E-4
4	1.04E-5	2.58E-4	1.62E-4	1.53E-4	1.74E-4
5	1.26E-4	3.13E-4	1.96E-4	1.85E-4	2.11E-4
6	1.26E-4	3.15E-4	1.97E-4	1.86E-4	2.12E-4

Table 46: Differences for homogeneous plates composed of five stacking sequences under CCCC conditions

a/h	Bending frequency	% Differences below a/h=30 $\bar{\omega}$				
		Hexagonal	BBB	FFF	BFB	FBF
10	1	5.73	7.89	10.67	8.48	9.78
	2	9.75	12.50	16.31	13.81	15.13
	3	9.75	12.50	16.31	13.81	15.13
	4	12.98	16.28	20.37	16.99	18.97
	5	14.29	18.53	22.96	18.92	21.80
	6	14.29	17.78	22.34	18.82	21.23
20	1	0.86	1.49	2.17	1.54	1.85
	2	1.84	2.27	3.60	2.86	2.52
	3	1.84	2.27	3.60	2.86	2.52
	4	2.88	3.49	4.32	3.27	4.02
	5	3.17	3.83	5.10	3.78	4.74
	6	2.38	3.81	5.08	3.76	4.72

6.4 FCFC Condition

Using a total of 16 in-plane terms and 12 layers, Figure 60 demonstrates the difference of the basic frequency for these five sequences under FCFC condition. Comparing with the previous conditions, reductions are much larger and frequency lines are more scattered under lateral boundary conditions.

Figure 61 gives the first seven frequencies of homogeneous plates made of hexagonal materials under FCFC condition and the first six corresponding mode shapes. For the first six frequencies, in-plane mode 6 which is indicated as a straight dashed line starts to appear in this condition. With lower slenderness, frequencies are more close to each other, while with large a/h ratios frequency lines are well separated. Two frequency lines relatively close

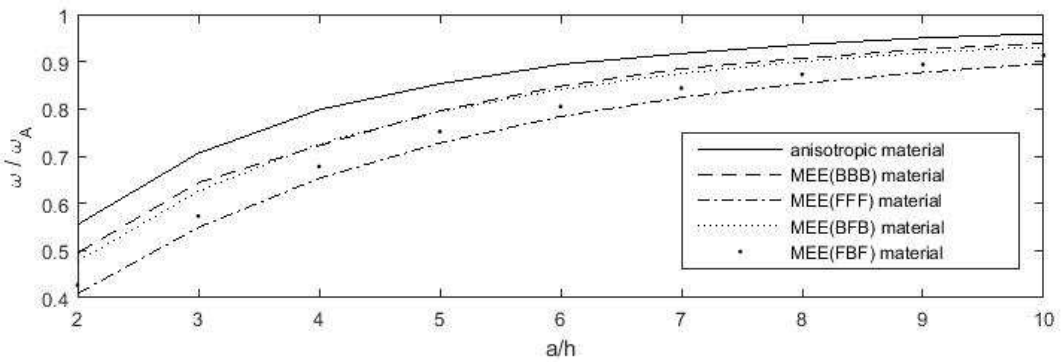

Figure 60: Differences of the fundamental frequency with five stacking sequences under FCFC condiitons

to each other represent the bending and torsional modes along the fixed-fixed edges, while the little separate lines are the bending modes along free edges.

Figures 62-65 show the influence of a/h ratio for the following four stacking sequences. Except for the order in sequence the arrangement of frequencies and mode shapes are almost the same as those of hexagonal materials.

Tables 47 and 48 give the values of the first seven mode frequencies according to these five materials at slenderness of 10 and 20, respectively. The order of these values are given as frequencies appear in sequences at a/h=10 ratio. Table 49 only gives the bending frequency values at a/h ratio of 30. Table 50 lists the difference of five stacking MEE plates under FCFC condition. Differences are increased gradually in this case. Reductions are smaller for the piezoelectric and piezomagnetic plates in the sixth frequency. This is apparent from the different curvature of each frequency lines. As a/h ratios approach 20, the percentages differences are within 5 percent.

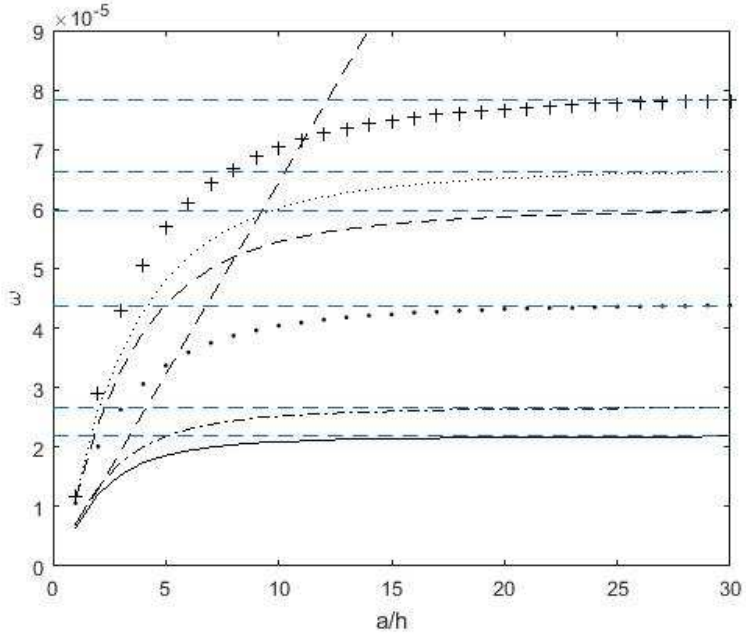

The influence of slenderness for the first seven frequencies for plates with anisotropic materials under FCFC conditions

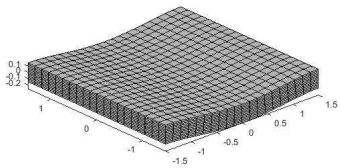

Mode 1

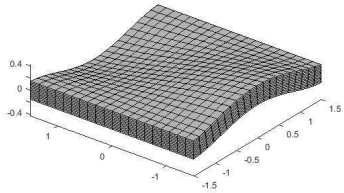

Mode 2

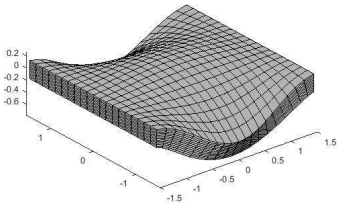

Mode 3

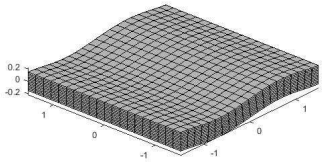

Mode 4

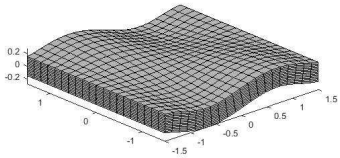

Mode 5

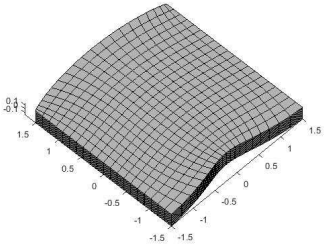

Mode 6

First six mode shapes for plates with anisotropic materials under FCFC conditions

Figure 61: First seven frequencies and first six mode shapes under FCFC conditions

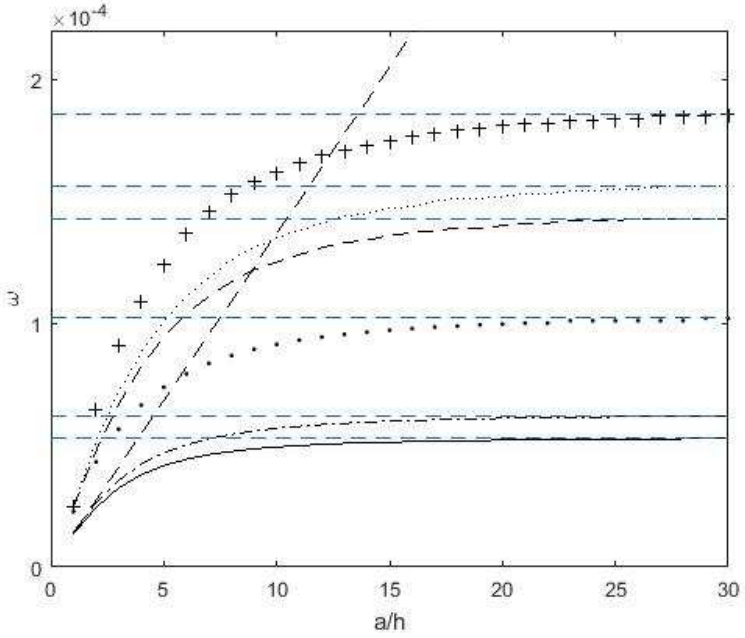

Figure 62: The influence of slenderness for the first six frequencies for plates with BBB materials under FCFC conditions

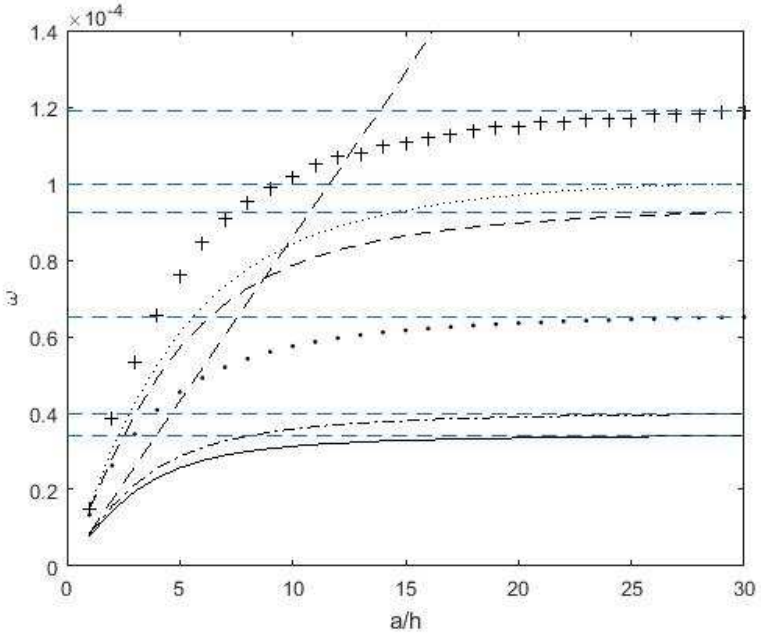

Figure 63: The influence of slenderness for the first six frequencies for plates with FFF materials under FCFC conditions

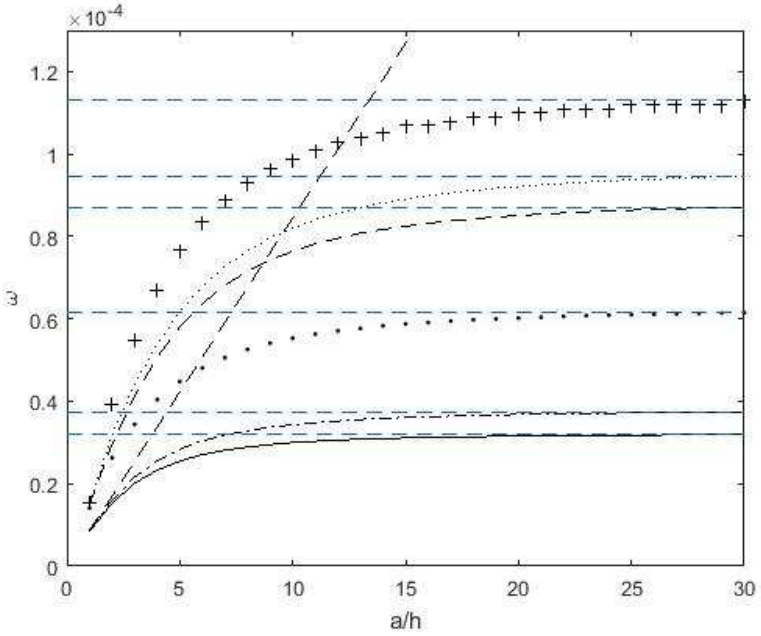

Figure 64: The influence of slenderness for the first six frequencies for plates with BFB materials under FCFC conditions

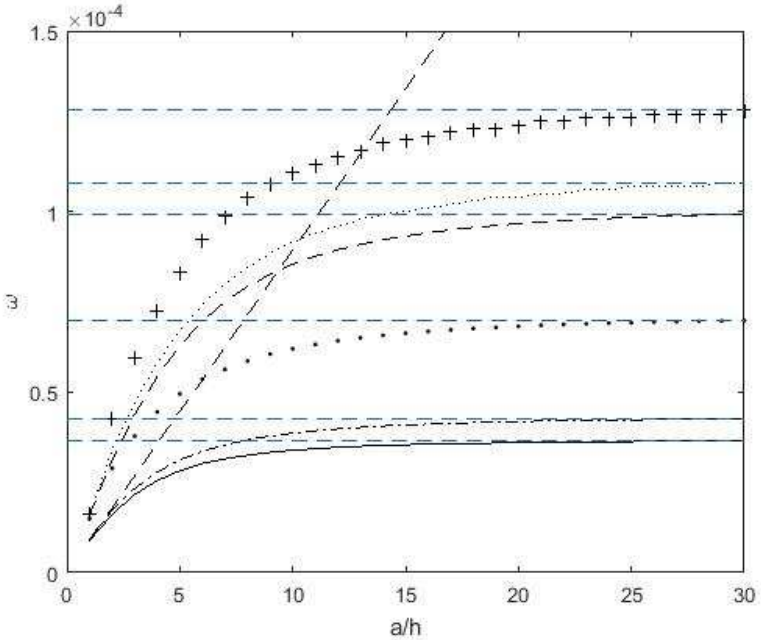

Figure 65: The influence of slenderness for the first six frequencies for plates with FBF materials under FCFC conditions

Table 47: Frequencies for homogeneous plates composed of five stacking sequences under FCFC condition at a/h=10

Mode	Hex	BBB	FFF	BFB	FBF
1	2.09E-5	4.92E-5	3.13E-5	3.00E-5	3.39E-5
2	2.52E-5	5.69E-5	3.58E-5	3.43E-5	3.86E-5
3	4.04E-5	9.13E-5	5.75E-5	5.53E-5	6.20E-5
4	5.45E-5	1.25E-4	7.86E-5	7.64E-5	8.54E-5
5	6.01E-5	1.35E-4	8.43E-5	8.20E-5	9.15E-5
6	6.44E-5	1.37E-4	8.60E-5	8.45E-5	8.93E-5
7	7.04E-5	1.62E-4	1.02E-4	9.89E-5	1.11E-4

Table 48: Frequencies for homogeneous plates composed of five stacking sequences under FCFC condition at a/h=20

Mode	Hex	BBB	FFF	BFB	FBF
1	2.16E-5	5.20E-5	3.35E-5	3.16E-5	3.60E-5
2	2.64E-5	6.10E-5	3.90E-5	3.68E-5	4.18E-5
3	4.32E-5	9.96E-5	6.35E-5	6.02E-5	6.82E-5
4	5.87E-5	1.40E-4	8.97E-5	8.51E-5	9.66E-5
5	6.52E-5	1.52E-4	9.70E-5	9.21E-5	1.04E-4
6	1.19E-4	2.67E-4	1.70E-4	1.66E-4	1.79E-4
7	7.68E-5	1.81E-4	1.15E-4	1.10E-4	1.24E-4

Table 49: Frequencies for homogeneous plates composed of five stacking sequences under FCFC condition at a/h=30

Bending Mode	Hex	BBB	FFF	BFB	FBF
1	2.18E-5	5.26E-5	3.40E-5	3.19E-5	3.65E-5
2	2.66E-5	6.20E-5	3.97E-5	3.74E-5	4.26E-5
3	4.38E-5	1.02E-4	6.51E-5	6.15E-5	6.98E-5
4	5.96E-5	1.43E-4	9.24E-5	8.71E-5	9.93E-5
5	6.63E-5	1.56E-4	1.00E-4	9.46E-5	1.08E-4
6	7.84E-5	1.86E-4	1.19E-4	1.13E-4	1.28E-4

Table 50: Differences for homogeneous plates composed of five stacking sequences under FCFC conditions

a/h	Bending frequency	% Differences below a/h=30 $\bar{\omega}$				
		Hexagonal	BBB	FFF	BFB	FBF
10	1	4.13	6.46	7.94	5.96	7.12
	2	5.26	8.23	9.82	8.29	9.39
	3	7.76	10.49	11.67	10.08	11.17
	4	8.56	12.59	14.94	12.28	14.00
	5	9.35	13.46	15.70	13.32	15.28
	6	10.20	12.90	14.29	12.48	13.28
20	1	0.92	1.14	1.47	0.94	1.37
	2	0.75	1.61	1.76	1.60	1.88
	3	1.37	2.35	2.46	2.11	2.29
	4	1.51	2.10	2.92	2.30	2.72
	5	1.66	2.56	3.00	2.64	3.70
	6	2.04	2.69	3.36	2.65	3.12

6.5 CFFF Condition

As an extension of cantilever beams, cantilever plates are also an important case for plates. Four terms are used in both x and y directions with 3 layers through the thickness. Figure 66 shows the difference of these five stacking sequences respect to the fundamental frequency. Reductions are less variable under this condition. BFB material has the biggest difference. Even with a/h=10 BFB material still maintains a 5 percent reduction.

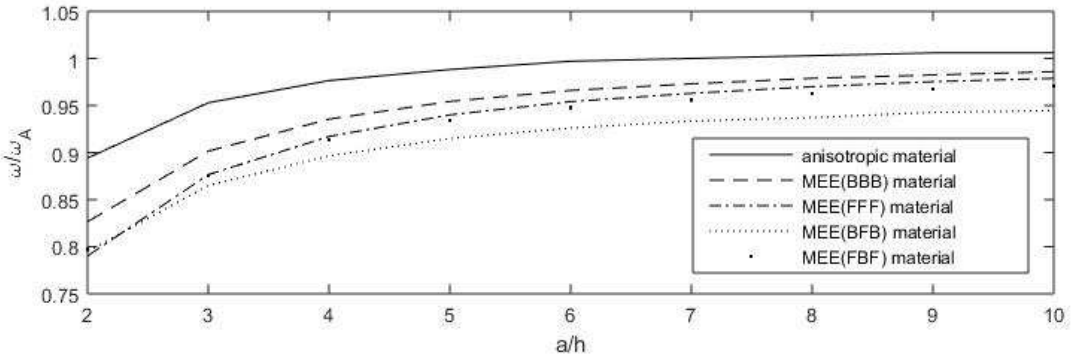

Figure 66: Differences of the fundamental frequency with five stacking sequences under CFFF conditions

Figure 67 displays the first eight frequencies as a function of a/h ratio and the first six mode shapes under CFFF condition. The straight dashed lines represent the in-plane modes. The mode shapes are almost the same as isotropic plates under this boundary condition. Figures 68-71 give the configuration of frequencies of the other four stacking sequences. The lines of the fourth and fifth frequencies are identical with large slenderness. Tables 51 and 52 show at fixing a/h of 10 and 20, the values of first eight frequencies with respect to these five materials. Table 53 lists the frequency values of the first six bending modes at a/h=30. Table 54 demonstrates the differences of these five stacking plates under frequencies at length-to-thickness ratio of 30. Differences are quite small for this condition. The percent difference are below 10 percent even up to the fifth frequency with a/h=10.

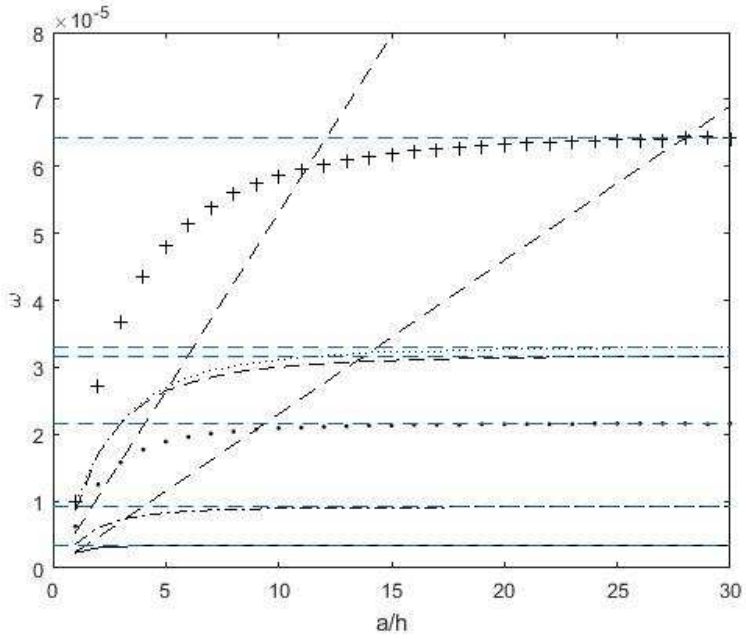

The influence of slenderness for the first eight frequencies for plates with anisotropic materials under CFFF condition

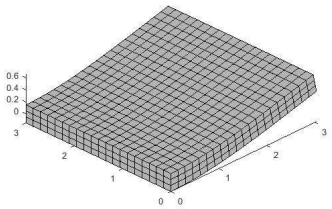

Mode 1

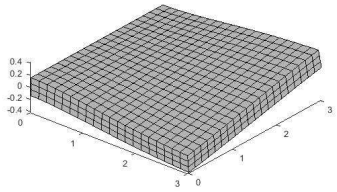

Mode 2

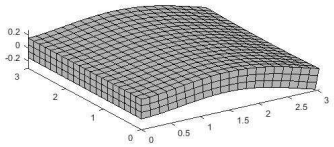

Mode 3

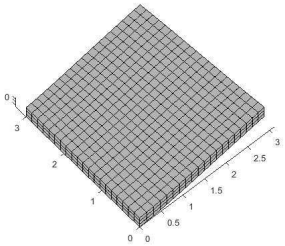

Mode 4

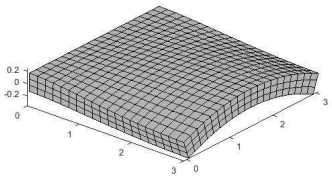

Mode 5

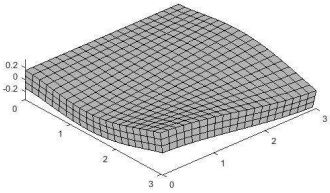

Mode 6

First six mode shapes for plates with anisotropic materials under CFFF condition

Figure 67: First eight frequencies and first six mode shapes under CFFF condition

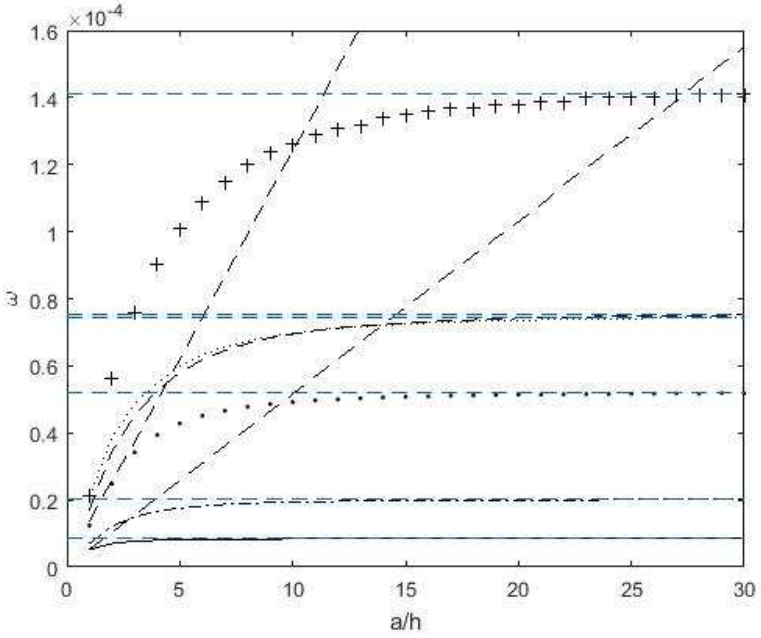

Figure 68: The influence of slenderness for the first six frequencies for plates with BBB materials under CFFF condition

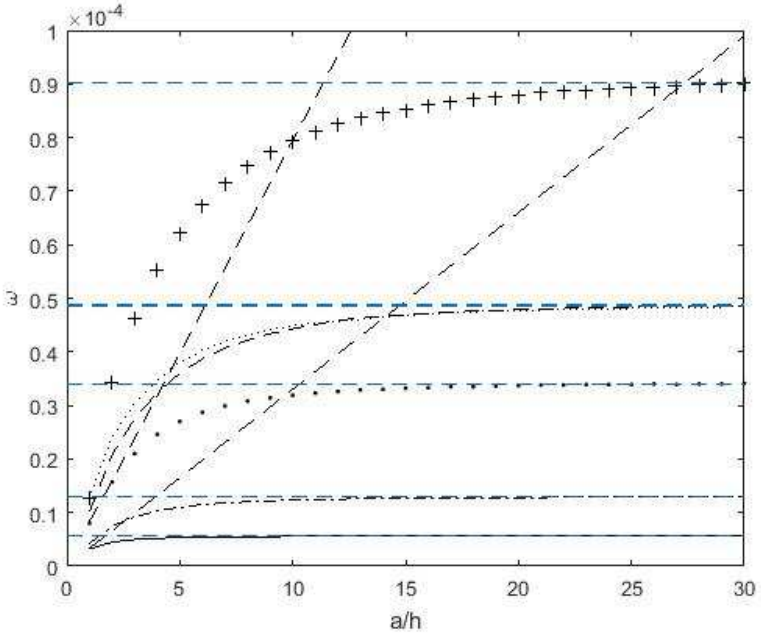

Figure 69: The influence of slenderness for the first six frequencies for plates with FFF materials under CFFF condition

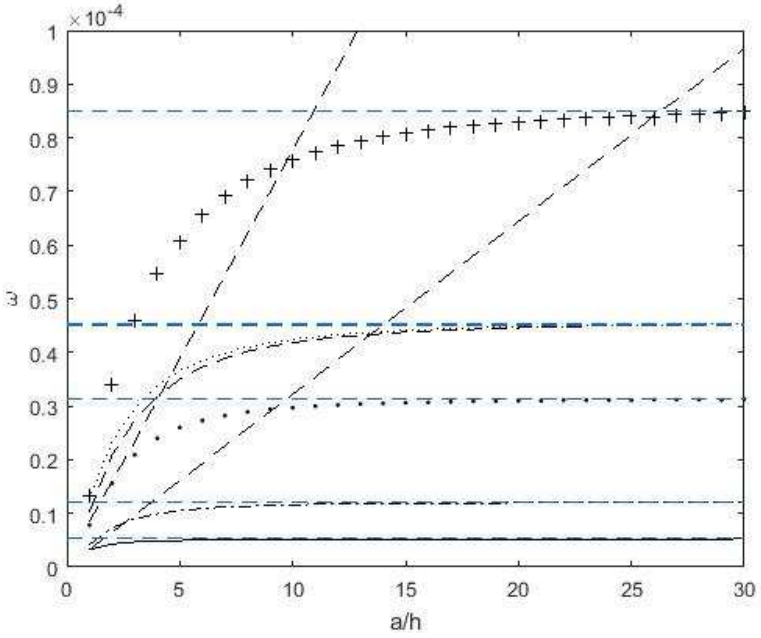

Figure 70: The influence of slenderness for the first six frequencies for plates with BFB materials under CFFF condition

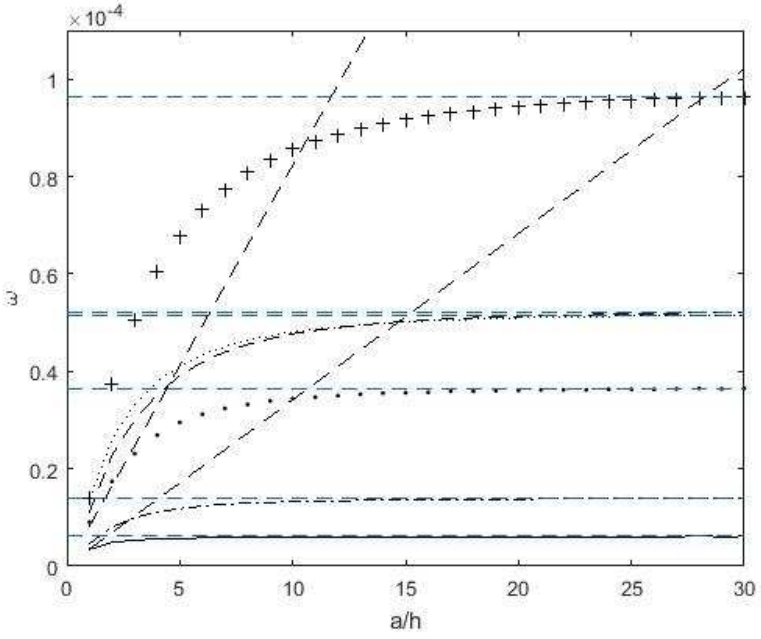

Figure 71: The influence of slenderness for the first six frequencies for plates with FBF materials under CFFF condition

When length-to-thickness ratio is 20, even for the sixth frequency reductions are nearly 2 percent. And since modes change sequence order, such as mode 5 and mode 6, differences for the forth bending frequency are larger than those of the fifth bending frequency.

Table 51: Frequencies for homogeneous plates composed of five stacking sequences under CFFF condition at a/h=10

Mode	Hex	BBB	FFF	BFB	FBF
1	3.42E-6	8.41E-6	5.55E-6	5.11E-6	5.93E-6
2	8.91E-6	1.94E-5	1.23E-5	1.16E-5	1.32E-5
3	2.09E-5	4.92E-5	3.19E-5	2.97E-5	3.42E-5
4	2.30E-5	5.16E-5	3.30E-5	3.22E-5	3.44E-5
5	3.00E-5	6.95E-5	4.43E-5	4.18E-5	4.77E-5
6	3.11E-5	6.97E-5	4.49E-5	4.24E-5	4.81E-5
7	5.31E-5	1.24E-4	7.95E-5	7.60E-5	8.23E-5
8	5.87E-5	1.26E-4	7.95E-5	7.77E-5	8.57E-5

Table 52: Frequencies for homogeneous plates composed of five stacking sequences under CFFF condition at a/h=20

Mode	Hex	BBB	FFF	BFB	FBF
1	3.44E-6	8.50E-6	5.65E-6	5.17E-6	6.02E-6
2	9.12E-6	2.00E-5	1.28E-5	1.20E-5	1.37E-5
3	2.15E-5	5.14E-5	3.37E-5	3.10E-5	6.83E-5
4	4.60E-5	1.03E-4	6.60E-5	6.44E-5	3.61E-5
5	3.14E-5	7.42E-5	4.79E-5	4.46E-5	5.13E-5
6	3.27E-5	7.36E-5	4.77E-5	4.48E-5	5.10E-5
7	1.06E-4	2.48E-4	1.59E-4	8.30E-5	1.65E-4
8	6.33E-5	1.38E-4	8.80E-5	1.55E-4	9.44E-5

3

Table 53: Frequencies for homogeneous plates composed of five stacking sequences under CFFF condition at a/h=30

Bending Mode	Hex	BBB	FFF	BFB	FBF
1	3.44E-6	8.53E-6	5.67E-6	5.41E-6	6.11E-6
2	9.16E-6	2.01E-5	1.29E-5	1.20E-5	1.38E-5
3	2.16E-5	5.18E-5	3.41E-5	3.13E-5	3.65E-5
4	3.17E-5	7.52E-5	4.87E-5	4.50E-5	5.21E-5
5	3.30E-5	7.45E-5	4.84E-5	4.52E-5	5.15E-5
6	6.43E-5	1.41E-4	9.01E-5	8.49E-5	9.65E-5

Table 54: Frequencies for homogeneous plates composed of five stacking sequences under CFFF condition

a/h	Bending frequency	% Differences below a/h=30 $\bar{\omega}$				
		Hexagonal	BBB	FFF	BFB	FBF
10	1	1.16	1.41	2.12	5.55	2.95
	2	2.73	3.48	4.65	3.33	4.35
	3	3.24	5.02	6.45	5.11	5.75
	4	5.36	7.58	9.03	7.11	8.45
	5	5.76	6.44	7.23	6.19	6.60
	6	8.71	10.64	11.76	10.48	11.19
20	1	0.58	0.35	0.35	4.44	1.47
	2	0.44	0.50	0.78	0.00	0.72
	3	0.46	0.77	1.17	0.96	1.10
	4	0.95	1.33	1.64	0.89	1.54
	5	0.91	1.21	1.45	0.88	0.97
	6	1.56	2.13	2.33	2.24	2.18

6.6 CCFF Condition

With 4 terms used in x and y with 3 sub-layers, Figure 72 demonstrates the reduction for the basic frequency various with a/h ratio. At a/h ratio around 6, percent difference can within 10 percent for each material.

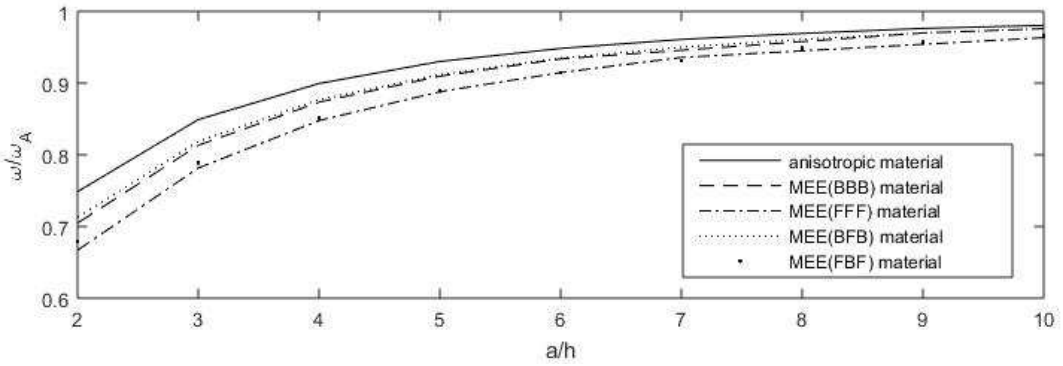

Figure 72: Differences of the fundamental frequency with five stacking sequences under CCFF conditions

Figure 73 shows the first nine frequencies and the first six mode shapes of the plates made of anisotropic materials under CCFF condition. More in-plane modes appear within these bending frequencies. Figures 74-77 give the influence of slenderness for the first nine frequencies for the rest four stacking sequences. The fifth frequency and the sixth frequency are well separated in these cases.

Tables 55 and 56 list the corresponding frequencies according to the sequence of these frequencies fixing an a/h ratio of 10. Table 57 illustrates the first six bending frequencies' values for the five material combinations, while Table 58 shows differences below these values respect to plates composed of five stacking sequences. It is apparent that there is a large reduction for the fifth frequency. Even as a/h is equal to 20, the reductions are still over 5 percent.

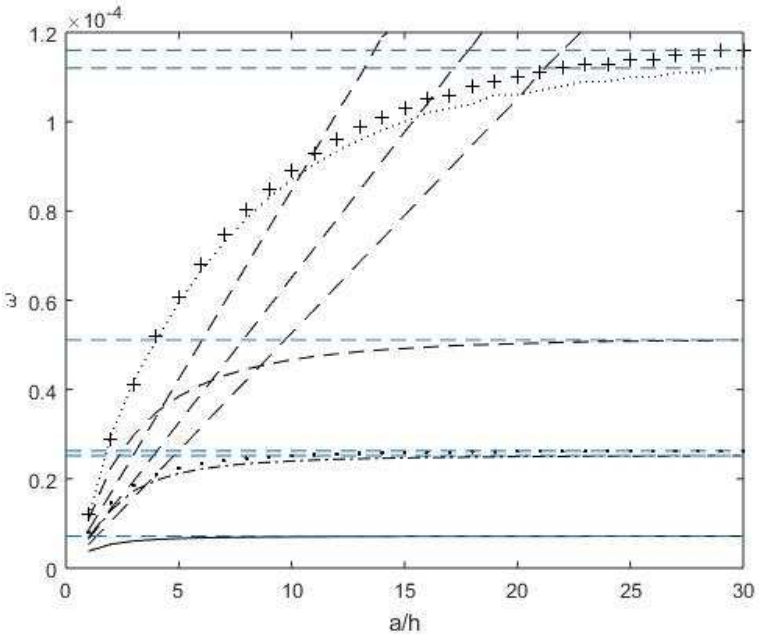

The influence of slenderness for the first nine frequencies for plates with anisotropic materials under CCFF condition

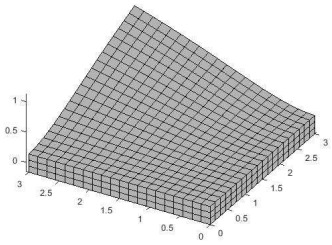

Mode 1

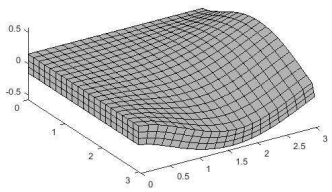

Mode 2

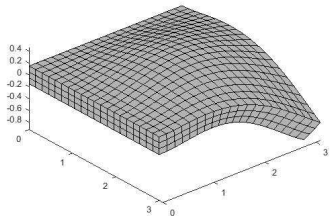

Mode 3

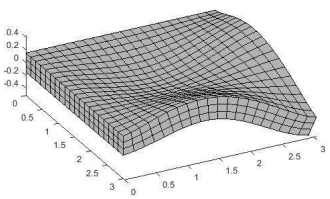

Mode 4

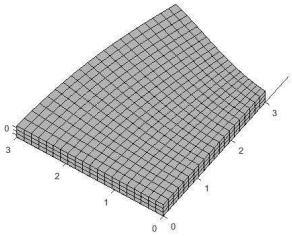

Mode 5

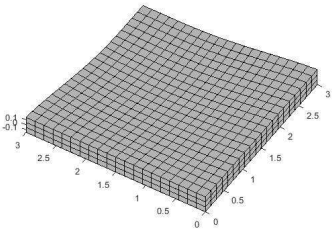

Mode 6

First six mode shapes for plates with FBF materials under CCFF condition

Figure 73: First nine frequencies and first six mode shapes under CCFF condition

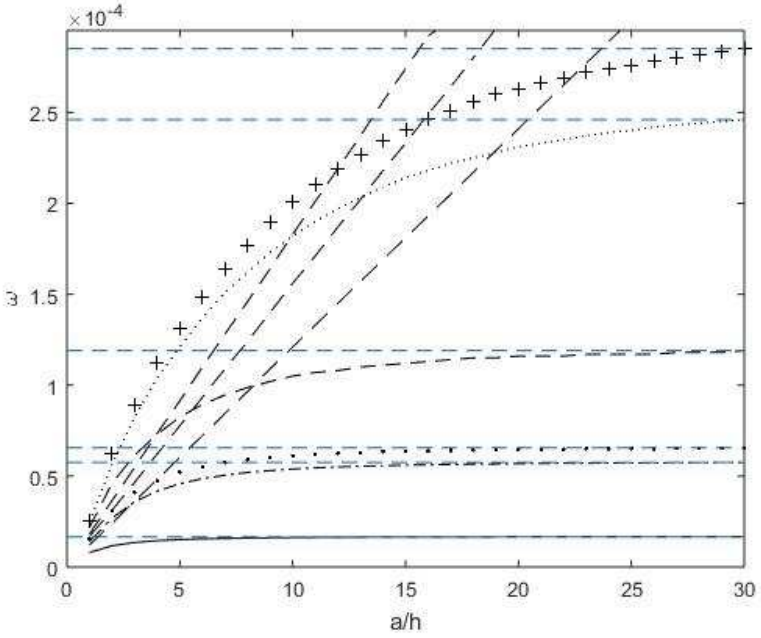

Figure 74: The influence of slenderness for the first nine frequencies for plates with BBB materials under CCFF condition

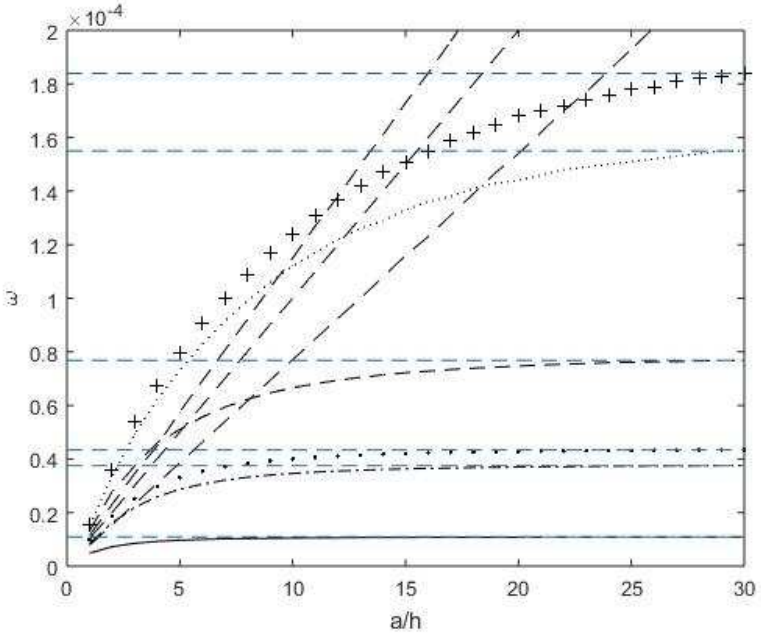

Figure 75: The influence of slenderness for the first six frequencies for plates with FFF materials under CCFF condition

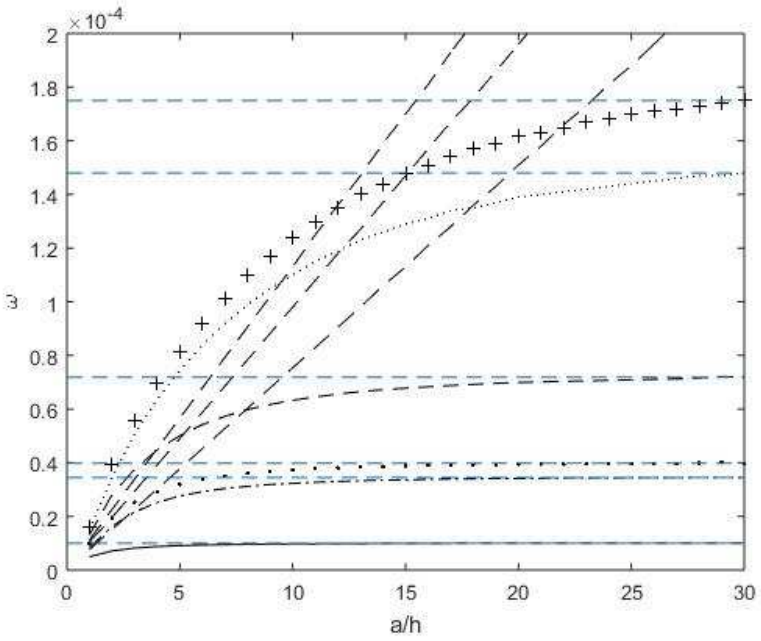

Figure 76: The influence of slenderness for the first six frequencies for plates with BFB materials under CCFF condition

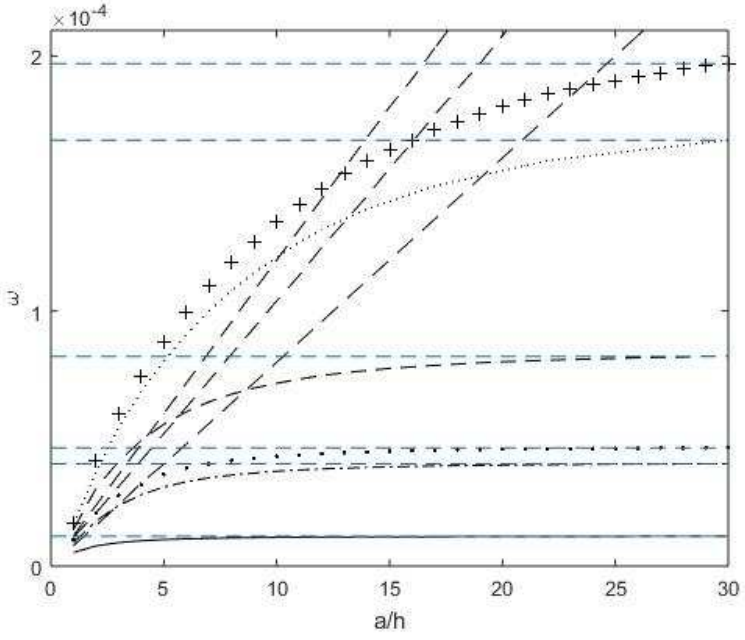

Figure 77: The influence of slenderness for the first six frequencies for plates with FBF materials under CCFF condition

Table 55: Frequencies for homogeneous plates composed of five stacking sequences under CCFF condition at a/h=10

Mode	Hex	BBB	FFF	BFB	FBF
1	7.02E-6	1.62E-5	1.05E-5	9.75E-6	1.13E-5
2	2.40E-5	5.39E-5	3.46E-5	3.23E-5	3.72E-5
3	2.52E-5	6.12E-5	4.00E-5	3.73E-5	4.31E-5
4	4.67E-5	1.05E-4	6.66E-5	6.33E-5	7.17E-5
5	5.27E-5	1.21E-4	7.71E-5	7.54E-5	7.99E-5
6	6.51E-5	1.56E-4	1.00E-4	9.80E-5	1.04E-4
7	8.47E-5	1.82E-4	1.12E-4	1.10E-4	1.20E-4
8	8.70E-5	1.83E-4	1.15E-4	1.13E-4	1.21E-4
9	8.92E-5	2.01E-4	1.24E-4	1.24E-4	1.35E-4

Table 56: Frequencies for homogeneous plates composed of five stacking sequences under CCFF condition at a/h=20

Mode	Hex	BBB	FFF	BFB	FBF
1	7.14E-6	1.66E-5	1.08E-5	9.98E-6	1.16E-5
2	2.50E-5	5.69E-5	3.70E-5	3.41E-5	3.96E-5
3	2.62E-5	6.46E-5	4.28E-5	3.94E-5	4.58E-5
4	5.03E-5	1.16E-4	7.47E-5	6.99E-5	8.01E-5
5	1.05E-4	2.41E-4	1.54E-4	1.51E-4	1.60E-4
6	1.30E-4	3.11E-4	2.00E-4	1.96E-4	2.08E-4
7	1.69E-4	2.31E-4	1.44E-4	1.39E-4	2.39E-4
8	1.06E-4	3.65E-4	2.31E-4	2.26E-4	1.55E-4
9	1.10E-4	2.63E-4	1.68E-4	1.62E-4	1.80E-4

Table 57: Frequencies for homogeneous plates composed of five stacking sequences under CCFF condition at a/h=30

Bending Mode	Hex	BBB	FFF	BFB	FBF
1	7.16E-6	1.66E-5	1.09E-5	9.99E-6	1.17E-5
2	2.52E-5	5.75E-5	3.75E-5	3.45E-5	4.01E-5
3	2.63E-5	6.56E-5	4.34E-5	3.98E-5	4.64E-5
4	5.11E-5	1.19E-4	7.68E-5	7.19E-5	8.22E-5
5	1.12E-4	2.46E-4	1.55E-4	1.48E-4	1.67E-4
6	1.16E-4	2.85E-4	1.84E-4	1.75E-4	1.97E-4

Table 58: Differences for homogeneous plates composed of five stacking sequences

a/h	Bending frequency	% Differences below a/h=30 $\bar{\omega}$				
		Hexagonal	BBB	FFF	BFB	FBF
10	1	1.96	2.41	3.67	2.40	3.42
	2	4.76	6.26	7.73	6.38	7.23
	3	4.18	6.71	7.83	6.28	7.11
	4	8.61	11.76	13.28	11.96	12.77
	5	22.32	26.02	27.74	25.68	27.54
	6	23.10	29.47	32.61	29.14	31.47
20	1	0.28	0.00	0.92	0.10	0.85
	2	0.79	1.04	1.33	1.16	1.25
	3	0.38	1.52	1.38	1.01	1.29
	4	1.57	2.52	2.73	2.78	2.55
	5	5.36	6.10	7.10	6.08	7.19
	6	5.17	7.72	8.70	7.43	8.63

6.7 SFSF Condition

Keeping 4 terms in two lateral directions and 12 layers, Figure 78 shows the difference of the fundamental frequency of five MEE composite materials. The configuration is similar to the all simply supported condition; however, reductions are slightly small with lower slenderness.

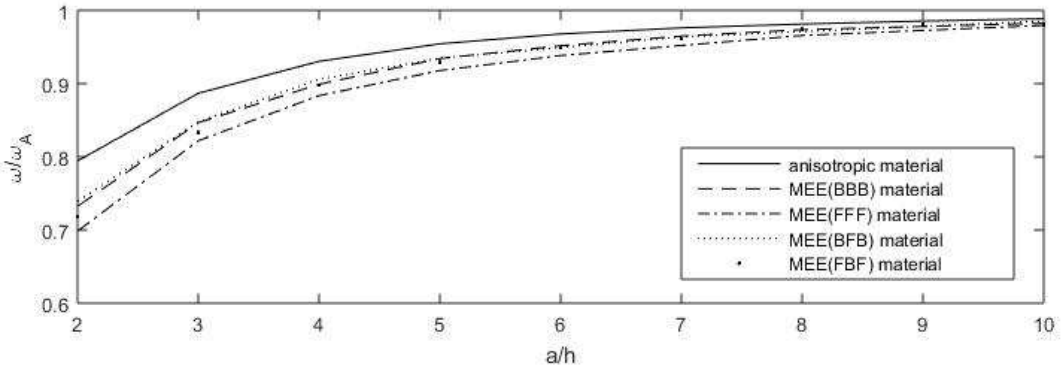

Figure 78: Differences of the fundamental frequency with five stacking sequences under SFSF conditions

Figure 79 demonstrates the configuration of the first seven frequencies and the first six modes of anisotropic materials under SFSF condition. The distribution of bending frequency lines are in a series of cascades, while the straight dashed line is corresponding to the in-plane mode 6. Figures 80-83 show the configuration of frequency lines for the following four materials. The arrangement of frequency lines are almost the same as those for anisotropic plates, except that the difference between the third and fourth bending frequencies which are the bending mode along simply supported edges and the bending mode along free edges are much smaller. Tables 59 and 60 give the frequency values with respect to the above figures at a/h=10 and 20. And Table 61 lists the first six bending frequencies of five stacking sequences at fixing a/h ratio is 30.

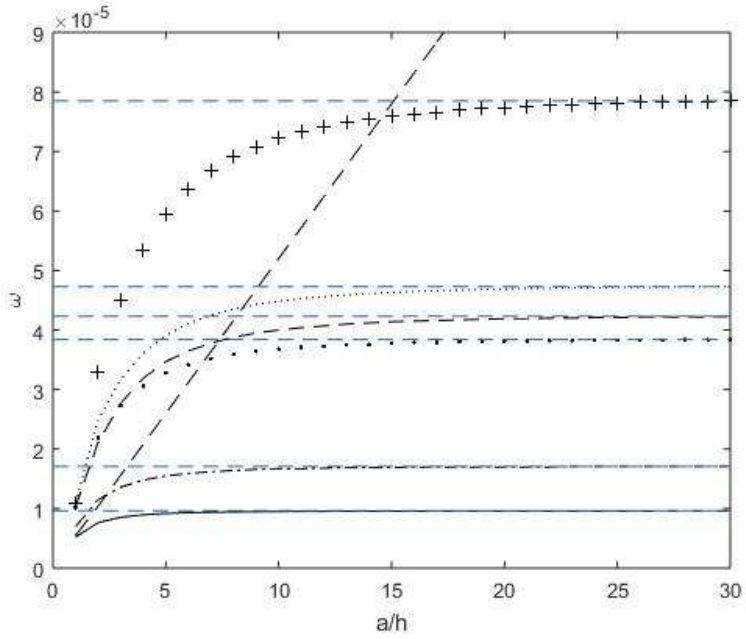

The influence of slenderness for the first eight frequencies for plates with anisotropic materials under SFSF conditions

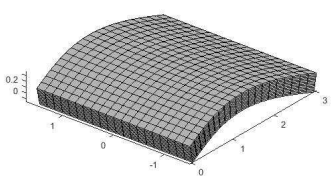

Mode 1

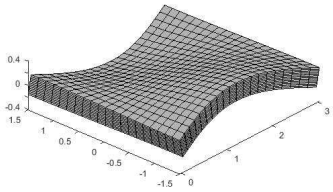

Mode 2

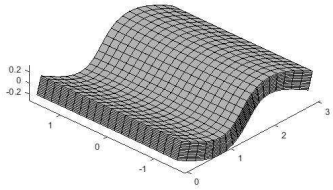

Mode 3

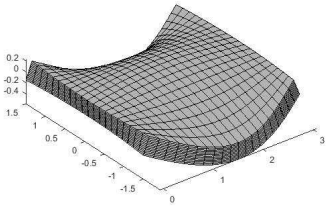

Mode 4

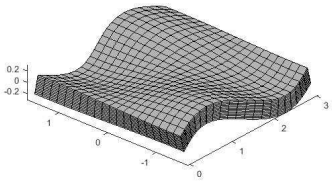

Mode 5

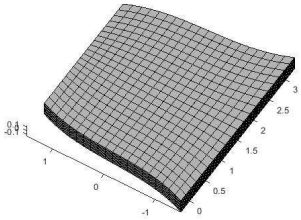

Mode 6

First six mode shapes for plates with FBF materials under SFSF conditions

Figure 79: First six frequencies and mode shapes under SFSF conditions

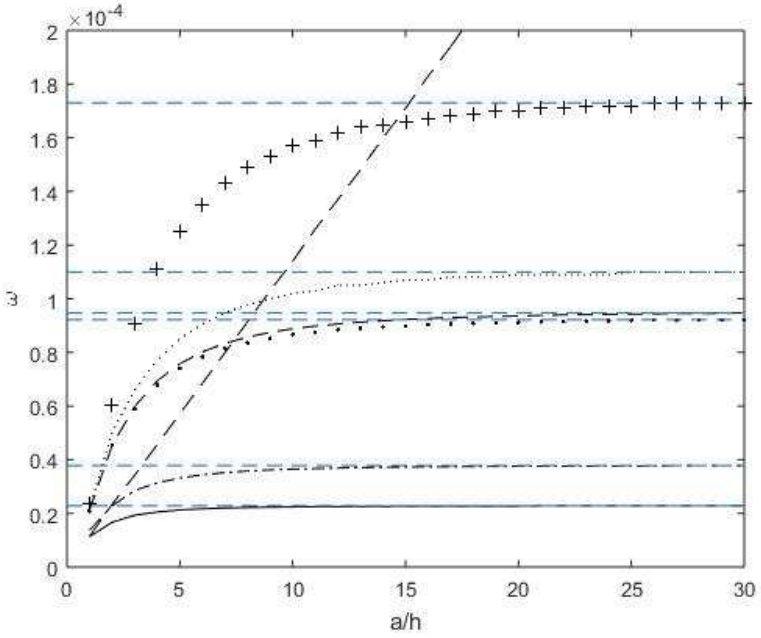

Figure 80: The influence of slenderness for the first six frequencies for plates with BBB materials under SFSF conditions

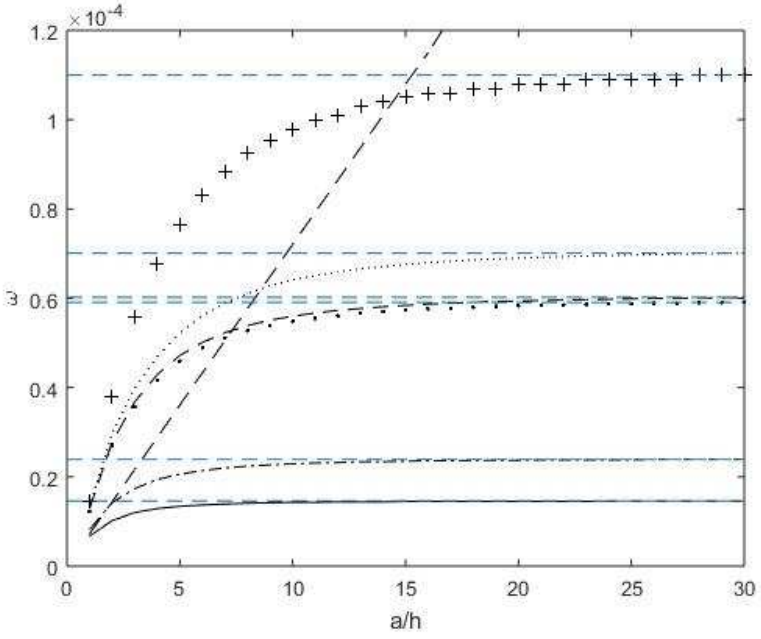

Figure 81: The influence of slenderness for the first six frequencies for plates with FFF materials under SFSF conditions

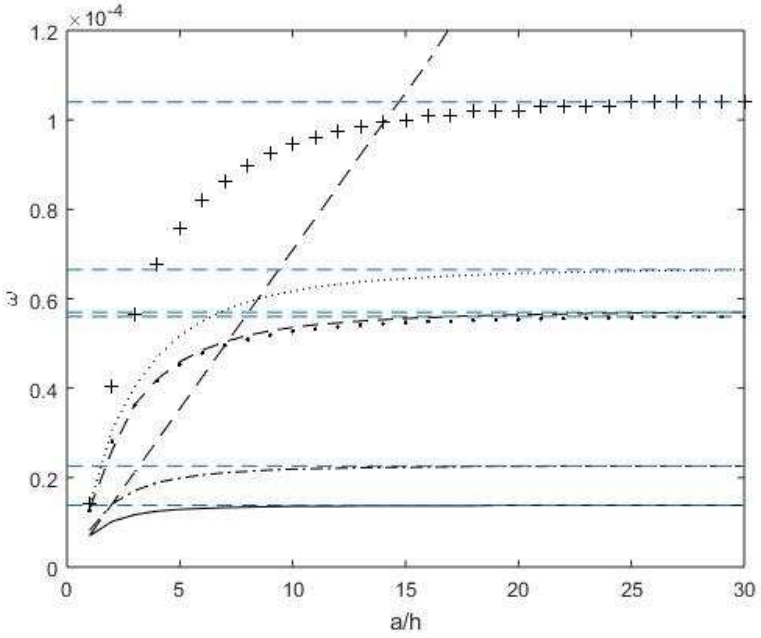

Figure 82: The influence of slenderness for the first six frequencies for plates with BFB materials under SFSF conditions

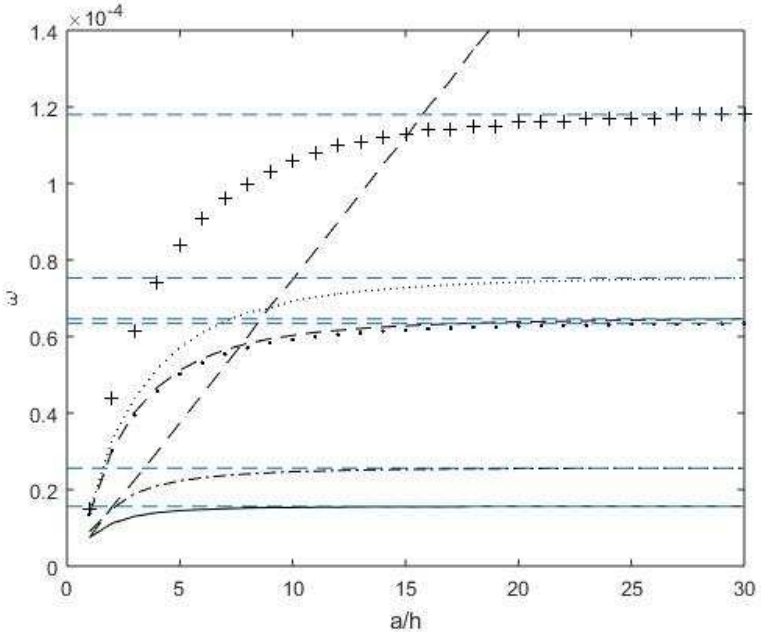

Figure 83: The influence of slenderness for the first six frequencies for plates with FBF materials under SFSF conditions

Table 59: Frequencies for homogeneous plates composed of five stacking sequences under SFSF condition at a/h=10

Mode	Hex	BBB	FFF	BFB	FBF
1	9.52E-6	2.24E-5	1.43E-5	1.36E-5	1.53E-5
2	1.67E-5	3.65E-5	2.29E-5	2.19E-5	2.47E-5
3	3.68E-5	8.66E-5	5.48E-5	5.27E-5	5.92E-5
4	4.00E-5	8.88E-5	5.60E-5	5.36E-5	6.03E-5
5	4.48E-5	1.02E-4	6.41E-5	6.17E-5	6.93E-5
6	5.20E-5	1.14E-4	7.21E-5	7.09E-5	7.49E-5
7	7.22E-5	1.57E-4	9.79E-5	9.46E-5	1.06E-4

Table 60: Frequencies for homogeneous plates composed of five stacking sequences under SFSF condition at a/h=20

Mode	Hex	BBB	FFF	BFB	FBF
1	9.61E-6	2.27E-5	1.45E-5	1.38E-5	1.56E-5
2	1.70E-5	3.76E-5	2.37E-5	2.25E-5	2.55E-5
3	3.81E-5	9.12E-5	5.83E-5	5.54E-5	6.27E-5
4	4.19E-5	9.36E-5	5.94E-5	5.64E-5	6.38E-5
5	4.69E-5	1.09E-4	6.90E-5	6.57E-5	7.42E-5
6	1.04E-4	2.28E-4	1.44E-4	1.42E-4	1.50E-4
7	7.74E-5	1.70E-4	1.08E-4	1.20E-4	1.16E-4

Differences for plates composed of these five materials are shown in Table 62. Based on the thin plate theory, normally 10 is the slenderness suggested for the isotropic plates. Hence, results are excellant as expected with classical plate theory. With slenderness of 10, the differences are within 10 percent. And within ratio of 20, the precent difference are smaller than 2.

Table 61: Frequencies for homogeneous plates composed of five stacking sequences under SFSF condition at a/h=30

Bending Mode	Hex	BBB	FFF	BFB	FBF
1	9.63E-6	2.28E-5	1.46E-5	1.38E-5	1.56E-5
2	1.71E-5	3.78E-5	2.39E-5	2.26E-5	2.56E-5
3	3.84E-5	9.22E-5	5.91E-5	5.60E-5	6.34E-5
4	4.23E-5	9.47E-5	6.02E-5	5.70E-5	6.46E-5
5	4.73E-5	1.10E-4	7.01E-5	6.65E-5	7.53E-5
6	7.85E-5	1.73E-4	1.10E-4	1.04E-4	1.18E-4

Table 62: Differences for homogeneous plates composed of five stacking sequences under SFSF condition

a/h	Bending frequency	% Differences below a/h=30 $\bar{\omega}$				
		Hexagonal	BBB	FFF	BFB	FBF
10	1	1.14	1.75	2.05	1.45	1.92
	2	2.34	3.44	4.18	3.10	3.52
	3	4.17	6.07	7.28	5.89	6.62
	4	5.44	6.23	6.98	5.96	6.66
	5	5.29	7.27	8.56	7.22	7.97
	6	8.03	9.25	11.00	9.04	10.17
20	1	0.21	0.44	0.68	0.00	0.00
	2	0.58	0.53	0.84	0.44	0.39
	3	0.78	1.08	1.35	1.07	1.10
	4	0.95	1.16	1.33	1.05	1.24
	5	0.85	0.91	1.57	1.20	1.46
	6	1.40	1.73	1.82	1.92	1.69

CHAPTER 7 CONCLUSION

In this studying, using the piecewise linear function through the thickness with appropriate approximate functions for the in-plane terms, the free vibration of laminated magneto-electro-elastic beams and plates are studied by a semi-analytical discrete-layer approach. Comparing with the classical beam and plate theories, and previous efforts, the discrete-layer model is accurate and efficient. By plotting the frequencies as a function of length-to-thickness ratio for isotropic materials, some significant phenomenons come out. Further, the DL model is applied to the MEE composite materials. The limitation of classical beam and plate theories under various laterial boundary conditions are shown for each case. From the analyses considered here, results are highlight as following:

- The non-zero Poisson ratio causes large reductions between real and analytical values for the axial and bending frequencies with lower slenderness. Otherwise, because the warping function is restricted at the fixed ends, torsional frequencies higher than the analytical values with respect to the lower a/h ratios.

- Drawing frequencies as a function of a/h ratio, it is clear that torsional and axial freqiencies are presented as linear functions, while the bending frequencies are tend to be curved lines.

- For MEE composite beams, contrary to some recommendations for isotropic beams, having a length-to-thickness ratio of 10 results in errors well into low double-digits for commonly computed frequencies under the simply-supported conditions. Situation gets worse for the fixed-fixed and cantilever beams. For an accurate application of

classical beam theory, a a/h ratio of at least 20 is suggested for errors within several percent for beams made of composite MEE materials.

- For the common used frequencies of composite MEE plates, the application of thin plate theory results around up to 10 percent errors in frequencies with slenderness of 10 for all simply supported and all-clamped conditiions. Keep using the a/h ratios over 20 can significantly lessen the differences within 5 percent for these cases. Adding more free edges can slightly reduce the percent differences caused by applying classical plate theory, as for FCFC, SFSF, and CFFF lateral boundary conditions. Otherwise, the unbalanced condition worsens the differences, as the fifth frequency under CCFF conditions.

The purpose of this study is to give a specification of the limits by using the classical thin beam and plate theories under various laterial boundary conditions. Some typical mode shapes are also plotted as a benefit for furture studying in this field. The present results of isotropic and composite MEE materials could be used as references for the furture investigation of MEE materials ranged from corrosion testing and weld evaluation to life testing and repair method validation.

REFERENCES

[1] S.S. Vel, R.C. Batra, Three-dimensional analytical solution for hybrid multilayered piezoelectric plates, *ASME Journal of Applied Mechanics* 67 (2000) 558-567.

[2] S.S. Vel, R.C. Mewer, R.C. Batra, Analytical solution for the cylindrical bending vibration of piezoelectric composite plates, *International Journal of Solids and Stuctures* 41 (2004) 1625-1643.

[3] E. Pan, P.R. Heyliger, Free vibrations of simply supported and multilayered magneto-electro-elastic plates, *Journal of Sound and Vibration* 252 (2002) 429-442.

[4] J.G. Wang, L.F. Chen, S.S. Fang, State vector approach to analysis of multilayered magneto-electro-elastic plates, *International Journal of Solids and Structure* 40 (2003) 1669-1680.

[5] J.Y. Chen, H.L. Chen, E. Pan, P.R. Heyliger, Modal analysis of magneto-electro-elastic plates using the state vector approach, *Journal of Sound and Vibration* 304 (2007) 722-734.

[6] W.Q. Chen, K.Y. Lee, H.J. Ding, On free vibration of non-homogeneous transversely isotropic magneto-electro-elastic plates, *Journal of Sound and Vibration* 279 (2005) 237-251.

[7] P. Kondaiah, k. Shankar, N. Ganesan. Studies on magneto-electro-elastic cantilever beam under thermal environment, Coupled systems mechanics (2012) pp.205-217

[8] J.Y. Chen, P.R. Heyliger, E. Pan, Free Vibration of Three-dimesional Multilayered Magneto-electro-elastic Plates under combined Clamped/Free Boundary Conditions, *Journal of Sound and Vibration* 333 (2014) 4017-4029.

[9] H.H. Demarest, Jr., Cube Resonance Method to Determine the Elastic Constants of Solids,*J. Acoust. Soc. Am.* 49, (1971) 768-775.

[10] E.P. Eer Nisse, Variational Method for Electroelastic Vibration Analysis, *IEEE Trans. Sonics Ultrason.* SU-14(1976) 153-160.

[11]P.R. Heyliger, Traction-free Vibration of Layered Elastic and Piezoelectric Rectangular Parallelepipeds, *The Journal of the Acoustical Society of America* 107, 1235 (2000).

[12] Rao, S. S. *Vibration of Continuous Systems*, John Wiley and Sons, Hoboken, NJ (2007). Technomic Publishing Co., Lancaster PA (1987).

[13] Whitney, J. M. *Structural Analysis of Laminated Composite Plates*, Technomic Publishing Co., Lancaster PA (1987).

[14] Hjelmstad, K. D. *Fundamentals of Structural Mechanics*, Prentice Hall, Upper Saddle River, NJ (1997).

[15] Ugural, A. C. and Fenster, S. K. *Advanced Strength and Applied Elasticity*, Third Edition, Prentice Hall, Englewood Cliffs, NJ (1995).

[16] Szilard, R. *Theory and Analysis of Plates* Prentice Hall, Englewood Cliffs, NJ (1974).

[17] H.F. Tiersten, Linear Piezoelectric Plate Vibrations, Plenum, New York (1969).

[18] S. Srinivas, C.V. Joga Rao, and A.K. Rao, *Some Results From an Exact Analysis of Thick Laminates in Vibration and Buckling*, J. Appl. Mech. 37, 868-870(1970).

[19] M. Abromowitz, I.A. Stegun, Handbook of Mathematical Functions, Dover, New York, 1965.

[20] I. Ohno, Free Vibration of a Rectangular Papallelepiped Crystal and its Application to Determination of Elastic Constants of Orthorhombic Crystals, *J. Phys. Earth.* 24, (1976) 355-379

[21] K. Nachbagauer, P. Gruber, and J. Gerstmayr, A 3D Shear Deformable Finite Element Based on the Absolute Nodal Coordinate Formulation, *Multibody Dynamics*, Springer Netherlands, (2013) pp 77-96.

[22] J.N. Reddy and N.D. Phan, Stability and Vibraiton of Isotropic, Orthotropic and Laminted Plates according to a Higher-order Shear Deformation Theory, *Journal of Sound and Vibration* 98(2), 157-170 (1985)

[23] K.M. Liew, Y.Xiang and S. Kitipornchai, Transverse vibration of thick rectangular plates-1. Comprehensive sets of boundary conditions,*Computers and Structures* 49(1) 1-29(1993).

APPENDIX A

$$K_{ij}^{11} = \int_V \left[C_{11} \frac{\partial \Psi_i^u}{\partial x} \frac{\partial \Psi_j^u}{\partial x} + C_{16} \left(\frac{\partial \Psi_i^u}{\partial x} \frac{\partial \Psi_j^u}{\partial y} + \frac{\partial \Psi_i^u}{\partial y} \frac{\partial \Psi_j^u}{\partial x} \right) + C_{55} \frac{\partial \Psi_i^u}{\partial z} \frac{\partial \Psi_j^u}{\partial z} + C_{66} \frac{\partial \Psi_i^u}{\partial y} \frac{\partial \Psi_j^u}{\partial y} \right] dV \tag{29}$$

$$K_{ij}^{12} = \int_V \left[C_{12} \frac{\partial \Psi_i^u}{\partial x} \frac{\partial \Psi_j^v}{\partial y} + C_{16} \frac{\partial \Psi_i^u}{\partial x} \frac{\partial \Psi_j^v}{\partial x} + C_{45} \frac{\partial \Psi_i^u}{\partial z} \frac{\partial \Psi_j^v}{\partial z} + C_{26} \frac{\partial \Psi_i^u}{\partial y} \frac{\partial \Psi_j^v}{\partial y} + C_{66} \frac{\partial \Psi_i^u}{\partial y} \frac{\partial \Psi_j^v}{\partial x} \right] dV \tag{30}$$

$$K_{ij}^{13} = \int_V \left[C_{13} \frac{\partial \Psi_i^u}{\partial x} \frac{\partial \Psi_j^w}{\partial z} + C_{45} \frac{\partial \Psi_i^u}{\partial z} \frac{\partial \Psi_j^w}{\partial y} + C_{55} \frac{\partial \Psi_i^u}{\partial z} \frac{\partial \Psi_j^w}{\partial x} + C_{36} \frac{\partial \Psi_i^u}{\partial y} \frac{\partial \Psi_j^w}{\partial z} \right] dV \tag{31}$$

$$K_{ij}^{14} = \int_V \left[e_{11} \frac{\partial \Psi_i^u}{\partial x} \frac{\partial \Psi_j^\phi}{\partial x} + e_{21} \frac{\partial \Psi_i^u}{\partial x} \frac{\partial \Psi_j^\phi}{\partial y} + e_{31} \frac{\partial \Psi_i^u}{\partial x} \frac{\partial \Psi_j^\phi}{\partial z} + e_{15} \frac{\partial \Psi_i^u}{\partial z} \frac{\partial \Psi_j^\phi}{\partial x} + e_{25} \frac{\partial \Psi_i^u}{\partial z} \frac{\partial \Psi_j^\phi}{\partial y} + e_{35} \frac{\partial \Psi_i^u}{\partial z} \frac{\partial \Psi_j^\phi}{\partial z} + e_{16} \frac{\partial \Psi_i^u}{\partial y} \frac{\partial \Psi_j^\phi}{\partial x} + e_{26} \frac{\partial \Psi_i^u}{\partial y} \frac{\partial \Psi_j^\phi}{\partial y} + e_{36} \frac{\partial \Psi_i^u}{\partial y} \frac{\partial \Psi_j^\phi}{\partial z} \right] dV \tag{32}$$

$$K_{ij}^{15} = \int_V \left[q_{11} \frac{\partial \Psi_i^u}{\partial x} \frac{\partial \Psi_j^\psi}{\partial x} + q_{21} \frac{\partial \Psi_i^u}{\partial x} \frac{\partial \Psi_j^\psi}{\partial y} + q_{31} \frac{\partial \Psi_i^u}{\partial x} \frac{\partial \Psi_j^\psi}{\partial z} + q_{15} \frac{\partial \Psi_i^u}{\partial z} \frac{\partial \Psi_j^\psi}{\partial x} + q_{25} \frac{\partial \Psi_i^u}{\partial z} \frac{\partial \Psi_j^\psi}{\partial y} + q_{35} \frac{\partial \Psi_i^u}{\partial z} \frac{\partial \Psi_j^\psi}{\partial z} + q_{16} \frac{\partial \Psi_i^u}{\partial y} \frac{\partial \Psi_j^\psi}{\partial x} + q_{26} \frac{\partial \Psi_i^u}{\partial y} \frac{\partial \Psi_j^\psi}{\partial y} + q_{36} \frac{\partial \Psi_i^u}{\partial y} \frac{\partial \Psi_j^\psi}{\partial z} \right] dV \tag{33}$$

$$K_{ij}^{22} = \int_V \left[C_{22} \frac{\partial \Psi_i^v}{\partial y} \frac{\partial \Psi_j^v}{\partial y} + C_{26} \left(\frac{\partial \Psi_i^v}{\partial y} \frac{\partial \Psi_j^v}{\partial x} + \frac{\partial \Psi_i^v}{\partial x} \frac{\partial \Psi_j^v}{\partial y} \right) + C_{44} \frac{\partial \Psi_i^v}{\partial z} \frac{\partial \Psi_j^v}{\partial z} + C_{66} \frac{\partial \Psi_i^v}{\partial x} \frac{\partial \Psi_j^v}{\partial x} \right] dV \tag{34}$$

$$K_{ij}^{23} = \int_V \left[C_{23} \frac{\partial \Psi_i^v}{\partial y} \frac{\partial \Psi_j^w}{\partial z} + C_{44} \frac{\partial \Psi_i^v}{\partial z} \frac{\partial \Psi_j^w}{\partial y} + C_{45} \frac{\partial \Psi_i^v}{\partial z} \frac{\partial \Psi_j^w}{\partial x} + C_{36} \frac{\partial \Psi_i^v}{\partial x} \frac{\partial \Psi_j^w}{\partial z} + \right] dV \tag{35}$$

$$K_{ij}^{24} = \int_V \left[e_{12} \frac{\partial \Psi_i^v}{\partial y} \frac{\partial \Psi_j^\phi}{\partial x} + e_{22} \frac{\partial \Psi_i^v}{\partial y} \frac{\partial \Psi_j^\phi}{\partial y} + e_{32} \frac{\partial \Psi_i^v}{\partial y} \frac{\partial \Psi_j^\phi}{\partial z} + e_{14} \frac{\partial \Psi_i^v}{\partial z} \frac{\partial \Psi_j^\phi}{\partial x} + e_{24} \frac{\partial \Psi_i^v}{\partial z} \frac{\partial \Psi_j^\phi}{\partial y} + e_{34} \frac{\partial \Psi_i^v}{\partial z} \frac{\partial \Psi_j^\phi}{\partial z} + e_{16} \frac{\partial \Psi_i^v}{\partial x} \frac{\partial \Psi_j^\phi}{\partial x} + e_{26} \frac{\partial \Psi_i^v}{\partial x} \frac{\partial \Psi_j^\phi}{\partial y} + e_{36} \frac{\partial \Psi_i^v}{\partial x} \frac{\partial \Psi_j^\phi}{\partial z} \right] dV \tag{36}$$

$$K_{ij}^{25} = \int_V \left[q_{12} \frac{\partial \Psi_i^v}{\partial y} \frac{\partial \Psi_j^\psi}{\partial x} + q_{22} \frac{\partial \Psi_i^v}{\partial y} \frac{\partial \Psi_j^\psi}{\partial y} + q_{32} \frac{\partial \Psi_i^v}{\partial y} \frac{\partial \Psi_j^\psi}{\partial z} + q_{14} \frac{\partial \Psi_i^v}{\partial z} \frac{\partial \Psi_j^\psi}{\partial x} + q_{24} \frac{\partial \Psi_i^v}{\partial z} \frac{\partial \Psi_j^\psi}{\partial y} + q_{34} \frac{\partial \Psi_i^v}{\partial z} \frac{\partial \Psi_j^\psi}{\partial z} + q_{16} \frac{\partial \Psi_i^v}{\partial x} \frac{\partial \Psi_j^\psi}{\partial x} + q_{26} \frac{\partial \Psi_i^v}{\partial x} \frac{\partial \Psi_j^\psi}{\partial y} + q_{36} \frac{\partial \Psi_i^v}{\partial x} \frac{\partial \Psi_j^\psi}{\partial z} \right] dV \tag{37}$$

$$K_{ij}^{33} = \int_V \left[C_{33} \frac{\partial \Psi_i^w}{\partial z} \frac{\partial \Psi_j^w}{\partial z} + C_{44} \frac{\partial \Psi_i^w}{\partial y} \frac{\partial \Psi_j^w}{\partial y} + C_{45} \frac{\partial \Psi_i^w}{\partial y} \frac{\partial \Psi_j^w}{\partial x} + C_{45} \frac{\partial \Psi_i^w}{\partial x} \frac{\partial \Psi_j^w}{\partial y} + C_{55} \frac{\partial \Psi_i^w}{\partial x} \frac{\partial \Psi_j^w}{\partial x} \right] dV \tag{38}$$

$$K_{ij}^{34} = \int_V \left[e_{13} \frac{\partial \Psi_i^w}{\partial z} \frac{\partial \Psi_j^\phi}{\partial x} + e_{23} \frac{\partial \Psi_i^w}{\partial z} \frac{\partial \Psi_j^\phi}{\partial y} + e_{33} \frac{\partial \Psi_i^w}{\partial z} \frac{\partial \Psi_j^\phi}{\partial z} + \right. \tag{39}$$
$$e_{14} \frac{\partial \Psi_i^w}{\partial y} \frac{\partial \Psi_j^\phi}{\partial x} + e_{24} \frac{\partial \Psi_i^w}{\partial y} \frac{\partial \Psi_j^\phi}{\partial y} + e_{34} \frac{\partial \Psi_i^w}{\partial y} \frac{\partial \Psi_j^\phi}{\partial z} +$$
$$\left. e_{15} \frac{\partial \Psi_i^w}{\partial x} \frac{\partial \Psi_j^\phi}{\partial x} + e_{25} \frac{\partial \Psi_i^w}{\partial x} \frac{\partial \Psi_j^\phi}{\partial y} + e_{35} \frac{\partial \Psi_i^w}{\partial x} \frac{\partial \Psi_j^\phi}{\partial z} \right] dV$$

$$K_{ij}^{44} = \int_V \left[-\epsilon_{11} \frac{\partial \Psi_i^\phi}{\partial x} \frac{\partial \Psi_j^\phi}{\partial x} - \epsilon_{22} \frac{\partial \Psi_i^\phi}{\partial y} \frac{\partial \Psi_j^\phi}{\partial y} - \epsilon_{33} \frac{\partial \Psi_i^\phi}{\partial z} \frac{\partial \Psi_j^\phi}{\partial z} \right] dV \tag{40}$$

$$K_{ij}^{55} = \int_V \left[-\mu_{11} \frac{\partial \Psi_i^\psi}{\partial x} \frac{\partial \Psi_j^\psi}{\partial x} - \mu_{22} \frac{\partial \Psi_i^\psi}{\partial y} \frac{\partial \Psi_j^\psi}{\partial y} - \mu_{33} \frac{\partial \Psi_i^\psi}{\partial z} \frac{\partial \Psi_j^\psi}{\partial z} \right] dV \tag{41}$$

APPENDIX B

Table 63: material coefficients of Hexagonal, $BaTiO_3$ and $CoFe_2O_4$

material coefficients of Hexagonal					
$c_{11} = c_{22}$	$298.2(10^9)$	$c_{44} = c_{55}$	$165.5(10^9)$	$c_{13} = c_{23}$	$11.0(10^9)$
c_{33}	$340.9(10^9)$	c_{66}	$135.3(10^9)$	c_{12}	$27.7(10^9)$
ρ	1850				
material coefficients of $BaTiO_3$					
$c_{11} = c_{22}$	$166(10^9)$	$\epsilon_{11} = \epsilon_{22}$	$11.2(10^{-9})$	$e_{31} = e_{32}$	-4.4
c_{33}	$162(10^9)$	ϵ_{33}	$12.6(10^{-9})$	e_{33}	18.6
$c_{44} = c_{55}$	$43(10^9)$	$\mu_{11} = \mu_{22}$	$5(10^{-6})$	$e_{24} = e_{15}$	11.6
c_{66}	$44.5(10^9)$	μ_{33}	$10(10^{-6})$		
c_{12}	$77(10^9)$				
$c_{13} = c_{23}$	$78(10^9)$	ρ	5800		
material coefficients of $CoFe_2O_4$					
$c_{11} = c_{22}$	$286(10^9)$	$\epsilon_{11} = \epsilon_{22}$	$0.08(10^{-9})$	$q_{31} = q_{32}$	580.3
c_{33}	$269.5(10^9)$	ϵ_{33}	$0.093(10^{-9})$	q_{33}	699.7
$c_{44} = c_{55}$	$45.3(10^9)$	$\mu_{11} = \mu_{22}$	$590(10^{-6})$	$q_{24} = q_{15}$	550
c_{66}	$56.5(10^9)$	μ_{33}	$157(10^{-6})$		
c_{12}	$173(10^9)$				
$c_{13} = c_{23}$	$170.5(10^9)$	ρ	5300		

the units here: $c_{ij}(N/m^2)$,$e_{ij}(C/m^2)$,$q_{ij}(N/Am)$,$\epsilon_{ij}(C^2/Nm^2)$, $\mu_{ij}(Ns^2/C^2)$,$\rho(kg/m^3)$